

**APPLICATION OF COLD PLATES TO
ELECTRONIC EQUIPMENT COOLING**

C. J. FELDMANIS

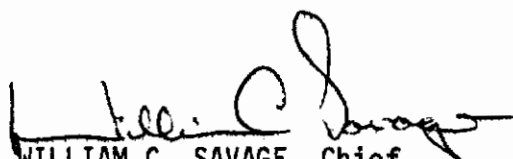
Distribution limited to U.S. Government agencies only; test and evaluation; statement applied May 1972. Other requests for this document must be referred to Air Force Flight Dynamics Laboratory (FEE), Wright-Patterson Air Force Base, Ohio 45433.

FOREWORD

This report was prepared by C. J. Feldmanis of the Environmental Control Branch, Vehicle Equipment Division, Air Force Flight Dynamics Laboratory. The study was conducted under Project 6146, "Environmental Control Systems For Military Aircraft".

The manuscript of this report was released by the author in June 1972.

This technical report has been reviewed and is approved.



WILLIAM C. SAVAGE, Chief
Environmental Control Branch
Vehicle Equipment Division
Air Force Flight Dynamics Lab.

ABSTRACT

Analytical and experimental work have been performed to investigate the feasibility for heat pipe technology for electronic equipment thermal control. Temperature level and uniformity, amplitude and the frequency of thermal cycling have significant adverse effect upon the reliability and operational characteristics of electronic equipment. In order to promote heat transfer and improve the temperature distribution, the electronic equipment cooling plates (cold plates) were provided with integral heat pipes. The experimental cold plates which were tested can be divided into three general categories: (1) conventional fin-tube configurations, (2) fin-tube configuration provided with temperature control capabilities (constant temperature or variable conductance cold plate), and (3) flat, continuous cavity configuration. Actual and simulated electronic components were attached to the plates and used as heat loads.

Test results have shown that the high thermal conductance of the heat pipes provided excellent temperature distribution throughout the plates, thus maintaining all of the equipment attached to them at a uniform temperature. Close temperature control of the plate could be achieved by utilizing variable conductance heat pipes with noncondensable gas reservoirs. Thermal cycling caused by equipment duty cycles or heat sink temperature changes was significantly reduced. Application of heat of fusion materials or evaporative coolants within the cold plates can also reduce thermal cycling or extend operational time for the safety of flight equipment under emergency conditions.

It must be pointed out, however, that all of the cold plates tested were quite sensitive to orientation. Only a few degrees of inclination

Contrails

with the evaporator section up caused degradation of the plate's thermal performance, while inclination with the condenser end up improved performance. Dynamic forces caused by aircraft maneuvers will also have effects upon heat pipe performance; these effects, however, were not investigated under this study.

Contrails

TABLE OF CONTENTS

<u>SECTION</u>		<u>PAGE</u>
I	INTRODUCTION	1
II	THERMAL PERFORMANCE OF HEAT PIPES	5
	1. Radial Heat Flux Limitations	8
	2. Constant Temperature Heat Pipe	15
III	COMPONENT MOUNTING AND HEAT REMOVAL	17
	1. Joint Thermal Resistance	25
	2. Plate Thermal Resistance	29
IV	EXPERIMENTAL RESULTS	31
	1. Electronic Equipment Cooling Plates Provided With Heat Sinks	31
	a. Cold Plate No. 1 Results	33
	b. Cold Plate No. 2 Results	38
	2. Electronic Equipment Cooling Plates With Integral Heat Pipes	42
	a. Cold Plate No. 3 Results	44
	(1) Thermal Resistance of the Evaporator Section	47
	(2) Thermal Resistance of the Condenser Section	49
	b. Sample Calculation	57
	(1) Thermal Resistance of Mounting Joint	59
	(2) Thermal Resistance of Plate	59
	(3) Thermal Resistance of Evaporator Section	60
	(4) Thermal Resistance of Condenser Section	60
	(5) Thermal Resistance of Forced Convection	61
	(6) Determination of Temperature Distribution	63
	c. Cold Plate No. 4 Results	67
	d. Cold Plate No. 5 Results	77
	e. Cold Plate No. 6 Results	94

Contrails

TABLE OF CONTENTS (Con'd)

<u>SECTION</u>		<u>PAGE</u>
V	SUMMARY OF RESULTS	104
VI	CONCLUSIONS	107
VII	REFERENCES	109

ILLUSTRATIONS

<u>FIGURE</u>	<u>PAGE</u>
1. Rating Chart of a Microelectronic Device	2
2. Schematic of a Heat Pipe	5
3. Results of Wick Boiling Tests with Freon 113	13
4. Condenser Section of Heat Pipe	14
5. Constant Temperature Heat Pipe	16
6. Component Mounting on Heat Sink	17
7. Rating Chart for RCA N-P-N Silicon Transistor	20
8. Rating Chart for RCA Germanium P-N-P Power Transistor	20
9. Stud Mounted Rectifier Assembly	21
10. Component Mounting on Cold Plate	22
11. Thermal Resistance Network of Evaporator Section	23
12. Total Thermal Resistance Network	24
13. Heat Flow Across Joint Direct Contact Area	26
14. Stress Distribution in a Bolted Joint	28
15. Resistance Network of Plate	29
16. Experimental Electronic Equipment Cold Plate (No. 1 and No. 2) Provided with Emergency Heat Sink	32
17. Temperature Change vs. Time of Cold Plate No. 1 at Different Power Input Rates and No Coolant Flow	37
18. Temperature Change vs. Time of Cold Plate No. 1 Under Periodic Heat Load Changes	39
19. Temperature Changes vs. Time of Cold Plate No. 2 at Different El Power Input Rates and No Coolant Flow	41
20. Comparison of Cold Plates No. 1 and No. 2 Thermal Performance	43

Contrails

<u>FIGURE</u>		<u>PAGE</u>
21.	Experimental Electronic Equipment Cold Plate No. 3	45
22.	Section A-A of Cold Plate No. 3	46
23.	Thermal Resistance Network	46
24.	Section B-B of Cold Plate No. 3	47
25.	Section C-C of Cold Plate No. 3	48
26.	Section D-D of Cold Plate No. 3	50
27.	Temperature Distribution of Cold Plate No. 3 (Long Section)	51
28.	Temperature Distribution from Component 1 Mounting Base to Coolant	53
29.	Comparison of Temperature Distribution Between Analytical and Experimental Results	54
30.	Temperature Distribution From Component 2 Mounting Base to Coolant	55
31.	Temperature Distribution From Component 3 Mounting Flange to Coolant	56
32.	Temperature Distribution of Cold Plate No. 3 (Short End) - All Components Energized	58
33.	Resistance Network of Evaporator Section	62
34.	Resistance Network of Symmetrical Section	63
35.	Experimental Electronic Equipment Cold Plate No. 4	68
36.	Temperature Distribution of Cold Plate No. 4	70
37.	Temperature Changes of Cold Plate No. 4 vs. Electric Power Input Rates	71
38.	Experimental Electronic Equipment Cold Plate No. 4 with Attached Two Power Transistors and a "Dummy" Component	72
39.	Section A-A of Cold Plate No. 4	73
40.	Temperature Distribution of Cold Plate No. 4 Under Coolant Flow and No Flow Conditions	75
41.	Temperature Distribution of Cold Plate No. 4 at Two Different El. Power Input Rates to Transistors	76

Contracts

<u>FIGURE</u>		<u>PAGE</u>
42.	Temperature Distribution of Cold Plate No. 4 - Mica Washers Used at Transistor Mounting Joints	78
43.	Temperature Distribution of Cold Plate No. 4 - Comparison of Different Transistor Mounting Techniques	79
44.	Temperature Distribution of Cold Plate No. 4 at Different El. Power Input Rates to "Dummy" Component 3	80
45.	Experimental Electronic Equipment Cold Plate No. 5 (Variable Conductance Cold Plate)	81
46.	Temperature Distribution of Cold Plate No. 5	83
47.	Temperature Distribution of Cold Plate No. 5	84
48.	Temperature Changes of Cold Plate No. 5 vs. Electric Power Input Rates to Heaters	86
49.	Effects of Orientation Upon Cold Plate's No. 5 Thermal Performance	87
50.	Experimental Electronic Equipment Cold Plate No. 5 With Attached Electronic Components	89
51.	Temperature Distribution From Component Mounting Base To Cold Plate	90
52.	Temperature Distribution From Component Mounting Base To Cold Plate	91
53.	Temperature Distribution From Component Mounting Base To Cold Plate	92
54.	Experimental Electronic Equipment Cold Plate No. 6	95
55.	Resistance Network of Evaporator Section	97
56.	Temperature Distribution of Cold Plate No. 6 at Different Power Input Rates to Transistor	100
57.	Temperature Distribution of Cold Plate No. 6 at Different Power Input Rates to Transistor	101
58.	Temperature Distribution of Cold Plate No. 6 at Two Different El. Power Input Rates	102

Contrails

SYMBOLS

A	area, sq. ft.
A_w	wick area, sq. ft.
c	specific heat, Btu/lb, °F
C	heat capacity, Btu/°F
D	diameter, ft
f_w	wick friction factor
g	acceleration due to gravity, ft./hr ² or ft/sec ²
G	mass velocity, lb/sec.
g_c	universal gravitational constant, ft. lb _m /lb _f hr ²
h	height of liquid column, ft or, heat transfer coefficient, Btu/ hr ft ² °F
H	Heat of fusion, Btu/lb
h_{fg}	latent heat of vaporization, Btu/lb
k	thermal conductivity, Btu/hr. ft. °F
K	thermal conductance, Btu/hr °F
K_p	permeability constant, ft ²
K_v	≤ 1 pressure recovery in the vapor (for zero pressure recovery $K_v = 1$)
L, ℓ	length, ft
L_a	length of adiabatic section, ft.
L_c	length of condenser section, ft.
L_e	length of evaporator section, ft.
\dot{m}	mass flow rate, lb/hr
M	mesh size, wires/inch
P	pressure, lb/ft ²

Contrails

ΔP_C	capillary pumping pressure, lb/ft ²
ΔP_L	pressure drop in liquid phase, lb/ft ²
ΔP_V	pressure drop in vapor phase, lb/ft ²
ΔP_g	pressure due to difference in elevation, lb/ft ²
Q	heat flow rate, Btu/hr
r_C	radius of the wick pores, ft
r_W	wire radius, in.
R_V	radius of the vapor channel, ft
R_W	inside radius of pipe, ft
R	resistance to heat flow, °F hr/Btu
R_{LV}	thermal resistance of liquid saturated wick, °F hr/Btu
T	temperature
U	overall heat transfer coefficient, Btu/hr ft ² °F
V	flow velocity, ft/sec
α	slope angle (measured from horizontal), degrees
θ	contact angle, degrees
ϵ	porosity, $\epsilon = (V_t - V_s)/V_t$
μ_L	absolute viscosity of liquid, lb/ft/hr
μ_V	absolute viscosity of vapor, lb/ft/hr
ν_L	kinematic viscosity of liquid, ft ²
ν_V	kinematic viscosity of vapor, ft ² /hr
ρ	density of liquid, lb/ft ³
ρ_V	density of vapor, lb/ft ³
σ	surface tension, lb/ft
τ	time, hrs

Contrails

Contrails

I INTRODUCTION

Effective heat transfer and removal is essential to the achievement of long life, high reliability and performance of electronic equipment. Operating temperature is a major factor in microelectronics reliability, and failure rates are commonly related to the junction temperature. Transistor characteristics, such as the transfer ratios, switching time, reverse current, breakdown voltage, etc. may vary with even small temperature changes. In order to minimize the failure rate and achieve successful operation of electronic equipment, low, stable temperatures are required. Reference 1 points out that failure rates increase by approximately a factor of 10 between 25⁰C and 125⁰C. In addition, for electronic stability, a constant temperature environment is also required. Most failure modes in integrated circuits are openings in the metal films that interconnect integrated circuit components, open bonds between the metal films, and lead wires that provide for electrical connections to the exterior. It is a known fact that cracking is caused by thermal cycling. Reference 2 points out that temperature cycling of electronic parts in a system have a significant adverse effect on the reliability of the system. The same reference has also shown that when the cycling environment was made less severe (reduced frequency of cycling), there was no observable difference between the reliability of the cycling systems and the constant temperature systems. Also, Reference 3 came to the conclusion that temperature cycled part life may be as much as six to seven times less than similar parts operated at constant temperature conditions. This reduction occurred even though the constant temperature parts were operated at a temperature approximately 100⁰F higher than

the maximum temperature of the cycled parts.

RADC Reliability Handbook (Reference 4) presents two rating points for each device: one for maximum permissible junction temperature and the other for the maximum case or ambient temperature at which 100 percent of the rated load can be dissipated without exceeding the specified maximum junction temperature (derating point, T_S). Some maximum ratings are based on operation at 25°C ambient temperature, while others on a 25°C case temperature (the latter generally for power devices used on heat sinks). Figure 1 shows a rating chart for a microelectronic device.

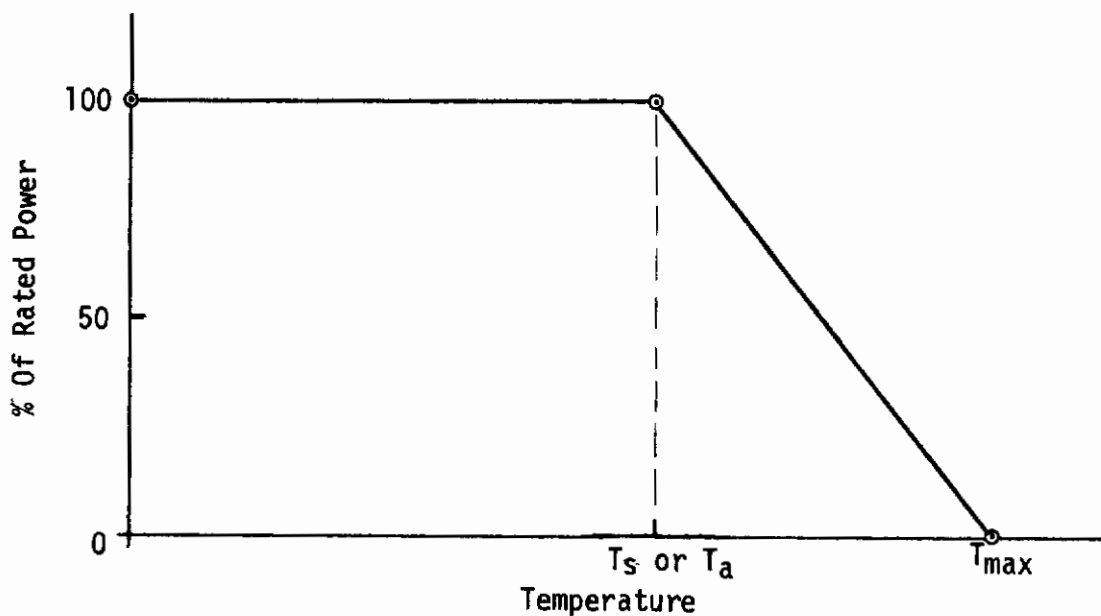


FIGURE 1. RATING CHART OF A MICROELECTRONIC DEVICE

T_S - the temperature derating point (usually 25°C)

T_{max} - maximum junction temperature

T_a - ambient or case temperature

Contrails

Maximum junction temperature is normally 175°C for silicon and 100°C for germanium devices. The maximum junction temperature for copper oxide rectifiers is from 65°C to 80°C , and for selenium about 85°C . In order to operate semiconductor devices at higher power levels, the environmental or heat sink temperature must be lowered. This has been done by using temperatures as low as that of liquid nitrogen. As far as air cooling is concerned, a common "rule-of-thumb" is that forced air cooling is not required if the heat flux (total dissipation divided by case surface area) is less than $1/4$ to $1/2$ watt/in². The higher value applies to well vented cases with parts mounted conductively. When forced air is used for cooling, heat fluxes of approximately 2 watts/in² can be removed. Reference 5 showed that a power transistor which could dissipate 70 watts when mounted on a heat sink at 25°C had a maximum power dissipation of approximately 2 watts when mounted in free air. Furthermore, present weapon systems, because of the large amount of electronic systems and thus large heat generation rates, impose limitations on the amount of air available for cooling. Also, conventional air cooling systems diminish in effectiveness at high vehicle speeds and high altitudes.

The above considerations, therefore, must eventually lead to alternative cooling methods such as circulating liquids, expendable coolants, and fuel heat sinks or combinations of these. Present and near future developments indicate that power densities can reach values up to 10^3 watts/in³ for conventional solid state devices. In IMPATT diodes the wafer power flux can reach values up to 10^6 watts/in² (Reference 6). These extremely high heat generation rates are well above the heat load capabilities of present conventional cooling systems.

Contrails

When considering the cooling of semi-conductor devices, the most practical method of removing waste heat from the device is by metallic conduction. Such cooling techniques can be best provided by application of cold plates cooled by a circulating liquid. Two general designs can be realized from such cold plates: (1) the cold plate is provided with passages through which coolant is circulated, and (2) the cold plate is provided with heat pipe passages which collect and transfer the equipment waste heat to the circulating coolant. This effort, however, will be mainly devoted to development of electronic equipment mounting plates (cold plates) provided with heat pipe passages. Such plates can provide not only uniform temperature equipment mounting surfaces, but can also provide temperature control by introducing non-condensable gas into the condenser section of the heat pipe. Quite a close temperature control can be achieved by this technique without application of sophisticated thermal control systems.

II THERMAL PERFORMANCE OF HEAT PIPES

Although thermal analysis and performance characteristics of heat pipes have been covered in many technical reports and papers, the basic theory and equations will be presented in this report. Figure 2 shows a schematic of a heat pipe consisting of a constant cross-sectional area vapor flow passage surrounded by an annular wick.

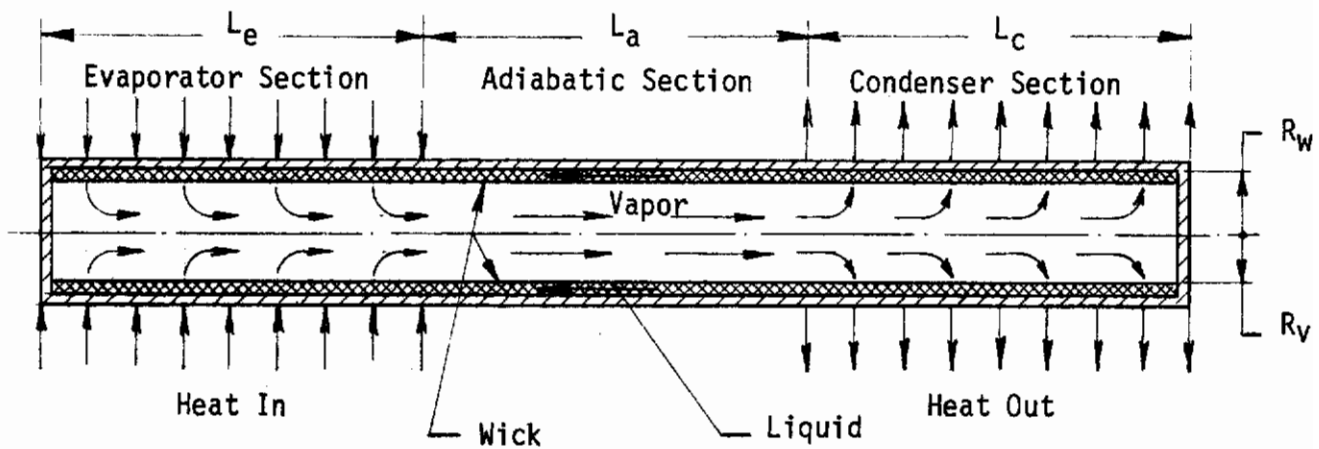


FIGURE 2. SCHEMATIC OF A HEAT PIPE

The working fluid is evaporated at the evaporator section, transferred through the vapor flow passage to the condenser section where it is condensed, and returned through the wick by capillary action to the evaporator section. As both the boiling and condensing processes take place at a constant temperature, the internal temperature of the heat pipe is practically constant (assuming a negligible pressure drop in the vapor space).

Contrails

For optimum operating conditions, the wick thickness can be determined from the following expression given by Reference 7.

$$\frac{R_V}{R_W} = \sqrt{2/3} \quad (1)$$

Assuming that the maximum heat flux which the heat pipe can transfer depends upon the capillary pumping pressure, the following equation must be satisfied:

$$\Delta P_\ell + \Delta P_V + \Delta P_g = \Delta P_C \quad (2)$$

When the heat pipe orientation is horizontal, $\Delta P_g = 0$, and

$$\Delta P_C = \Delta P_\ell + \Delta P_V \quad (3)$$

The capillary pumping pressure or driving force results from the adhesive force of interfacial wetting and can be expressed as

$$\Delta P_C = \frac{2\sigma \cos \theta}{r_c} \quad (4)$$

The maximum driving pressure occurs when the wetting angle $\theta = 0$, and under such conditions

$$\Delta P_C = \frac{2\sigma}{r_c} \quad (5)$$

The gravity head is given by

$$\Delta P_g = \rho_\ell \frac{g}{g_c} L \sin \alpha \quad (6)$$

Neglecting effects of gravity, the wick provides the only resistance to liquid flow from the condenser to the evaporator. Because of the low flow rates and velocities encountered in capillary flow, it can be assumed that the flow is laminar and Darcy's law, therefore, will apply

$$\Delta P_{\ell} = \frac{\dot{m}_{\ell} \mu_{\ell} L_a}{K_p A_w \rho_{\ell}} \quad (7)$$

Another expression, based also on Darcy's law, can be used for determining the liquid pressure drop as a function of heat flow

$$\Delta P_{\ell} = \frac{1}{K_p} \frac{\nu_{\ell}}{A_w g_c} \frac{Q}{h_{fg}} \left(\frac{L_e}{2} + L_a + \frac{L_c}{2} \right) \quad (8)$$

For a cylindrical pipe, the pressure drop in the vapor passage as given by RCA is:

$$\Delta P_v = \frac{K_v G^2 g}{8 R_v^4 p_v g_c} \quad (9)$$

Equation (8) is based on the assumption of uniform heat input in the evaporator section, and uniform rejection in the condenser section.

The only unknown in the above equation is the permeability constant, K_p , which can be determined experimentally using laboratory test techniques. Neglecting ΔP_v and assuming that $L_a = 0$ and $\theta = 0$ Reference 8 gives the following expression for Q_{\max} :

$$Q_{\max} = 4 \left(\frac{\sigma h_{fg}}{\nu_{\ell}} \right) \frac{K_p A_w g_c}{r_c L} - 2 \left(\frac{\rho_{\ell} h_{fg}}{\nu_{\ell}} \right) K_p A_w g \sin \alpha \quad (10)$$

Neglecting gravity forces the second term disappears, and

$$Q_{\max} = 4 \left(\frac{\sigma h_{fg}}{\nu_{\ell}} \right) \frac{K_p A_w g_c}{r_c L} \quad (11)$$

The wick friction factor, expressed as $f_w = 1/K_p$ can be measured by passing fluid at a known rate through a sample of known size. The pressure drop across the sample can be measured, and f_w can be determined from the following expression:

Contrails

$$f_w = \frac{A_t}{\Delta x} \frac{\rho_l}{\mu_l} \frac{\Delta P_f}{W_l} \quad (12)$$

where A_t is the total cross-sectional area of the sample perpendicular to the liquid flow direction, Δx is the length of the sample, ΔP_f is the pressure drop across the sample, and W_l is the liquid flow rate.

With reference to Equation (5), accurate prediction of ΔP_c , however, is impossible because wick surfaces do not exhibit clearly defined uniform circular openings with measurable radii. In addition, wettability is a function of the working fluid and wick material, and values of θ cannot always be obtained or assumed to be zero. ΔP_c can, however, be determined experimentally by using wick capillary pressure tests. Reference 9 gives the following expression for determining capillary radius of wire cloth wick

$$r_c = \frac{1}{2M} - r_w \quad (13)$$

Where M - mesh size, wires/inch

r_w - wire radius, inches

1. Radial Heat Flux Limitations

There are two limiting factors which must be considered in the design of heat pipes: (1) when the vaporization rates are too high, the capillary forces may not be sufficient to deliver liquid to the evaporator section of the heat pipe, and (2) if vapor does not leave the vaporization interface at the rate it is produced then, liquid will be excluded from the interface and the vapor will expand and blanket the heated surface. In either of the two cases the effects would be a sharp increase in the heat pipe wall temperature at the evaporator

section.

Although there is a very small temperature drop along the longitudinal axis of the heat pipe, the main temperature gradient occurs in the radial direction at both the evaporator and condenser sections. Only limited effort has been devoted to heat transfer studies of wick covered surfaces and only limited data are available about boiling and condensing heat transfer coefficients from wick covered surfaces. The heat transfer rate, based on the overall heat transfer coefficient, can be expressed as follows:

$$Q = UA\Delta t \quad (14)$$

The total thermal resistance of a heat pipe consists of the series resistances of the evaporator and condenser

$$R_t = R_e + R_c = \left(\frac{1}{UA}\right)_e + \left(\frac{1}{UA}\right)_c \quad (15)$$

For a tight, low porosity wick, RCA gives the following radial conduction equation:

$$K_r = \frac{2\pi L_e k_w^{l_v}}{\ln \left(\frac{R_w}{R_v}\right)} \quad (16)$$

where

$k_w^{l_v}$ - Composite thermal conductivity of the wick, liquid and possibly intrapped vapor bubbles

When nucleate boiling takes place within the wick, the evaporator conductance is expressed by:

$$K_e = 2\pi R_w L_e h \quad (17)$$

where

h - boiling heat transfer coefficient determined for the specific fluid, heat pipe and operating heat flux.

$$h = \frac{k_{w\ell}}{\delta_w} \quad (18)$$

$k_{w\ell}$ - Thermal conductivity of liquid saturated wick -
condition at low heat fluxes

δ_w - thickness of wick, ft

For heat transfer surfaces covered with thin metallic wicks, equation (18) will give values which are too high, and other analytical expressions must be used for determining evaporative heat transfer coefficients. Reference 10 has investigated evaporative heat transfer coefficients for a 1.0 inch outside diameter horizontal copper tube embedded in water saturated ceramic fiber wick. The data were correlated over a heat flux range from 1000 to 10,000 Btu/hr. ft.² °F by using the following equation:

$$\left(\frac{h}{CG'}\right) \left(\frac{C_\mu}{k}\right)^{0.6} \left(\frac{\rho \ell \sigma}{p^2}\right)^{0.21} = 0.072 \left(\frac{D_e G'}{\mu}\right)^{-0.77} \quad (19)$$

Where $G' = \frac{Q}{A_e h_{fg}}$ lb/hr ft² (20)

$$D_e = 4r_h = 4 \frac{\epsilon}{A_s} \quad (21)$$

$$A_s = \pi D_f L_f \quad (22)$$

In the above reference the author concluded that, at low heat flux, the evaporative heat transfer coefficient for a wick covered surface was higher than that for pool boiling from a plain surface. The following reasons have been given for the above phenomena: (1) wick fibers

increase the effective transfer surface area and provide active sites for bubble formation, and (2) the wick fibers greatly increase the ratio of heated surface to liquid volume (this increases the rate of superheat of liquid near the surface, thus aiding the formation of vapor bubbles).

Reference 11 presents results of pool boiling of distilled water (at one atmosphere pressure) from horizontal, stainless steel tubes spiraled by 1/8 and 1/4 inch diameter organic fiber wicking in a coil-like manner. The test runs were performed with eight, sixteen and twenty six evenly spaced spirals. It was observed that the wick spirals around the heater section produced much earlier nucleation in the saturated liquid pool. At about 20°F, superheat sites were activated while about 10°F was required without wicking. Also, as the number of spirals increased, the greater was the improvement in the film coefficient over no wicking runs. With 26 spirals of wicking around a six inch heater length, the film coefficient was four times greater than for a non-wicked surface at Δt_{sat} of 20°F. The wicking spirals, however, did not increase the critical heat flux of the heater surface. The improvement in heat transfer could be observed at the lower heat fluxes only. The results are in complete agreement with Reference 10.

Extensive experimental data have been presented in Reference 12, where evaporative heat transfer coefficients were determined from planar wick covered surfaces using water and Freon 113 as evaporants. This reference points out that equivalent or superior

performance can be obtained with wick covered surfaces as compared to surfaces with no wicks. The data, however, indicate that, depending on the structure of the wicking material, the entrapment of vapor bubbles in the wick matrix may cause premature film boiling in the wick at relatively low heat fluxes. Reference 12 also points out that the boiling heat transfer coefficient of two-layer thick screen is significantly higher than that of the seven-layer thick sample. Figure 3 shows results of wick boiling tests with Freon 113 as presented in Reference 12.

Based on the studies performed, a conclusion can be made that the approximate critical heat flux can be determined by a semi-empirical equation developed by Rohsenow and Griffith (Reference 13).

$$q_{cr} = 143 h_{fg} \rho_v \left(\frac{g}{g_c}\right)^{0.25} \left(\frac{\rho_l - \rho_v}{\rho_v}\right)^{0.6} \quad (23)$$

or the following equation developed by Zuber

$$q_{cr} = 0.18 h_{fg} \rho_v \left[\frac{\sigma(\rho_l - \rho_v) g g_c}{\rho_v^2}\right]^{-0.25} \left(\frac{\rho_l - \rho_v}{\rho_l}\right)^{0.5} \quad (24)$$

Correlations with Equations 23 and 24 have also been performed for Freons E2 and C51-12.

The condensing heat transfer coefficient can be estimated by Nusselt's equation for film condensation on horizontal tubes

$$h_c = 0.725 \left(\frac{g^2 h_{fg} k^3}{D \mu \Delta t}\right)^{0.25} \quad (25)$$

or, when the value of g (4.17×10^8 ft/hr²) is removed from the brackets, the equation may be expressed as

$$h_c = 103.7 \left(\frac{k^3 \rho^2 h_{fg}}{D \mu \Delta t}\right)^{0.25} \quad (26)$$

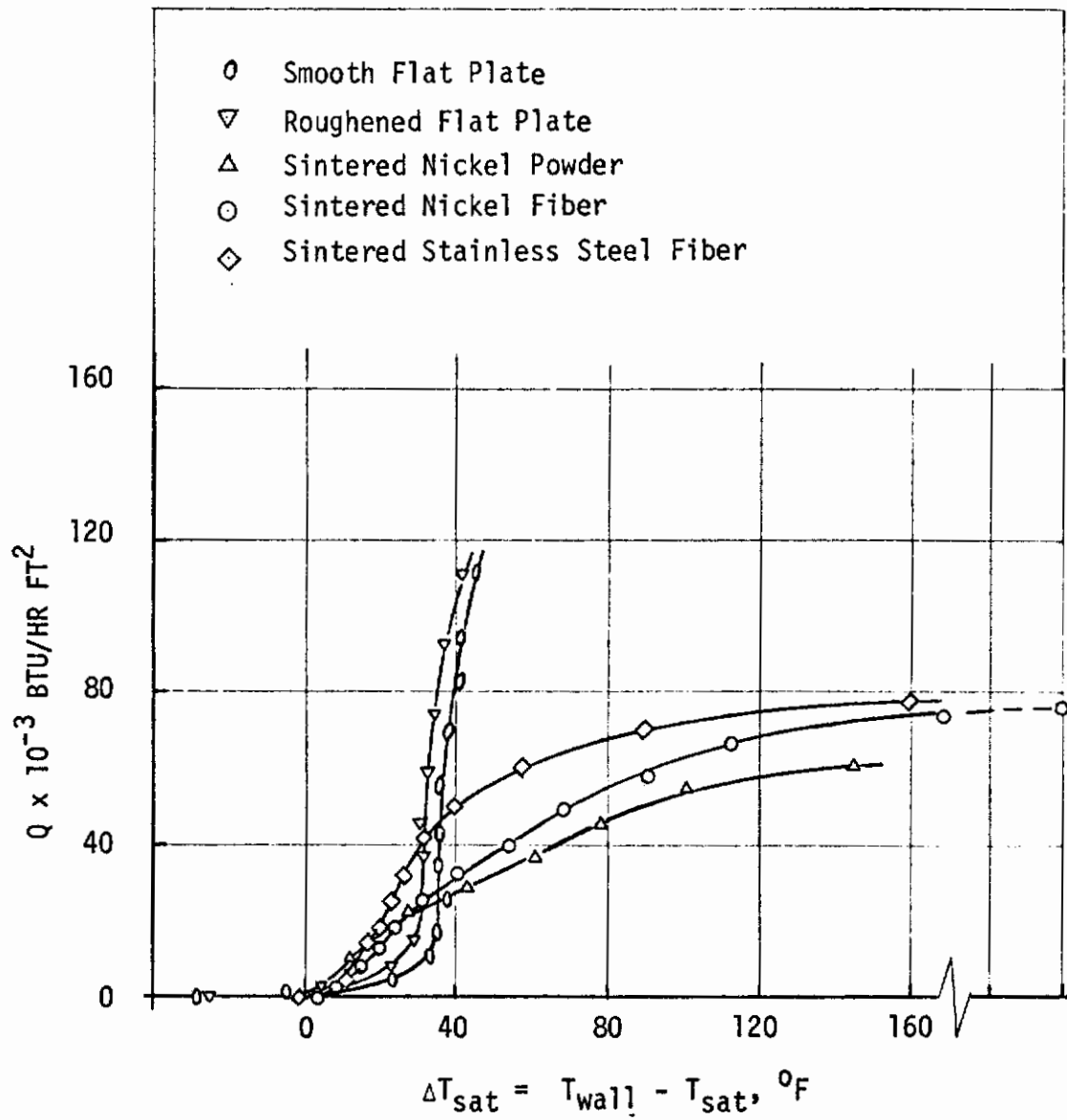


FIGURE 3. RESULTS OF WICK BOILING TESTS WITH FREON 113 (REF 12)

where Δt - difference in temperature of the vapor and wall, $^{\circ}\text{F}$.

If the thermal resistance of the liquid saturated wick is large compared with thermal resistance of condensation, the following equation may be used for determining condensing heat transfer coefficient:

$$h_c = \frac{k_{w\ell}}{\delta_w} \quad (27)$$

Reference 9 gives the following equation for determining thermal conductance of liquid saturated wick:

$$k_{w\ell} = \epsilon k_\ell + (1-\epsilon) k_w \quad (28)$$

where ϵ is porosity of the wicking material.

Heat transfer through the condenser section of the heat pipe, (see Figure 4), can be divided into four separate items.

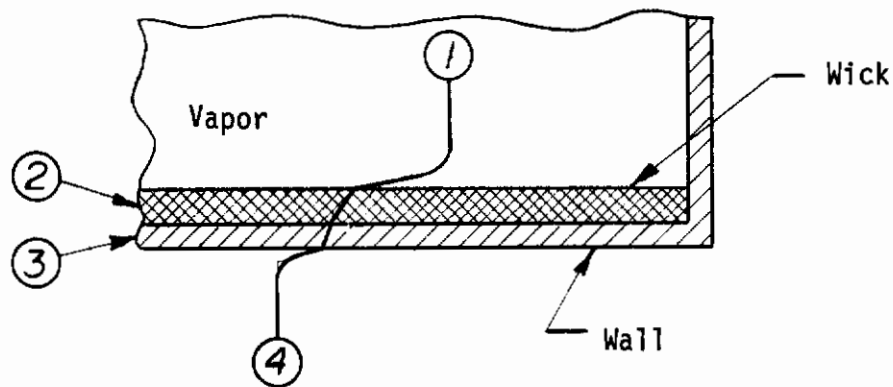


FIGURE 4. CONDENSER SECTION OF HEAT PIPE

- (1) Condensation heat transfer coefficient on the wick covered surface.
- (2) Conduction heat transfer through liquid saturated wick.

(3) Conduction through tube wall.

(4) Convection heat transfer to coolant (heat sink).

The overall heat transfer coefficient at the condenser section of the heat pipe, therefore, can be expressed as follows:

$$\frac{1}{U} = \frac{1}{h_i} + \frac{x_1}{k_1} + \frac{x_2}{k_2} + \frac{1}{h_o} \quad (29)$$

or

$$U = \frac{1}{\frac{1}{h_i} + \frac{x_1}{k_1} + \frac{x_2}{k_2} + \frac{1}{h_o}} \quad (30)$$

Both the evaporator and condenser surface areas are important items in heat pipe thermal performance. When the evaporator is covered with a vapor film, a critical heat flux is reached which will cause a drastic rise in the temperature of the evaporator surface. This condition should be avoided. For a given heat load, the evaporator surface area must be properly sized to ensure operation below the critical heat flux. Similarly, care must be taken for properly designing the condenser section in order to reduce the radial temperature drop. Under gravity conditions some portion of the condenser can be designed without a wick, significantly reducing the resistance to heat flow.

2. Constant Temperature Heat Pipe

The constant temperature heat pipe was an early development at RCA employing an inert gas blanket in the condenser section. Figure 5 shows such an arrangement.

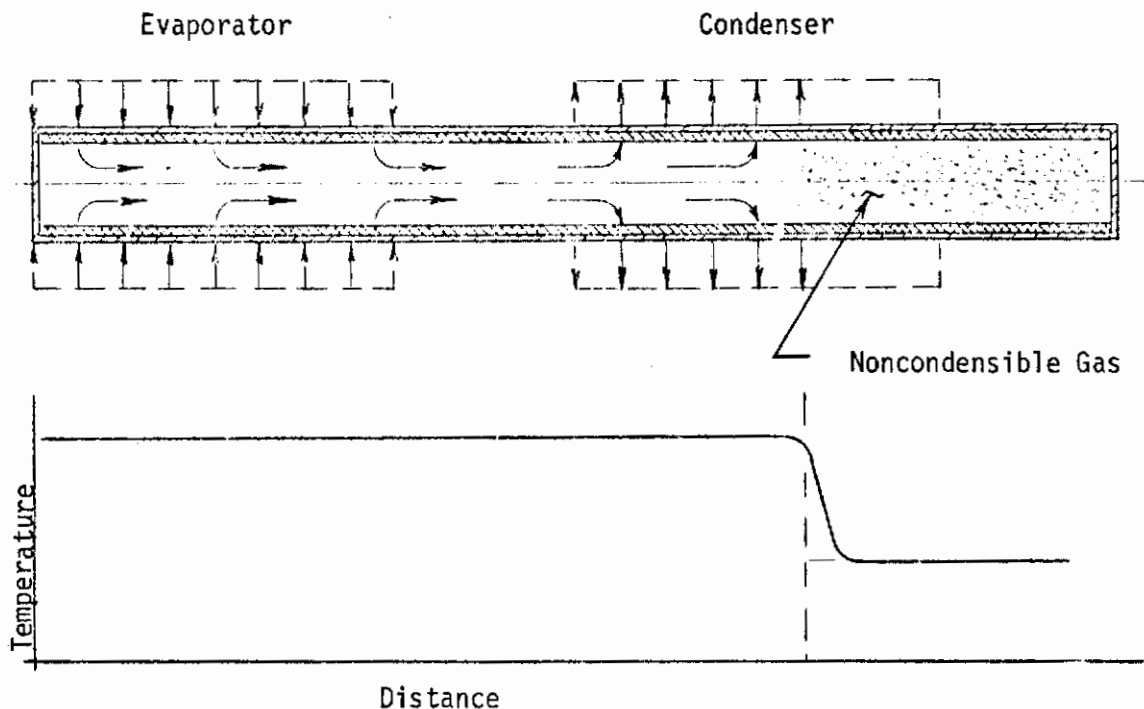


FIGURE 5. CONSTANT TEMPERATURE HEAT PIPE

The inert or noncondensable gas is employed to control the heat rejection area of the condenser section. Under low heat transfer rates the noncondensable gas will occupy most of the condenser length reducing the heat transfer area. As the heat load is increased the noncondensable gas will be forced by the working fluid vapor flow into the reservoir exposing a larger condensing surface area. As a result, the heat pipe becomes a device of nearly constant temperature. Because of the short mean free path of the vapor molecules at normal internal pressures, the vapor penetration into the non-condensable gas is quite small and the interface has a very sharp temperature gradient.

Although the operating temperature of the constant temperature heat pipe will be higher at lower heat dissipation rates than an equivalent conventional heat pipe's temperature, fluctuations caused by heat load changes can be significantly reduced by this simple passive thermal control technique. This technique of temperature control can be applied to electronic equipment cooling when the amplitude of thermal cycling must be reduced.

III COMPONENT MOUNTING AND HEAT REMOVAL

Semiconductor devices (rectifiers, transistors, resistors, etc.) of medium and high power dissipation have power losses which cannot be sufficiently transferred to the heat absorbing medium without special provisions. For air cooling techniques this usually has been achieved by specifically designed heat sinks consisting of heavy and large metal bases provided with extended surfaces. For forced air or liquid cooling systems the heat generating components are mounted on the fluid cooled chassis or cold plates. Because the forced flow heat transfer coefficients are much higher than the natural convection coefficients, particularly when liquid coolants are used, a significant weight and volume savings can be achieved.

Consider an ordinary air cooled heat sink with a power diode or rectifier mounted on it. Heat, generated by the device flows mainly to the base of the device, then across the mounting joint and through the heat sink to the surrounding air. Figure 6 shows a rectifier mounted on an air cooled heat sink.

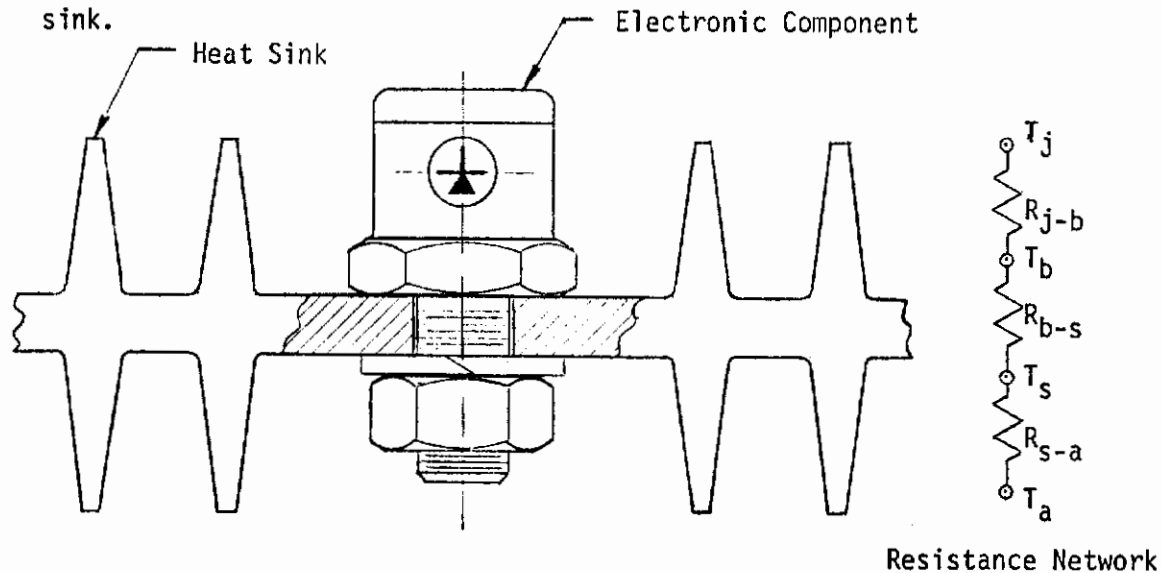


FIGURE 6. COMPONENT MOUNTING ON A HEAT SINK

The total thermal resistance (R_t) can be expressed as follows

$$R_t = R_{j-a} = R_{j-b} + R_{b-s} + R_{s-a} \quad (31)$$

where

R_{j-b} - thermal resistance from junction to mounting base

R_{b-s} - thermal resistance from component mounting base to heat sink
(contact thermal resistance)

R_{s-a} - thermal resistance between the heat sink and the ambient air.

Actually, the heat sink will also have a certain resistance to heat flow and will cause a temperature drop. However, because of the large cross-sectional area and high thermal conductance of the material, this resistance is usually neglected. The above thermal resistances can be found in manufacturers handbooks, and the junction temperature can be determined from the following expression:

$$T_j - T_a = P (R_{j-b} + R_{b-s} + R_{s-a}) \quad (32)$$

where P is the power generation rate in watts.

The junction temperature for stud or flange mounted devices is the base or flange temperature plus the product of the thermal resistance (R_{j-b}) and the power dissipated in the device, or

$$T_j = T_b + PR_{j-b} \quad (33)$$

The thermal resistance from junction to ambient or any other type of heat absorbing medium is an important characteristic in design of transistor circuits. Increase in temperature from the specified value will result in changes of the transistor characteristics. Operating a transistor at or near its maximum power dissipation limits can cause a

Contrails

condition known as "thermal runaway". If the heat generated at the transistor junction is not dissipated at a proper rate, current flow through the junction will increase and the transistor will burn out. Figures 7 and 8 show rating charts for two types of RCA transistors. It can be seen that when the temperature is increased over a specified limit, the power dissipation rate must be reduced. The AFSC Design Handbook for Microelectronics indicates that: "The thermal engineering design of equipments incorporating integrated circuits must be oriented toward lowest practical junction temperatures. In no case, however, should such designs allow these temperatures to be higher than 50°C below the maximum junction temperature specified for the circuit". Power transistors are generally furnished in packages that can be attached to heat sinks or cold plates. All germanium power transistors are packed in air-tight hermetically sealed metal cases. Many silicon transistors are made in hermetic cases, but since the surface of silicon devices can be passivated to prevent contamination, molded plastic packages are also used. Such packages can provide economy and good performance but require more careful heat sink design. In accordance with Reference 14 for power transistors in which the junction is mounted directly on the header or pedestal, the total internal resistance from junction to case (or mount) varies from 50°C/watt to less than 1°C/watt. Thermal resistance from the mounting flange or base to the heat sink can be made quite small, and usually is within a fraction of a degree per watt. To compensate for the low convection heat transfer coefficient from the heat sink to the ambient air, and thus reduce the thermal resistance, the heat transfer area of the heat sink must be made large.

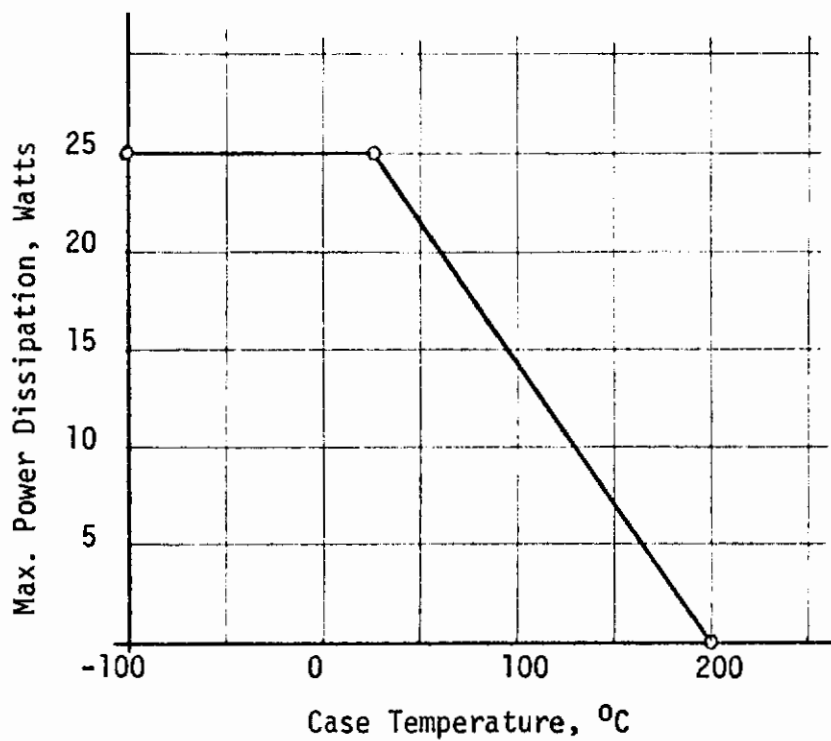


FIGURE 7. RATING CHART FOR ANRCA N-P-N SILICON TRANSISTOR

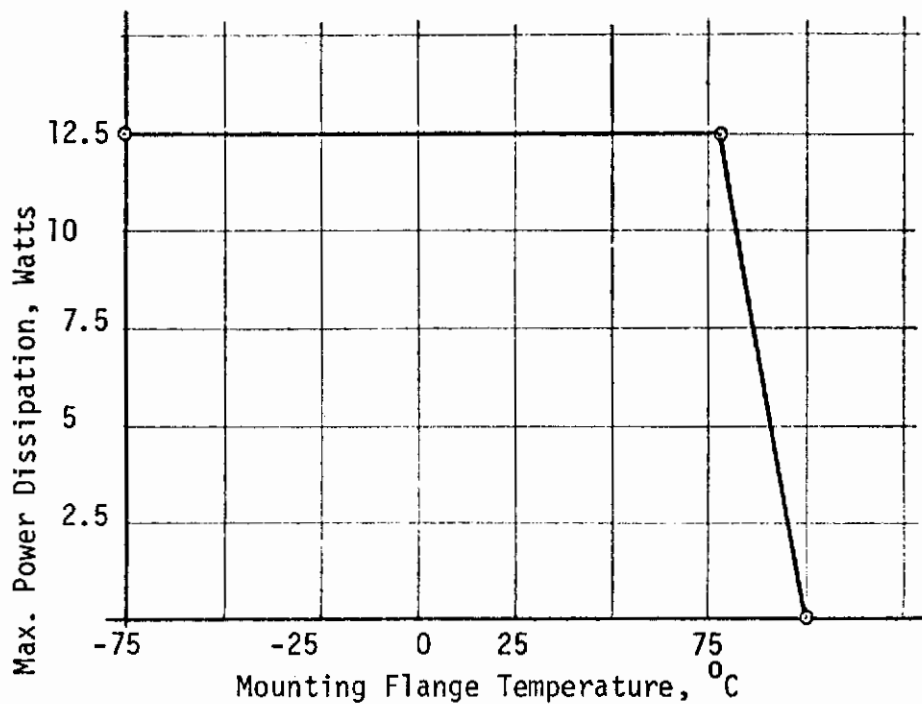


FIGURE 8. RATING CHART FOR AN RCA P-N-P GERMANIUM POWER TRANSISTOR

Under many conditions (unless a grounded collector circuit is used) some form of electrical isolation must be provided between the case and the heat sink or cold plate. The best washer materials for this application are mica, teflon, beryllium oxide and anodized aluminum. Figure 9 shows an arrangement when washers are used for electrical isolation. The increase in thermal resistance using mica or aluminum oxide washers is about $0.5^{\circ}\text{C}/\text{watt}$ minimum. Beryllium oxide, however, is five to six times better as a heat conductor than aluminum oxide. It can be assumed that application of such washers will increase the contact resistance, R_{b-s} , by a factor of about 10. Since the total thermal resistance must have a fixed maximum value for a given power dissipation and cooling medium temperature, the increase of R_{b-s} has to be compensated by a reduction of R_{s-a} .

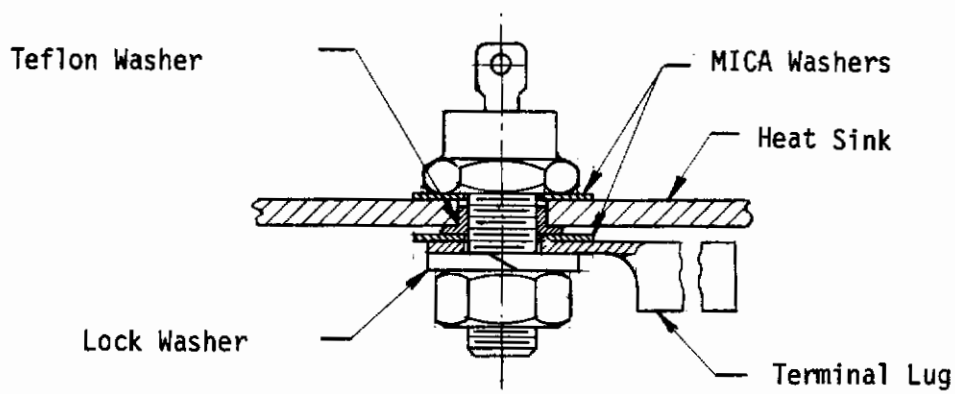


FIGURE 9. STUD MOUNTED RECTIFIER ASSEMBLY

This can be achieved by using larger heat sinks, or cold plates cooled by circulating liquid coolant. Compared with air cooled chassis or cold plates, liquid cooled cold plates are much more efficient.

Conventional cold plates can be cooled by a fluid forced through tubes which are in contact with one side of the plate or plates, or the plate may consist of a sandwich type heat exchanger. Effectiveness

of such cold plates will depend upon spacing of fluid passages, fluid flow rates and fluid properties, plate thickness and thermo-physical properties. If an avionics system cooling was based on such a cold plate design, a significant length of tubing would be required making the system vulnerable to general leaks and battle damage, besides pressure drop and flow distribution problems. Application of heat pipes in cold plate design will not only significantly reduce the length and amount of tubing, but will provide simple, passive control techniques for temperature sensitive electronic equipment. Furthermore, the heat pipes can also be utilized as structural members thus providing a weight advantage.

Consider a cold plate having heat pipe passages and some circulated fluid as an ultimate heat sink. Heat, generated by the electronic component, will be transferred into the component's mounting base or flange and from there, crossing the mounting joint, into the plate. Figure 10 shows such an arrangement.

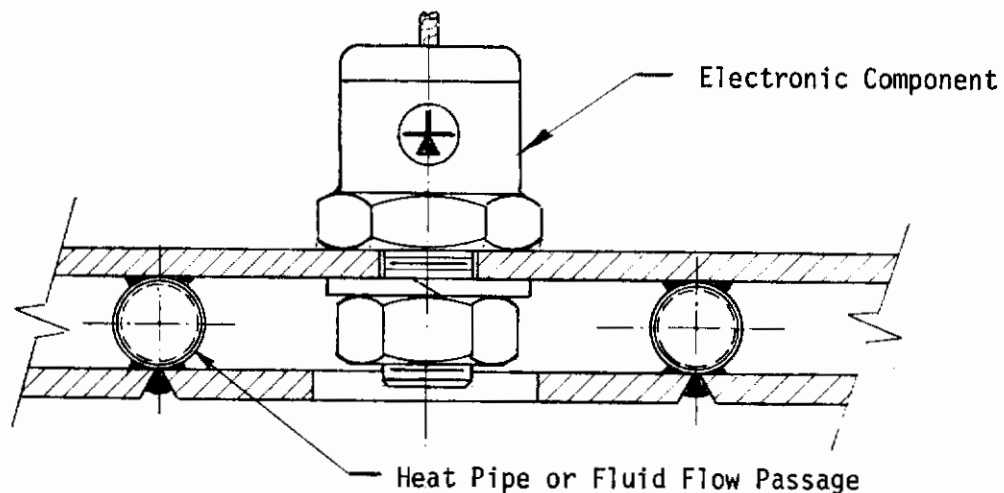


FIGURE 10. ELECTRONIC COMPONENT MOUNTING ON A COLD PLATE

Figure 11 shows all the thermal resistances from junction to the heat pipe working fluid.

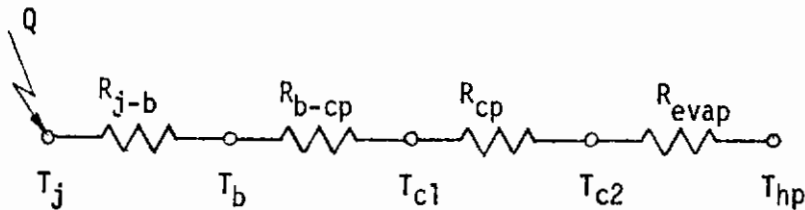


FIGURE 11. THERMAL RESISTANCE NETWORK OF EVAPORATOR SECTION

As already indicated, the first two resistances are given by the manufacturer of the electronic components and the heat sinks. The joint thermal resistance between the base of the device and the cold plate, however, will depend upon the mounting plate (cold plate) thickness, assuming other aspects such as surface finish and flatness constant. Also, the thermal resistance of the plate itself cannot be neglected. Previous studies (Reference 15) performed on joint thermal performance indicated that the plate itself induces the largest resistance to heat flow and not the actual joint interface. As far as the interface is concerned, the effective contact area is not changed significantly by the surface finish if at least one of the surfaces is of soft material such as copper. Fillers, such as silicone grease, applied to the surface will also reduce the joint thermal resistance. Neglecting thermal resistance to and across the wall of the heat pipe, heat is transferred to the working fluid by evaporation, which has been discussed previously (Section II).

It can be assumed that there is no temperature drop along the heat pipe, and the heat pipe passage itself, therefore, will not provide any resistance to heat flow. A certain thermal resistance will occur at

the condenser section associated with some temperature drop (see Section II). Figure 12 shows the overall thermal resistance network from the component junction to the ultimate heat sink - circulating fluid.

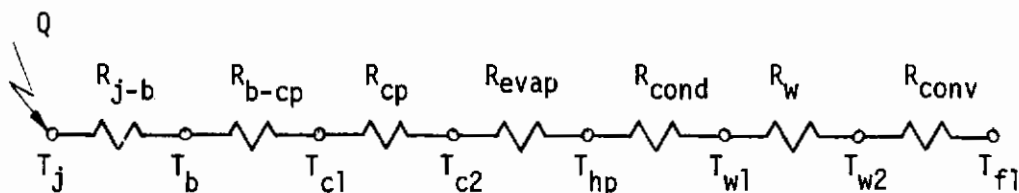


FIGURE 12. TOTAL THERMAL RESISTANCE NETWORK

Thermal resistances of the thin walls at both the evaporator and condenser sections have been neglected. The total thermal resistance, therefore, can be expressed as follows:

$$R_{tot} = R_{j-b} + R_{b-cp} + R_{cp} + R_{evap} + R_{cond} + R_{lW} + R_{conv} \quad (34)$$

where

R_{b-cp} - thermal resistance from component mounting base to cold plate.

R_{cp} - thermal resistance of cold plate.

R_{evap} - thermal resistance of evaporation.

R_{cond} - thermal resistance of condensation.

R_{lW} - thermal resistance of liquid saturated wick.

R_{conv} - thermal resistance of convection.

There is certainly another path of heat flow, i.e., from the component case and plate by radiation and convection to the ambient air. This thermal resistance, however, is very high unless the component is liquid immersed.

The most significant thermal resistance will probably occur within the component mounting surfaces and in the condenser section. Steps, therefore, should be taken to reduce these resistances to a minimum.

Resistance of mounting surfaces can be reduced by selecting materials of high thermal conductivity and reasonable thickness. More careful design will be required to reduce thermal resistance of the condenser section where consideration must be given to two main items: (1) conduction heat transfer across the liquid saturated wick, and (2) convection heat transfer to the circulating coolant. Under the conditions when the whole condenser surface area is covered with wick, the liquid saturated wick can induce quite a significant thermal resistance, because the working fluids generally used in low temperature heat pipes have a low thermal conductivity. Under gravity conditions, however, it will not be always necessary to cover the whole condenser surface area with a wick. Depending on the plate's orientation, condenser arrangement and configuration, a wick might be required only on a portion of the condenser section.

Transferring heat into the circulating coolant is another problem associated with heat pipes. The convection heat transfer coefficient will depend on the coolant properties and flow regime, and will therefore, be limited to a certain value. The only possibility of reducing the convection heat transfer resistance would be by increasing the heat transfer surface area. Design of the condenser section of the cold plate will probably be one of the most important items in designing cold plates with integral heat pipes.

1. Joint Thermal Resistance

Heat transfer rate across the interface of a joint can be expressed by the following equation:

$$Q = AK\Delta t \quad (35)$$

Where

A - area of interface, ft²

K - thermal conductance of joint, Btu/hr ft² °F

Δt - temperature difference across joint, °F

If the heat transfer rate, area of the interface, and the temperature differential are known, thermal conductance across the joint can be determined from equation (35)

$$K = \frac{Q}{A\Delta t} \quad (36)$$

Approximate analytical techniques for determining joint thermal performance as developed by Lindh et al, Fontenot and Whitehurst are presented in Reference 15; the general equations and procedures, however, will also be presented in this report.

Heat transfer across the direct contact area of a joint may be considered as consisting of two components or conduction paths (See Fig. 13): (1) heat conducted across the actual contact points, and (2) heat conducted across the interstitial fluid filling the gap.

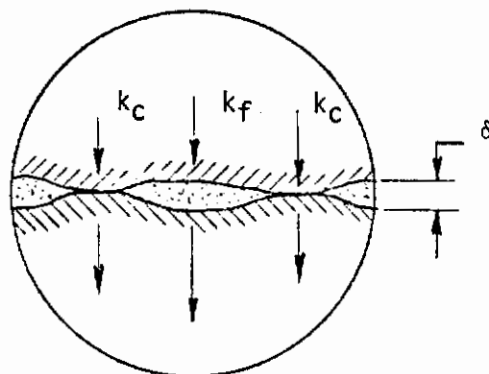


FIGURE 13. HEAT FLOW ACROSS JOINT DIRECT CONTACT AREA

Total heat flow across the direct contact area can be expressed as:

$$K = k_c + k_f \quad (37)$$

where k_c - direct contact conductance, Btu/hr ft² °F

k_f - gap conductance, Btu/hr ft² °F

The total heat transfer rate across the direct contact area can be determined by equation (35). When some information about interface surface conditions is available, thermal conductance across the area of direct contact may be determined from the following equation:

$$K = \frac{1.56 k_f}{i_a + i_b} + 2 n \bar{a} k_m \quad (38)$$

$$k_m = \frac{2 k_1 k_2}{k_1 + k_2} \quad (39)$$

k_1 and k_2 are thermal conductances of the materials making up the joint.
 i_a and i_b are the root mean square values of surface irregularity (roughness plus waviness) for surfaces a and b respectively.

k_f - thermal conductivity of the interstitial fluid, Btu/Hr ft °F

\bar{a} - average radius of contact points

n - number of contact points per unit area

Conductance across a gap can be determined from the following equation

$$K = \frac{k_f}{\delta} \quad (40)$$

Based on known R.M.S. (approximate values of i_a and i_b can be obtained) $n\bar{a}$ values versus contact pressure, as determined by Fontenot (Reference 16), can be obtained from charts.

Figure 14 shows stress distribution in a bolted joint.

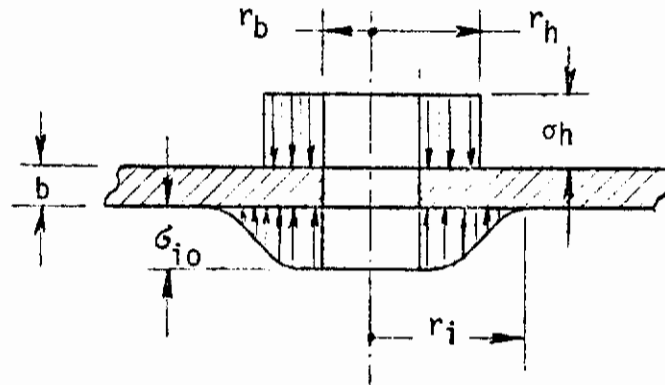


FIGURE 14. STRESS DISTRIBUTION IN A BOLTED JOINT

Using Lieb's (Reference 17) stress distribution parameters, r_i can be found and thus also the average interface pressure

$$\bar{\sigma}_i = \frac{F}{A_i} \quad (41)$$

$$F = \frac{T}{0.2D} \quad (42)$$

$$A_i = \frac{\pi}{4} (D_i^2 - D_b^2) \quad (43)$$

A_i - direct contact area, ft^2

F - induced axial force, lbs

T - bolt torque, in-lbs

D - bolt diameter, in.

Any joint can be divided into direct contact area and gap area, and total conductance or resistance determined

$$K = \frac{1}{R} \quad (44)$$

or

$$R = \frac{1}{K} \quad (45)$$

2. Plate Thermal Resistance

It has been found from previous studies that the largest thermal resistance does not occur at the joint (if the joint is properly made), but rather within the plate. Figure 15 shows resistance network of a plate (see Figs. 22 and 23).

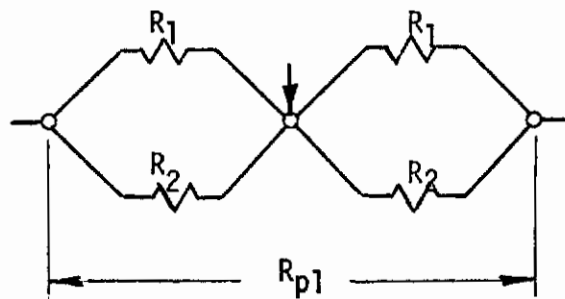


FIGURE 15. RESISTANCE NETWORK OF PLATE

Total thermal resistance of the plate can be expressed as follows:

$$\frac{1}{R_{pl}} = \frac{1}{R_1} + \frac{1}{R_1} + \frac{1}{R_2} + \frac{1}{R_2} = \frac{2}{R_1} + \frac{2}{R_2} \quad (46)$$

and

$$R_{pl} = \frac{1}{\frac{2}{R_1} + \frac{2}{R_2}} \quad (47)$$

The rate of heat flow between isothermal boundaries can be obtained from the flux plots outlined in Section IV. Each heat flow tube may be assumed as a composite wall with equal series resistances through which the rate of heat flow can be expressed by the following equation:

$$\Delta q = \frac{k}{M} (t_1 - t_2) \quad (48)$$

where M is the number of curvilinear squares in the channel. For N channels of unit thickness the heat flow rate becomes

$$Q = \frac{N}{M} k (t_1 - t_2) \quad (49)$$

and for plate thickness b

$$Q = b \frac{N}{M} k (t_1 - t_2) \quad (50)$$

Letting $\frac{N}{M} = s$, and $K = bsk$

$$Q = bsk (t_1 - t_2) \quad (51a)$$

or $Q = K \Delta t \quad (51b)$

where N is the number of channels in a section.

IV EXPERIMENTAL RESULTS

Under this study program six cold plates of different design were fabricated and tested. All of the cold plates can be divided into the following two general categories: (1) cold plates with integral heat pipes provided with heat sinks, and (2) cold plates with integral heat pipes or cavities.

1. Electronic Equipment Cold Plates Provided with Heat Sinks

In aircraft cooling systems provided with circulating fluid loops, electronic equipment cooling will be performed mainly by cold plates or chassis, cooled by the circulating fluid. If such a system, because of enemy action or other reasons, would develop a leak, overheating of the electronic equipment would follow within a very short time. To avoid a catastrophic failure of some of the equipment essential to "safe return", a means must be provided to extend the operational time of such equipment without causing damage to the equipment by overheating. A way of doing this could be by providing the equipment mounting plate (cold plate) with some additional heat sink, for example heat of fusion material or evaporative coolant.

Two cold plates of similar design, shown on Figure 16, were fabricated and tested. The cold plates are made of copper (for fabrication reasons) and incorporate 1/2 inch diameter heat pipes. Space, formed between the two mounting surfaces, is sealed and can be filled with some heat absorbing material. Heat, generated by the electric heaters, is transferred to the heat pipes and from there to the circulating coolant. Heat of fusion materials were used on Cold Plate No. 1, while evaporative coolants were used in Cold Plate No. 2.

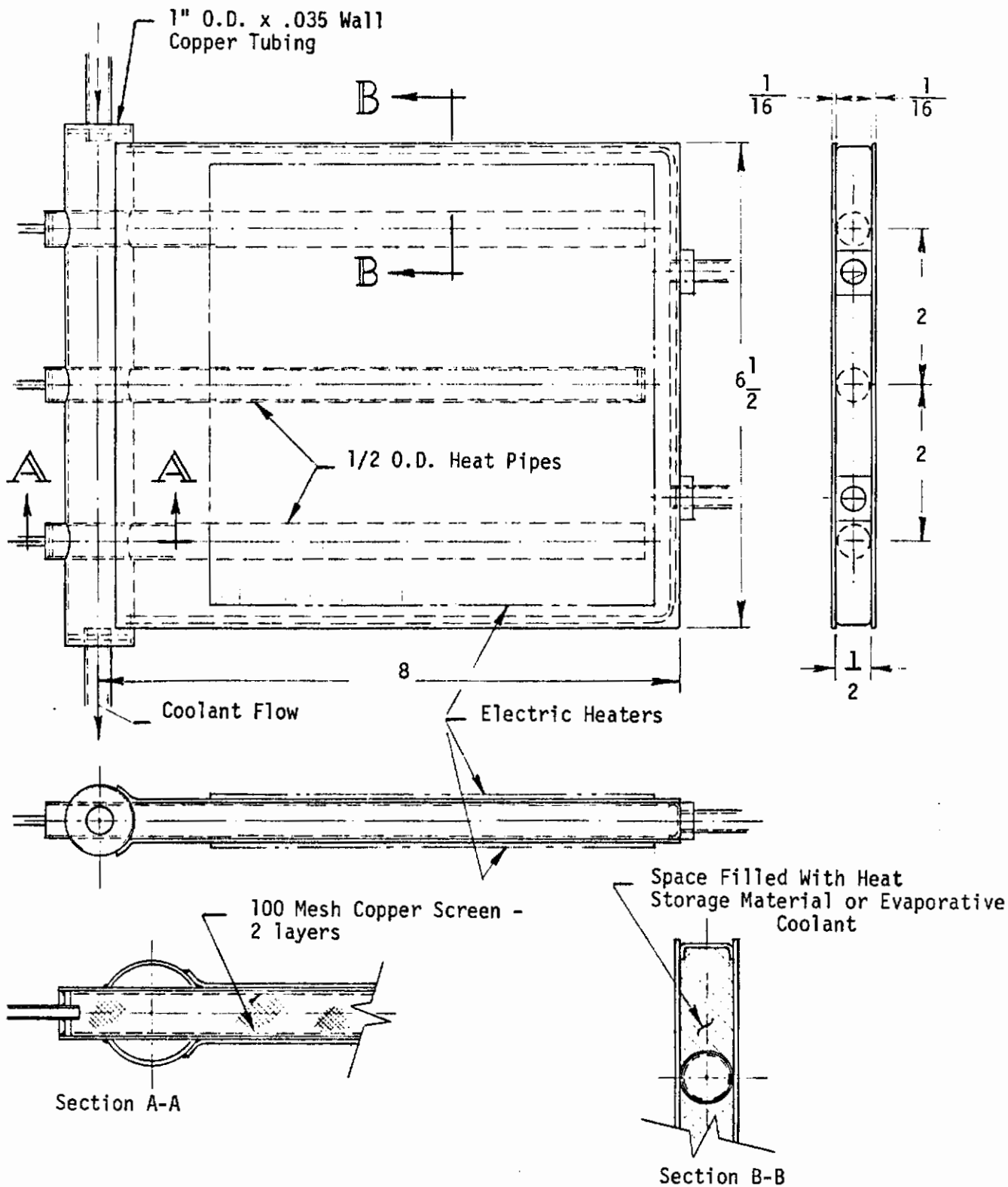


FIGURE 16 EXPERIMENTAL ELECTRONIC EQUIPMENT COLD PLATE (NO'S 1 AND 2) PROVIDED WITH EMERGENCY HEAT SINK

a. Cold Plate No. 1 Results

Filling the plate with the heat of fusion material was performed through the two filler tubes located at one end of the plate. The experiments were performed with the plate in a horizontal position and the filler tubes left open. Most heat of fusion materials expand approximately 10 percent during melting and, therefore, an allowance, must be provided for such expansion within the plate housing so that deformation and damage can be prevented. Another filling technique has also been used, where the space is filled with liquid fusible material at higher temperature than the expected maximum plate temperature and the filling ports sealed.

The cold plate shown here is not very effective as far as speed of response is concerned. The heat of fusion materials have a rather low thermal conductivity, and to accelerate heat transfer into this material, a finned type internal structure is needed. It is also important that the distance between the heat transfer passages be kept as small as practical. To avoid manufacturing difficulties the plate was made without internal fins.

Many chemical compounds are available for use in heat storage devices. However, in selecting such a material several aspects must be considered; for example, they must be non-toxic, non-corrosive, non-flammable and chemically stable. They should also have large heat of fusion, high thermal conductivity and specific heat. Furthermore, selection should be based on the melting temperature of the material so that phase change will take place at some temperature above the initial cold plate temperature and below the maximum allowable cold plate temperature. The total operational time of a cold plate (after

Contrails

coolant circulation is discontinued) provided with heat of fusion material is the sum of the following three items: (1) the time required to heat the cold plate with the heat of fusion material to the transition temperature, (2) the time required to transfer the heat of fusion material from solid to liquid, and (3) the time required to heat the cold plate and liquid heat of fusion material to the maximum allowable temperature.

Considering a cold plate filled with a certain amount of heat of fusion material, the total thermal capacitance of the system will consist of the heat of fusion material plus the plate itself, or

$$C_t = C_{fm} + C_{p\ell} \quad (52)$$

where $C = Wc$ heat capacitance, BTU/°F

When the specific heat is assumed to be constant, the rate of heat flow to a heat storage device can be expressed as follows:

$$Q = Wc \frac{dt}{d\tau} = C \frac{dt}{d\tau} \quad (53)$$

where

$d\tau$ is a time increment

dt is temperature change during the time increment

From equation (53) the time during which a certain amount of heat can be absorbed, can be expressed as follows:

$$\tau = \frac{C (t_1 - t_2)}{Q}, \text{ hrs.} \quad (54)$$

t_1 - temperature at the beginning of the time interval, °F

t_2 - temperature at the end of the time interval, °F

The time required to heat the heat storage device (cold plate and heat of

Contrails

fusion material) to the maximum allowable temperature can, therefore, be expressed as follows:

$$\tau = \frac{1}{Q} [(C_{p\ell} W_{p\ell} + C_{fs} W_f) (t_{tr}-t_i) + H W_f + (C_{p\ell} W_{p\ell} + C_{f\ell} W_f) (t_{max}-t_{tr})] \quad (55)$$

- τ - Operational time, hrs
- Q - heat input rate, Btu/hr
- $C_{p\ell}$ - specific heat of cold plate, Btu/lb^oF
- C_{fs} - specific heat of solid heat of fusion material, Btu/lb^oF
- $C_{f\ell}$ - specific heat of liquid heat of fusion material, Btu/lb^oF
- $W_{p\ell}$ - weight of cold plate, lbs
- W_f - weight of heat of fusion material, lbs
- t_{tr} - heat of fusion material transition temperature, ^oF
- t_i - initial temperature of cold plate, ^oF
- t_{max} - maximum temperature of cold plate, ^oF
- H - heat of fusion, Btu/lb

As far as thermal performance prediction of heat storage devices is concerned, very little information is available about heat transfer at the melt interface. Likewise, very limited data is available about thermophysical properties of such materials.

The experimental cold plate (shown on Figure 16) was cooled by circulating an ethylene glycol - water coolant at a flow rate of approx. 100 lbs/hr at an inlet temperature of approximately 75^oF. Two types of heat of fusion materials (purchased from E. H. Sargent and Company) were used in the cold plate.

1. Beeswax
Heat of fusion 72 Btu/lb
Melting temperature 143^oF

2. Acetamide, C_2H_5ON
Heat of fusion 104 Btu/lb
Melting temperature 160°F

The cold plate was filled with 300 grams of the heat of fusion material, and two types of tests performed: (1) a constant electric power was applied to the electric heaters attached to the plate, while the coolant was circulated through the condenser section of the cold plate. After equilibrium conditions were reached, the coolant flow was discontinued leaving the power input at the same level. (2) Power input cycling tests where the power dissipated by the plate was changed from a minimum to a maximum value.

Figure 17 shows temperature changes at the central section of the plate versus time during constant electric power input to the electric heater of 25, 50, and 75 watts. As seen from the figure, at electric power input of 25 watts a time period of more than two hours was needed before the plate's temperature reached 170°F. At a power input of 75 watts the plate's temperature reached 170°F in about 18 minutes. This short time period of reaching the high temperature, and the form of the high heat load curves indicate that the melting process of the heat of fusion material was retarded. The curves should show a level-off section when the heat of fusion material reaches its melting point. Absence of the internal fins slowed heat transfer to the heat of fusion material, and the temperature of the heated plate, therefore, rose at a faster rate. Connecting the two external plates with conducting fins, heat transfer into the heat of fusion material would be promoted and the time period for reaching the maximum temperature extended.

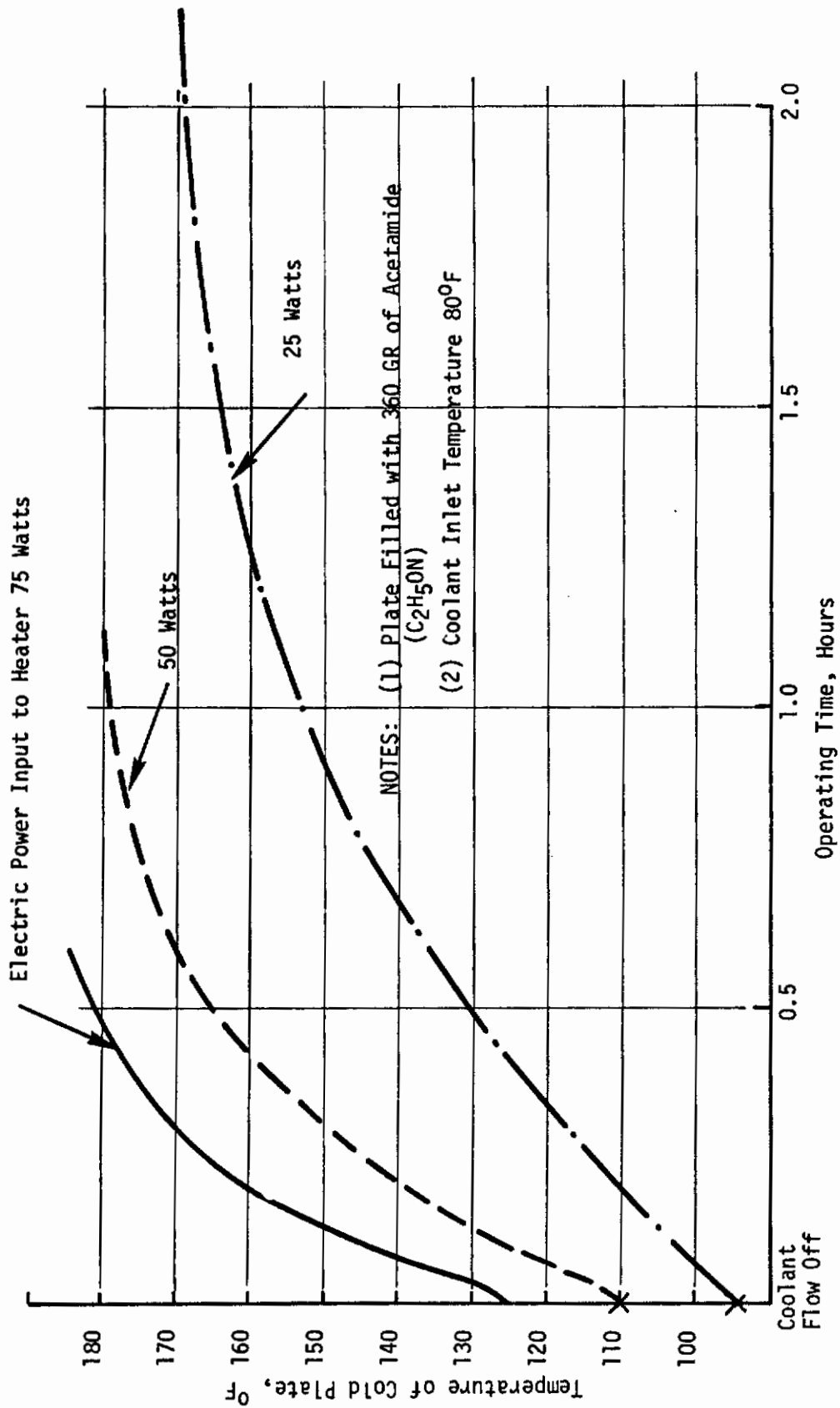


FIGURE 17. TEMPERATURE CHANGES VS TIME OF COLD PLATE NO. 1 AT DIFFERENT POWER INPUT RATES AND NO COOLANT FLOW

Figure 18 shows a comparison of the thermal performance of cold plate no. 1 with and without heat of fusion material under variable power input rates. The electric power input to the plate was varied periodically (15 minute intervals) from 50 to 100 watts; as can be seen, the amplitude of the temperature cycling was reduced from approximately $\pm 15^{\circ}\text{F}$ to $\pm 8^{\circ}\text{F}$ when the plate was filled with bees wax. With improved design of the cold plate, amplitude of the temperature cycling can be further reduced. Using an electronic equipment mounting plate with heat of fusion material, two general goals can be achieved: (1) reduced amplitude of temperature cycling during heat load changes, and (2) emergency cooling when the fluid coolant loop fails.

b. Cold Plate No. 2 Results

Problems of extreme heat concentration and high ambient temperature are usually solved by the evaporation cooling technique. In this cooling technique, heat is removed from the electronic components and/or systems by a change in state when the coolant evaporates during absorption of heat. For a given weight of coolant, vaporization cooling provides more effective heat removal than any other method. Similarly as in the case of the heat of fusion material, the evaporating liquid can be stored within the equipment mounting plate and will provide cooling when an emergency occurs. The evaporating liquid can be simply discharged overboard as a vapor. To insure wetting of the equipment mounting surfaces, the space filled with the evaporant should be provided with a wick. Selection of the liquid should be based on the allowable temperature of the mounting plate. Water has the greatest latent heat of vaporization, but it has disadvantages in its high boiling temperature

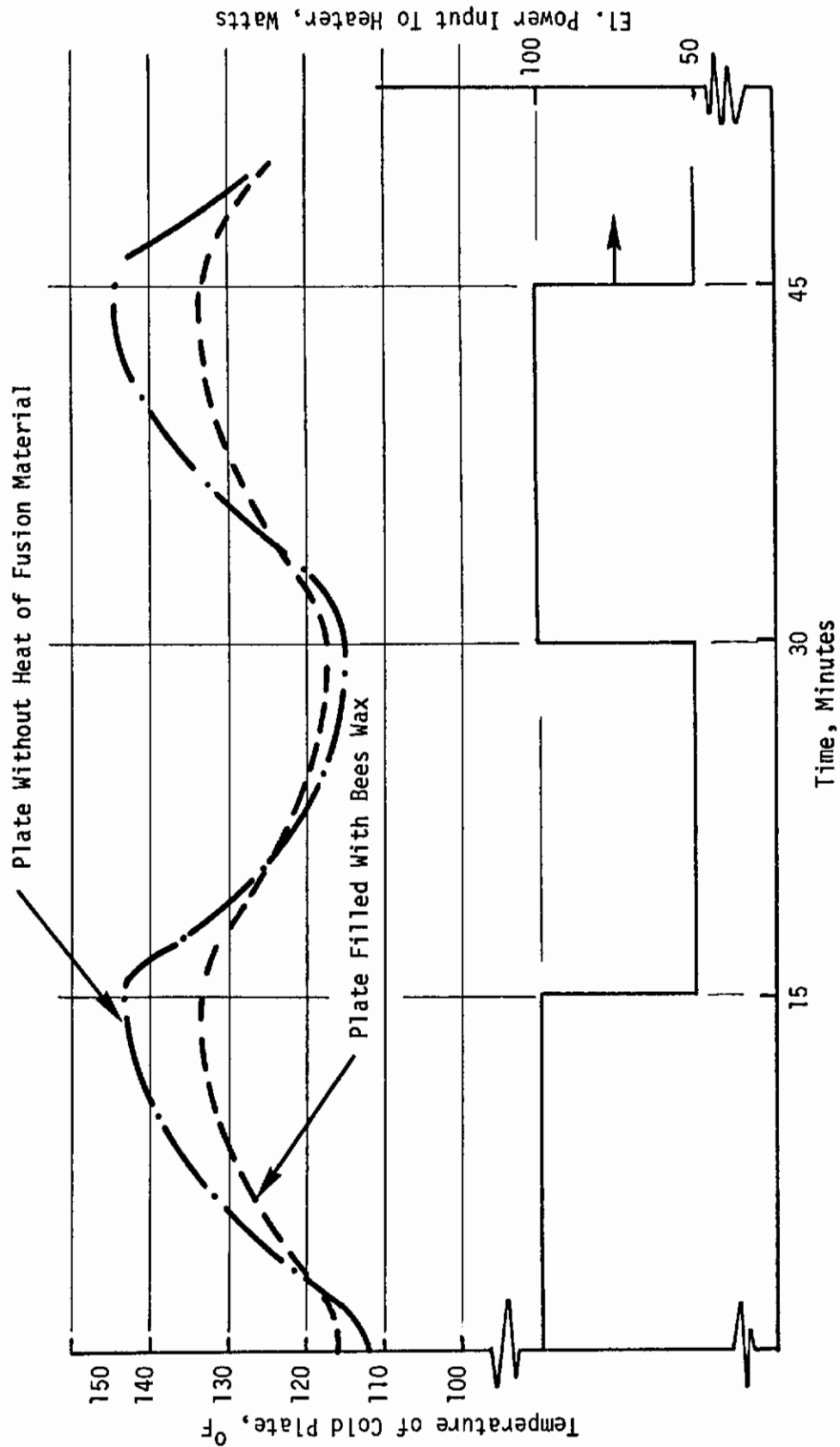


FIGURE 18. TEMPERATURE CHANGES VS TIME OF COLD PLATE NO. 1 UNDER PERIODIC HEAT LOAD CHANGES

and freezing point. The boiling temperature, however, is lowered with increasing altitude, and the freezing temperature can be lowered by adding methanol. When liquid distribution is not required, the freezing problem is not so severe if space for expansion is provided. Other fluids, Freons for example, can be used if the plate temperature must be maintained below the boiling temperature of water.

When coolant flow through the system is interrupted, the temperature of the equipment mounting plate will start to rise until it reaches the boiling temperature of the evaporant stored within the plate. Temperature rise of the plate at this point will stop until all the evaporant is evaporated. Heat capacity of the liquid filled cold plate can be determined from the following equation:

$$Q = W_l C_l (t_{op} - t_b) + W_{pl} C_{pl} (t_{op} - t_b) + W_l h_{fg} \quad (56)$$

W_l - Weight of evaporant, lbs

W_{pl} - Weight of the equipment mounting plate, lbs

C_l - Specific heat of the liquid, Btu/lb^oF

C_{pl} - Specific heat of the plate material, Btu/lb^oF

t_{op} - Operating temperature of the plate, ^oF

t_b - Boiling temperature of the evaporant, ^oF

Time, during which a certain amount of heat can be absorbed, can be expressed as follows:

$$\tau = \frac{Q}{Q_{gen}} \text{ hrs} \quad (57)$$

Q_{gen} - heat generated by the equipment, Btu/hr

Figure 19 shows the thermal performance of an experimental equipment mounting plate (cold plate no. 2) provided with an evaporative coolant. General design of the plate is the same as shown on Figure 16 except

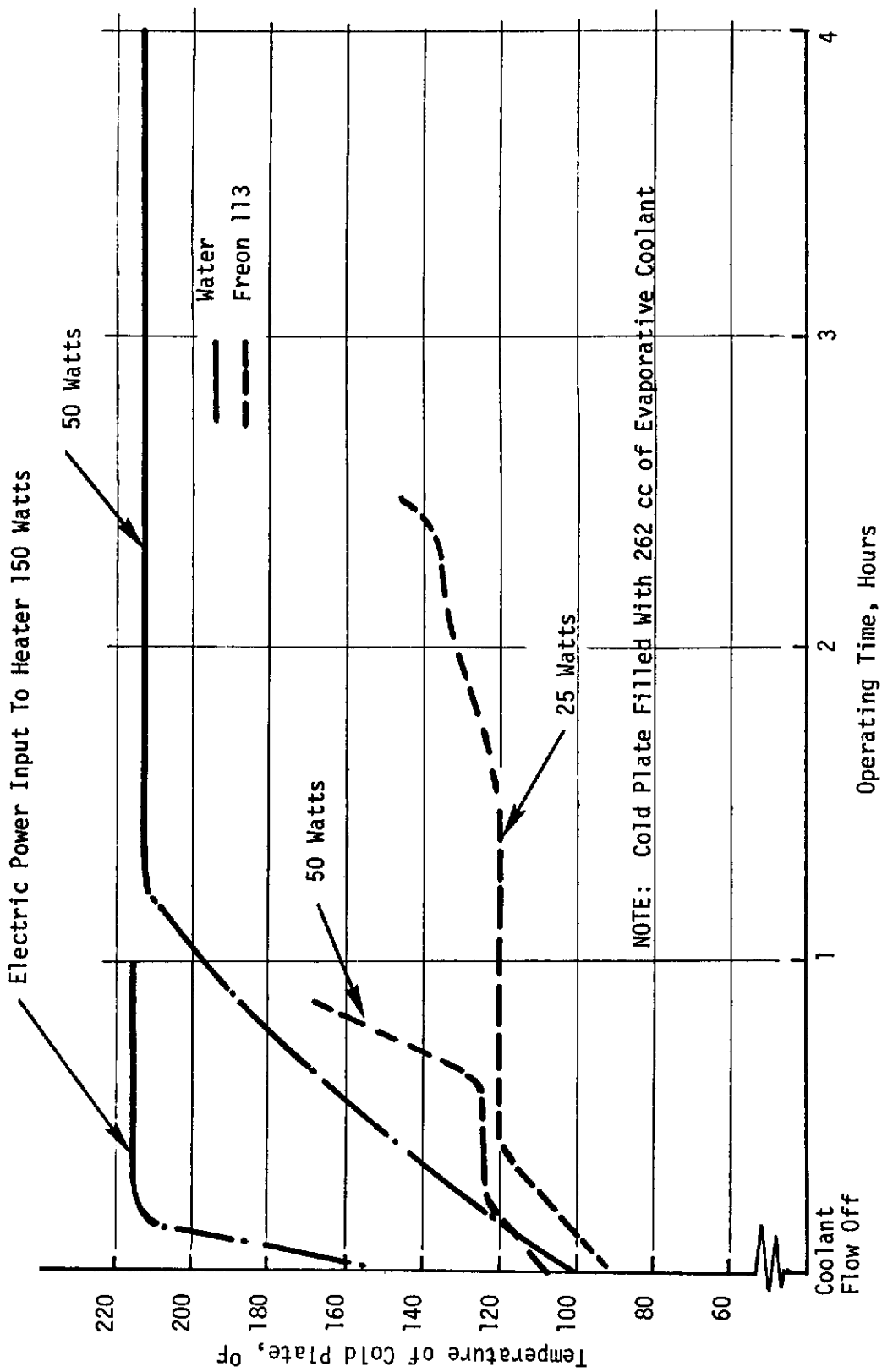


FIGURE 19. TEMPERATURE CHANGES VS TIME OF COLD PLATE NO. 2 AT DIFFERENT EL POWER INPUT RATES AND NO COOLANT FLOW

for the loose wick installed between the mounting surfaces. Experiments have been performed with two types of coolants, i.e., water and Freon 113, and simulated equipment heat loads ranging from 25 watts to 150 watts. As can be seen from the figure, water provides the best heat sink as far as time of operation is concerned. The 262 cubic centimeters of water provided an operational time of over 4 hours at a heat load of 50 watts after the coolant flow was stopped. The temperature of the plate, however, is quite high when operation occurs at sea level. Using Freon 113 as the heat sink, the plate temperature can be maintained at quite a low level, but the operational time, because of the low latent heat of evaporation, is short. The operating time can be increased by providing additional space for the evaporant.

Figure 20 shows comparison of cold plates' no. 1 and no. 2 thermal performance with the same electric power input of 50 watts, and conditions indicated on the figure. The figure is self explanatory and shows the advantage (in case of emergency) of providing the cold plate with some additional heat sink.

2. Electronic Equipment Cooling Plates With Integral Heat Pipes

Four experimental electronic equipment cooling plates (cold plates), provided with heat pipe passages for promoting temperature distribution and heat transfer, have been fabricated locally or purchased, and the thermal tests performed. In order to accommodate variations in heat load resulting from equipment duty cycles, one of the plates was provided with thermal control. Design of the cold plates, their thermal performance, and methods used for electronic equipment heat load simulation will be described in the following paragraphs.

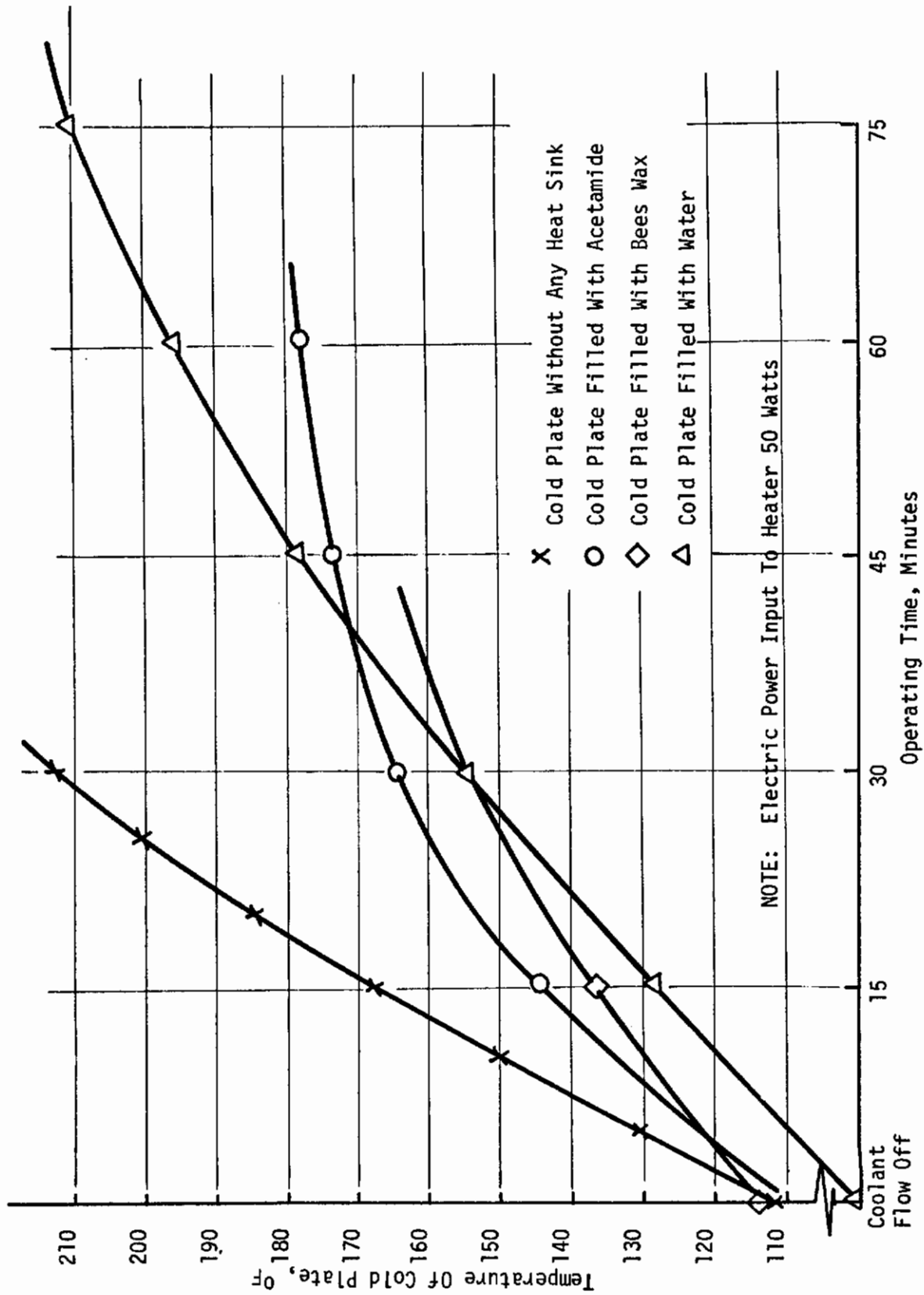


FIGURE 20. COMPARISON OF COLD PLATES' NO. 1 AND NO. 2 THERMAL PERFORMANCE

a. Cold Plate No. 3 Results

Figure 21 shows Cold Plate No. 3 which has been fabricated locally. It is a welded construction made of aluminum. For reliability reasons the heat pipe passages of the cold plate are divided into two separate sections each of which is cooled by circulating liquid. The heat pipe passages are provided with two layers of 100 mesh screen as a wicking material and charged with Freon 11. A total of six "dummy" components, four stud mounted and two flange mounted, were bolted to the 1/8 inch thick plates as shown on the figure. The "dummy" components were made of copper, and are similar in size and configuration to some electronic components selected from the Philips Semiconductor Handbook. A 150 watt blanket type heater was also attached to one of the plate's surfaces.

Figure 22 shows Section A-A of Cold Plate No. 3 with a simplified flux plot. Heat, generated by the "dummy" component, will be transferred from the component's mounting flange across the joint into the plate, and from there into the heat pipe passage. For simplicity reasons it is assumed that all of the heat flow takes place in a direction perpendicular to the axis of the two parallel heat pipe passages only. Actually the heat flow will be two-dimensional; however, because of the much longer heat flow path in the other direction, this resistance will be quite large and is, therefore, neglected.

Figure 23 shows the total resistance network from the component mounting flange to the heat pipe passages. Starting with the mounting joint, determination of all the thermal resistances will be outlined.

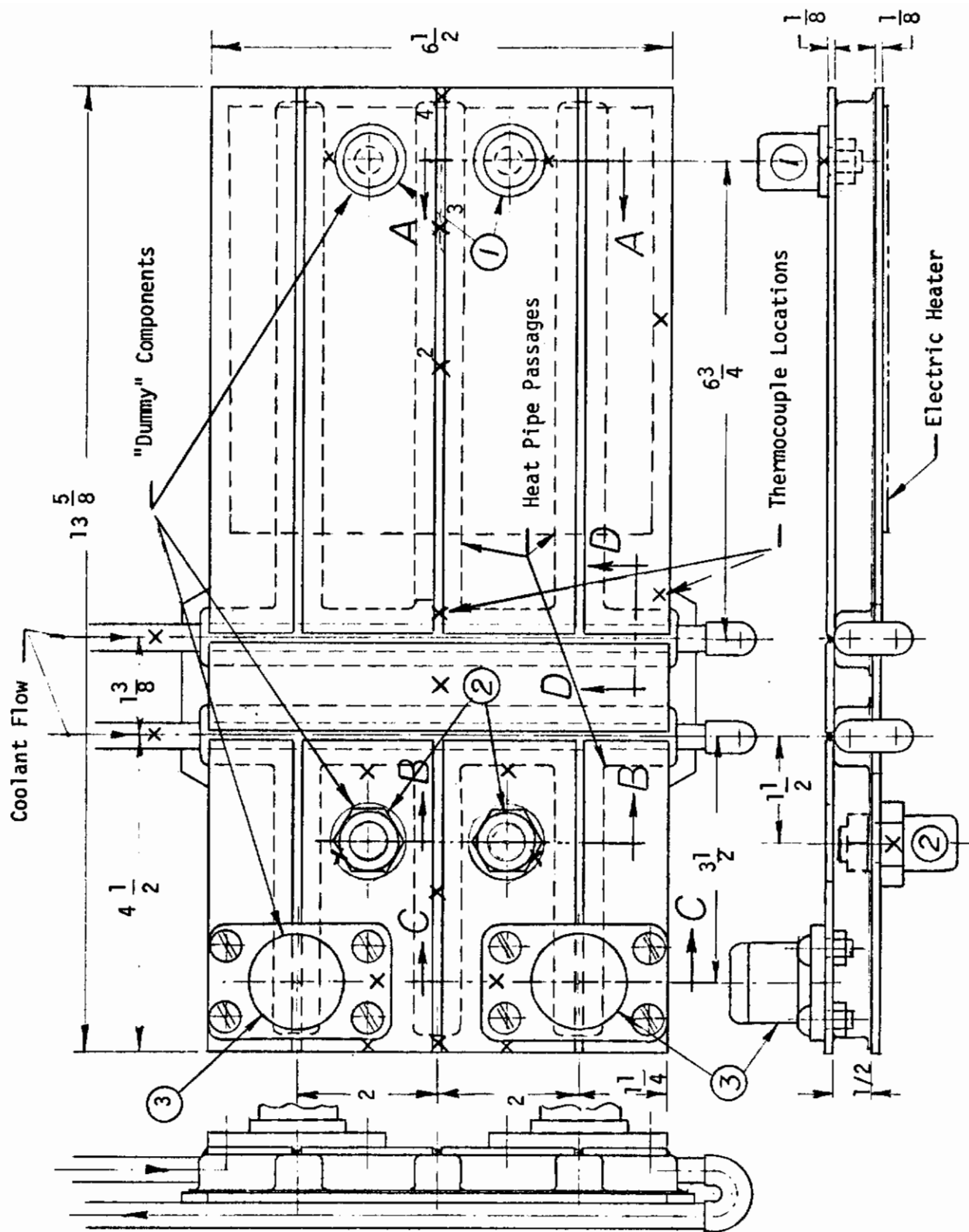


FIGURE 21. EXPERIMENTAL ELECTRONIC EQUIPMENT COLD PLATE NO. 3

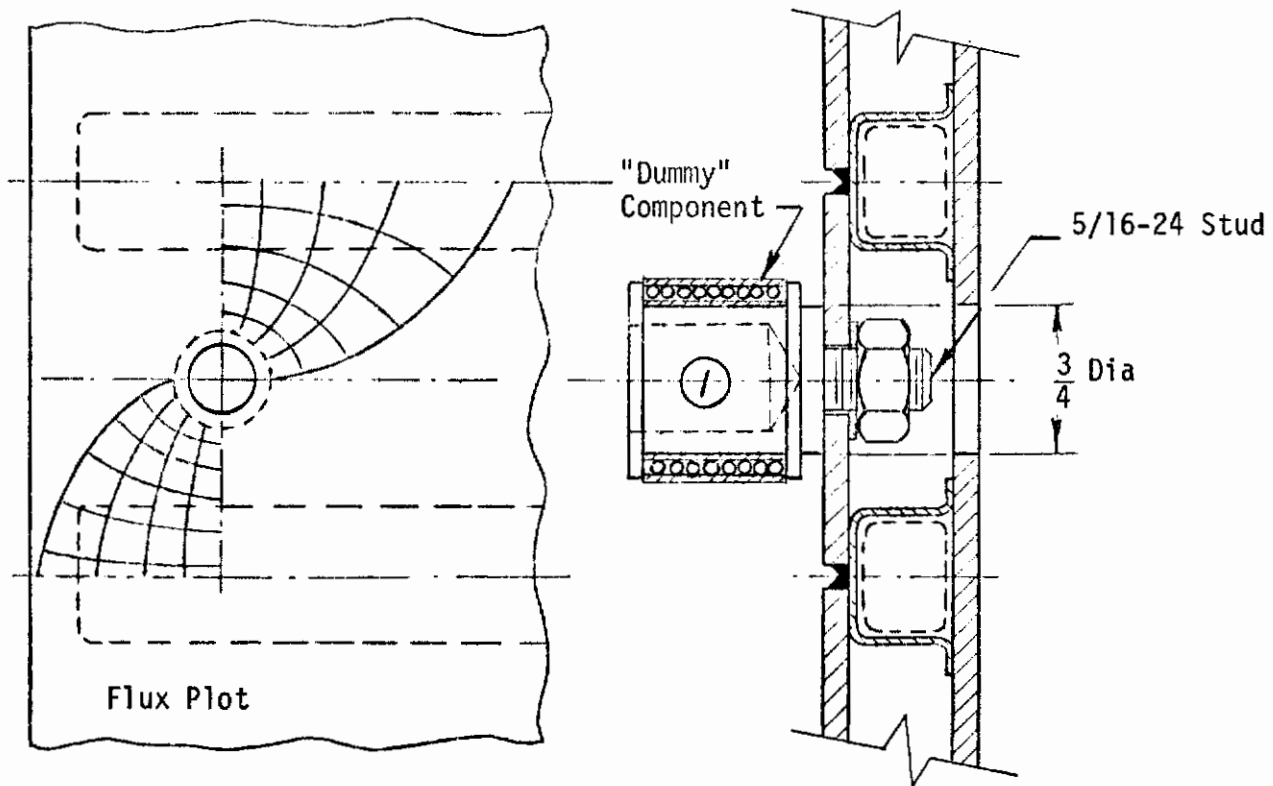


FIGURE 22. SECTION A-A OF COLD PLATE NO. 3

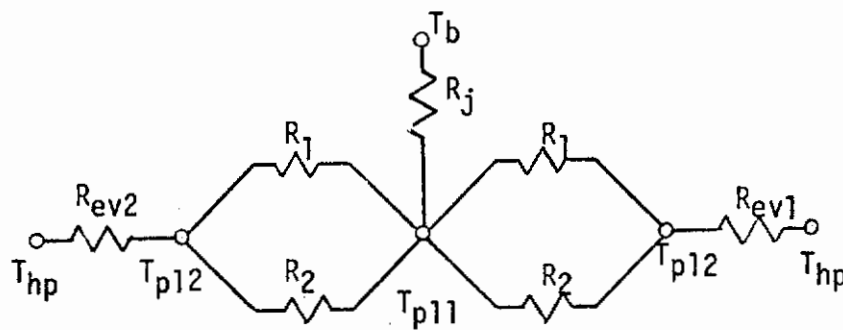


FIGURE 23. THERMAL RESISTANCE NETWORK

Figures 24 and 25 show sections and flux plots of Cold Plate No. 3.

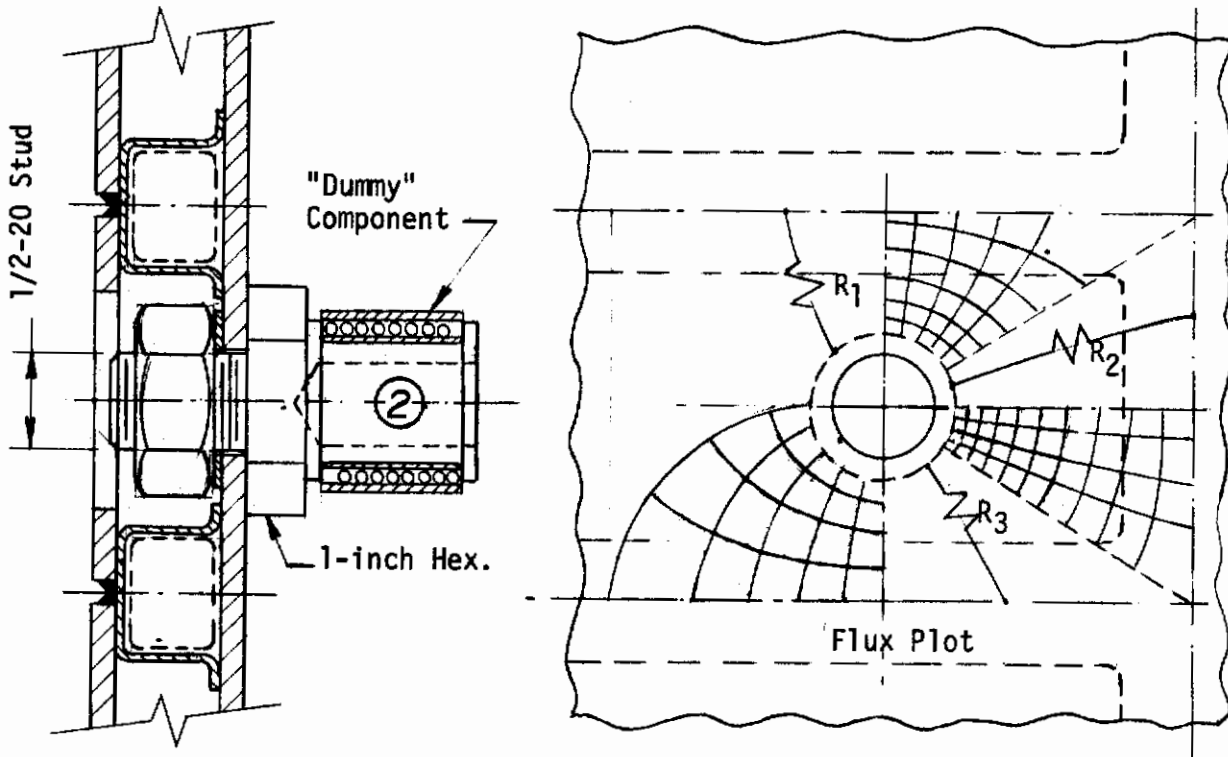


FIGURE 24. SECTION B-B OF COLD PLATE NO. 3

(1) Thermal Resistance of the Evaporator Section

The heat transfer rate from the plate into the evaporator section of the heat pipe passage can be expressed as follows:

$$Q = UA\Delta t \quad (58)$$

where U is the overall coefficient of heat transfer, Btu/hr ft² °F.

For flat or slightly curved walls the overall heat transfer coefficient can be determined from the following equation

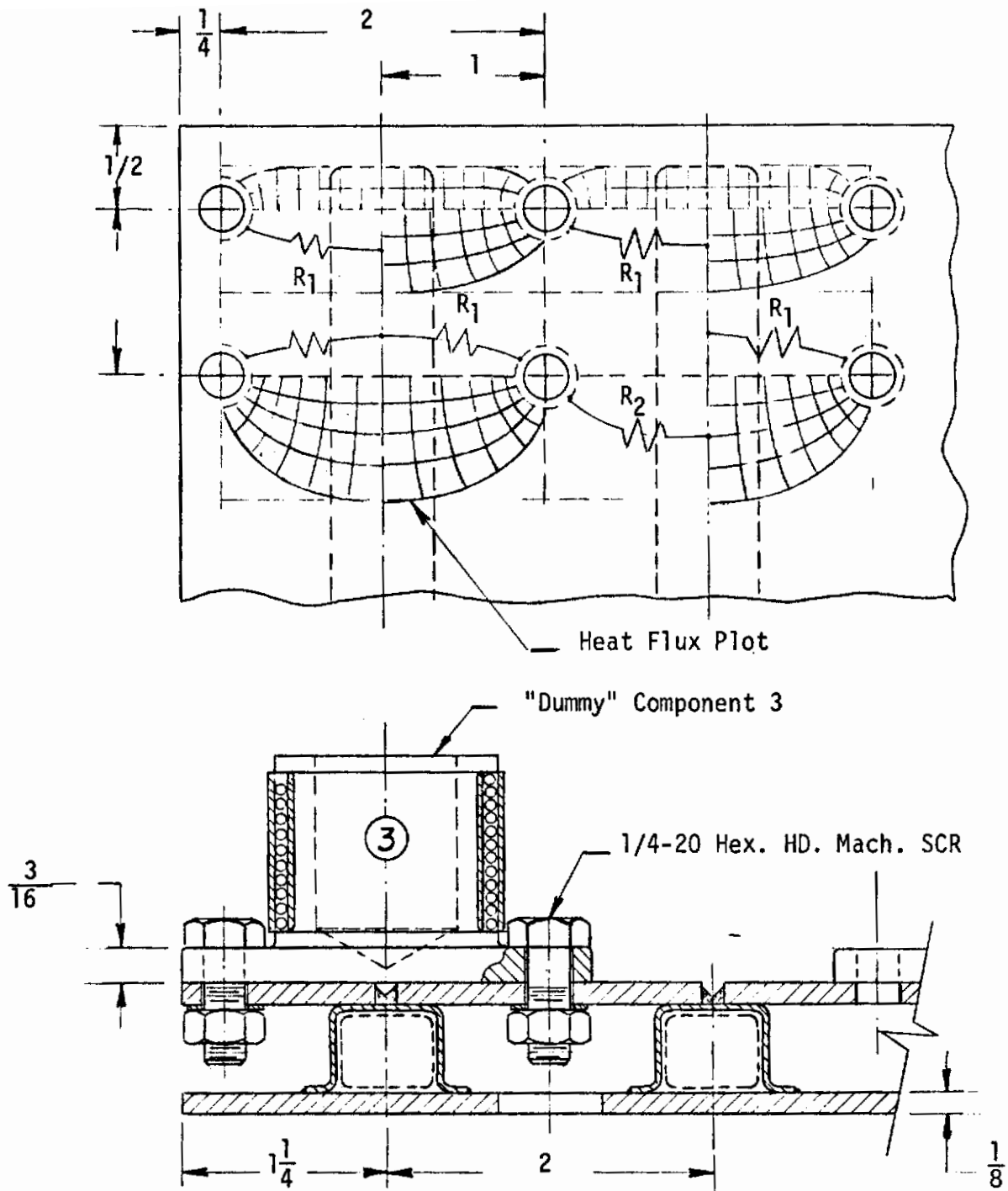


FIGURE 25. SECTION C-C OF COLD PLATE NO. 3

$$\frac{1}{U} = \frac{\ell}{k} + \frac{1}{h} \quad (59)$$

where

ℓ - thickness of the wall, ft

h - evaporative heat transfer coefficient, Btu/hr ft² °F

k - thermal conductivity of the wall, Btu/hr ft⁰F

For practical purposes, sufficiently accurate results of the overall heat transfer coefficient for thin walls and high thermal conductance passages can be obtained by assuming

$$U = h$$

and the thermal resistance of evaporator section can be expressed as:

$$R = \frac{1}{hA} \quad (60)$$

Determination of the evaporative heat transfer coefficient on wick covered surfaces is discussed in Section II of this report. Determination of the exact heat transfer area, because of the fin effect, is difficult, and, depending upon the analytical technique used, only some approximate values could be obtained.

(2) Thermal Resistance of the Condenser Section

Heat transfer through the condenser section of the heat pipe has been discussed in Section II of this report. Figure 26 shows arrangement of the condenser of cold plate no. 3. As can be seen, only the lower part of the condensing area is covered with wick, thus providing better heat transfer at the upper part of the condenser. Gravity force is here utilized for returning condensate to the wick covered surface. Neglecting thermal resistance of the coolant tube and heat pipe passage walls, the overall heat transfer coefficients for the two portions of the condenser can be determined as follows:

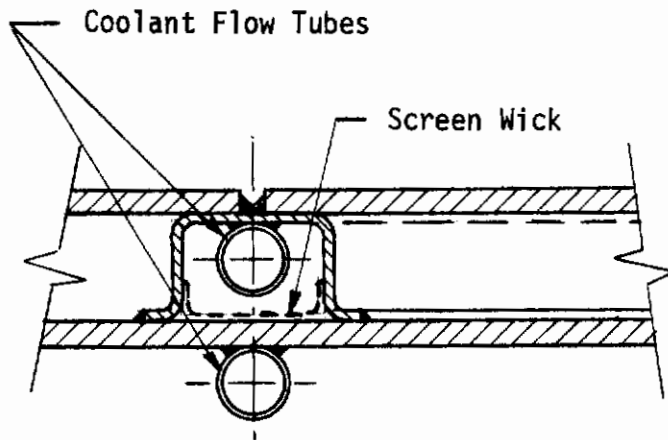


FIGURE 26. SECTION D-D OF COLD PLATE NO. 3

$$\frac{1}{U} = \frac{1}{h_c} + \frac{1}{h_{cv}} \quad (61)$$

$$\frac{1}{U} = \frac{1}{h_c} + \frac{X}{k_{wl}} + \frac{1}{h_{cv}} \quad (62)$$

k_{wl} (thermal conductance of liquid saturated wick) can be determined from equation (28)

X is thickness of the wick

h_{cv} is convection coefficient of coolant, Btu/hr ft² °F

The convection coefficient, depending on flow regime, can be determined from equations found in numerous heat transfer handbooks.

Figure 27 shows temperature distributions for Cold Plate No. 3 as measured at the central heat pipe passage. The tests were performed at three different levels of electric power inputs to the electronic component heat flux simulators (two "dummy" components and a blanket type electric heater). A condition was also investigated when there was no working fluid in the heat pipe passages. It can be seen from the figure that temperature gradients within the cold plate can be significantly reduced by application of heat pipes. The largest temperature

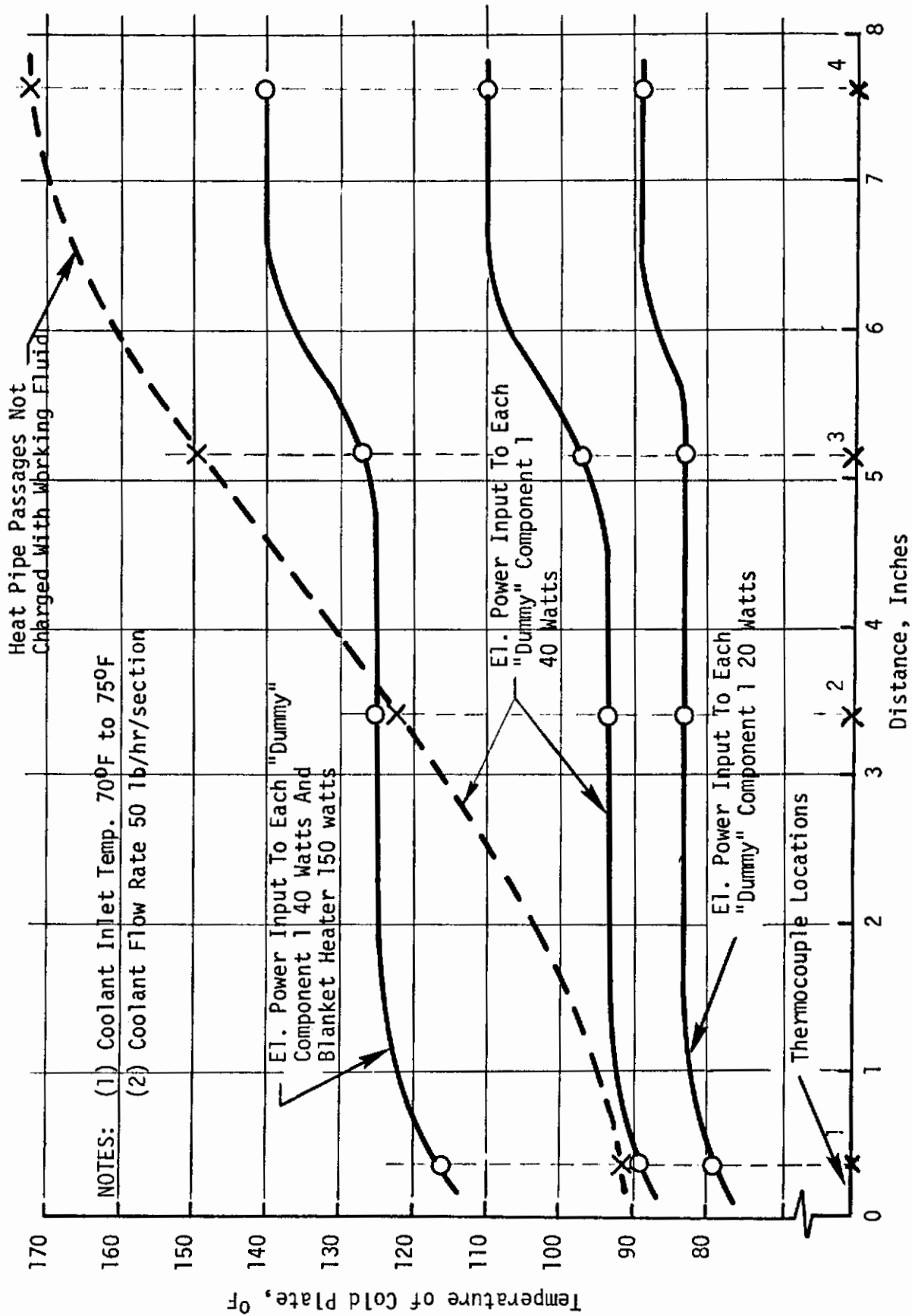


FIGURE 27. TEMPERATURE DISTRIBUTION OF COLD PLATE NO. 3 (LONG SECTION)

distortion within the plate occurred at the evaporator section, where the concentrated heat load from the "dummy" components were applied. Based on the total heat transfer rate of 230 watts (approx. 780 Btu/hr) and coolant inlet temperature of 75°F, a temperature drop of 50°F occurred at the condenser section with the largest portion accounted to convection heat transfer.

Figure 28 shows temperature distributions from the "dummy" component's mounting base to the circulating coolant at the different electric power input rates indicated on the chart. The figure clearly shows that the largest temperature drops occur within the component mounting surfaces, and at the plate's condenser section - transferring heat into the circulating coolant.

Figure 29 shows comparison between analytically and experimentally determined temperature distribution from the mounting base of "dummy" component 1 to the circulating coolant. As can be seen, quite a close agreement between the predicted and actually measured temperatures was obtained. The largest difference of only 7°F occurred at the highest heat input rate. A certain inconsistency between the analytical results, however, must be pointed out. While at the higher heat input rates the predicted component mounting base temperature was higher than measured, at the lower heat input rates it was lower. Because of the limited data available about evaporative heat transfer coefficients from wick covered surfaces, these coefficients were determined from temperature and heat transfer rate measurements.

Figure 30 shows temperature distributions for Cold Plate No. 3 (short section) when both "dummy" components "2" were energized. Figure 31

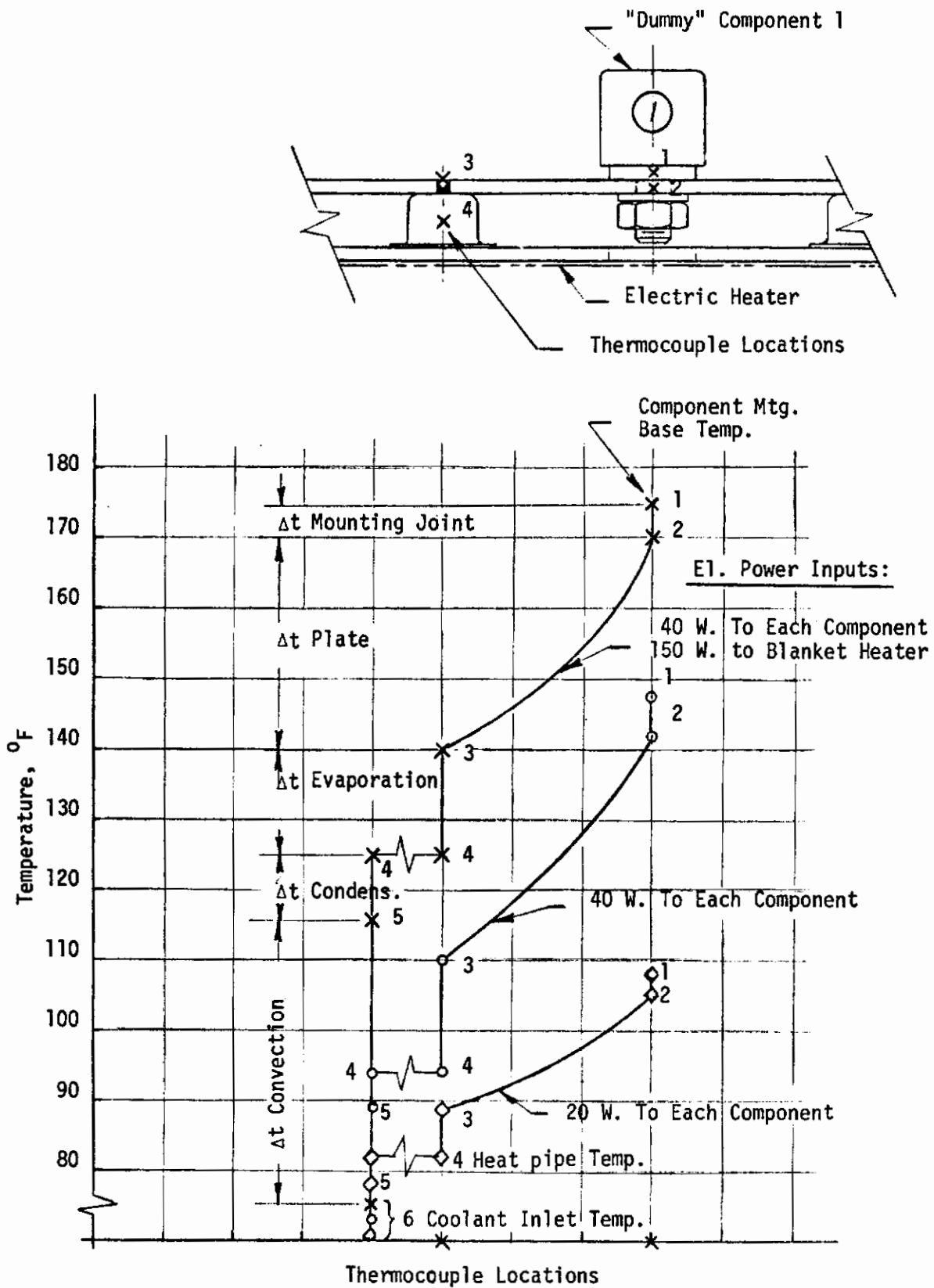


FIGURE 28. TEMPERATURE DISTRIBUTION FROM COMPONENT 1 MOUNTING BASE TO COOLANT

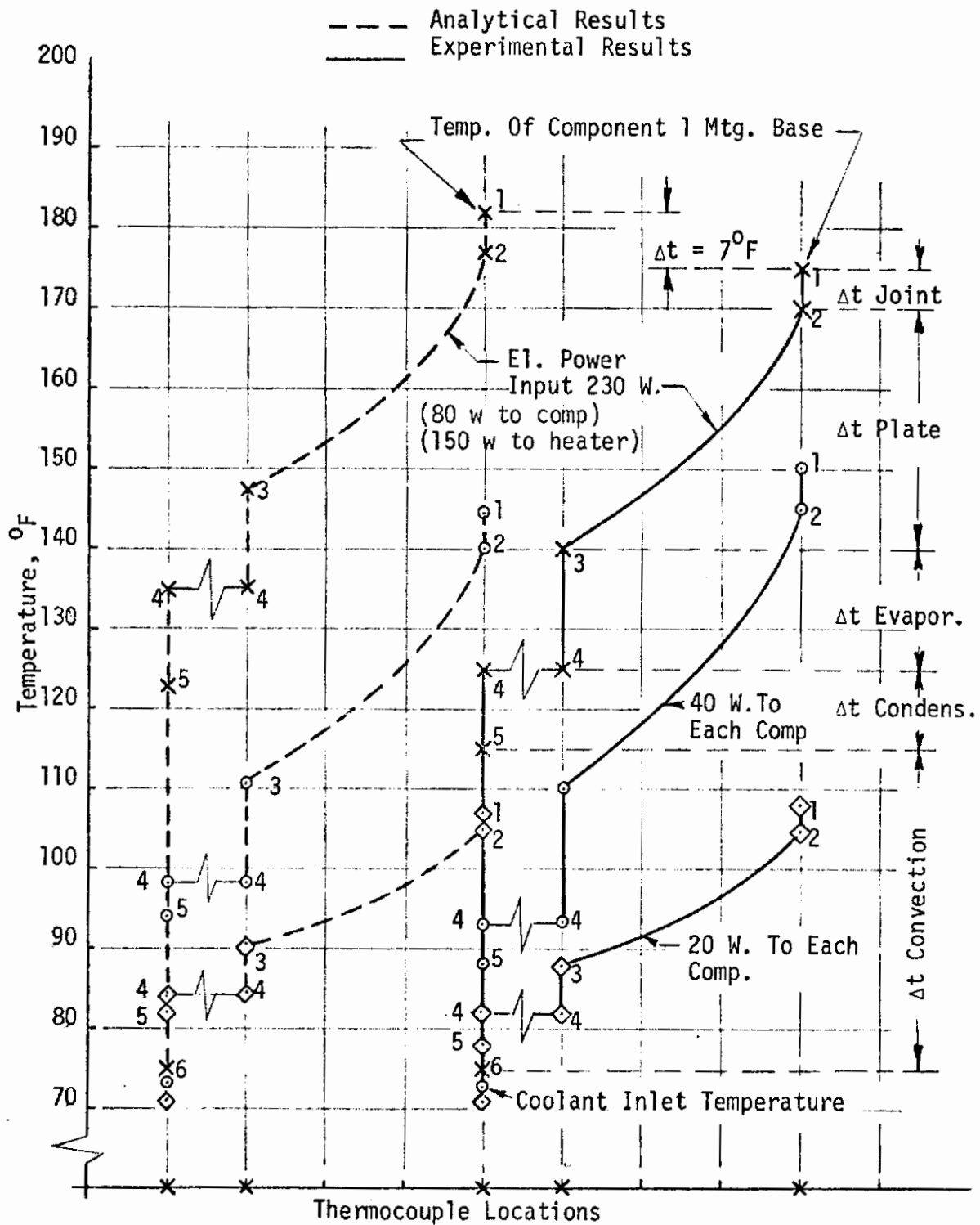


FIGURE 29. COMPARISON OF TEMPERATURE DISTRIBUTION BETWEEN ANALYTICAL AND EXPERIMENTAL RESULTS

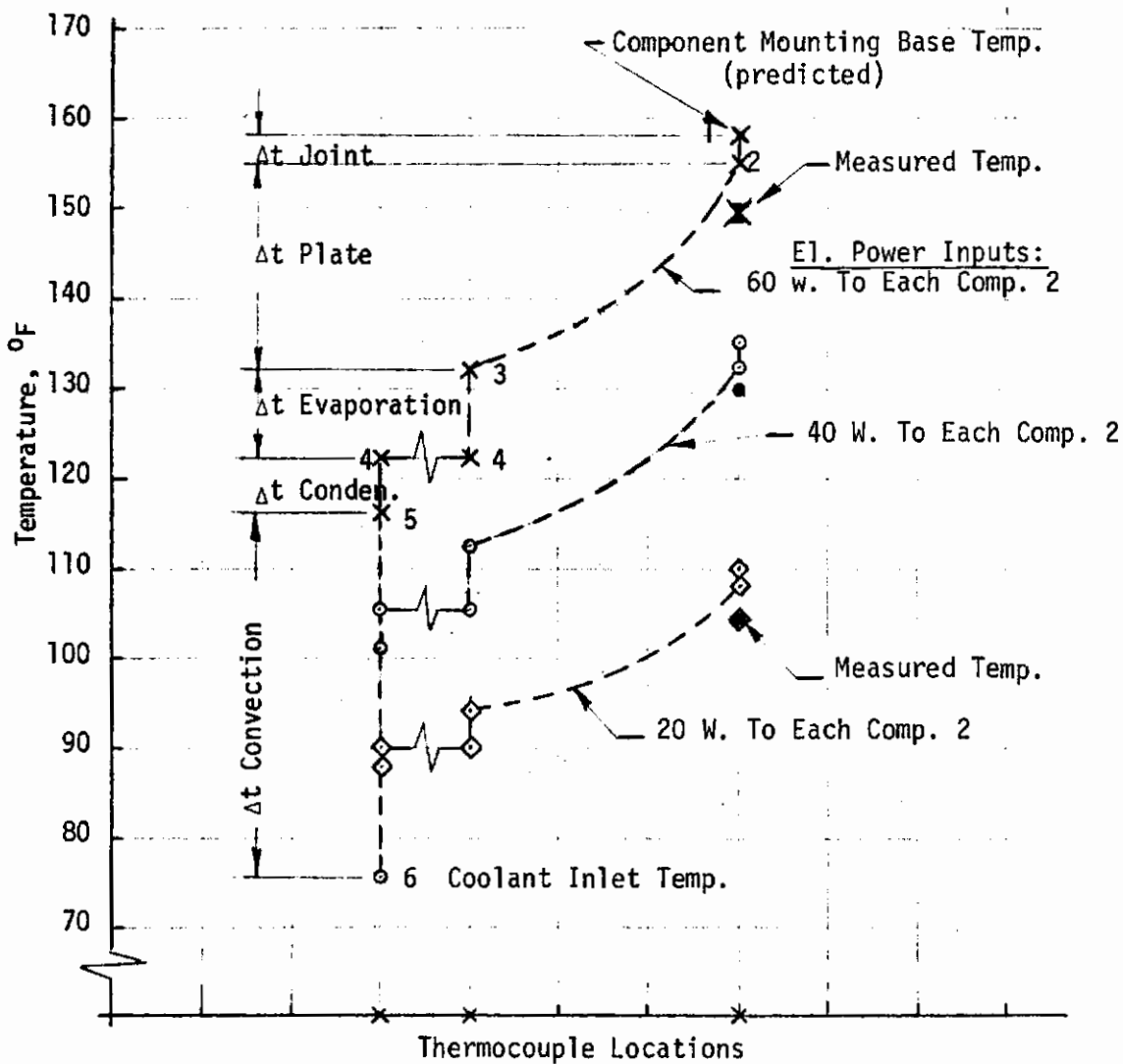
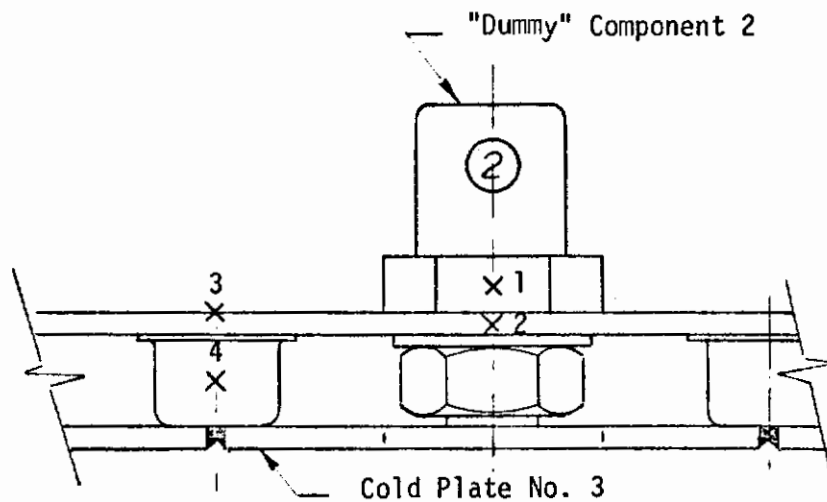


FIGURE 30. TEMPERATURE DISTRIBUTION FROM COMPONENT 2 MOUNTING BASE TO COOLANT

Contrails

- × El. Power Input to Each Component 3 75 watts
- + El. Power Input to Each Component 3 60 watts
- El. Power Input to Each Component 3 40 watts
- ◇ El. Power Input to Each Component 3 20 watts

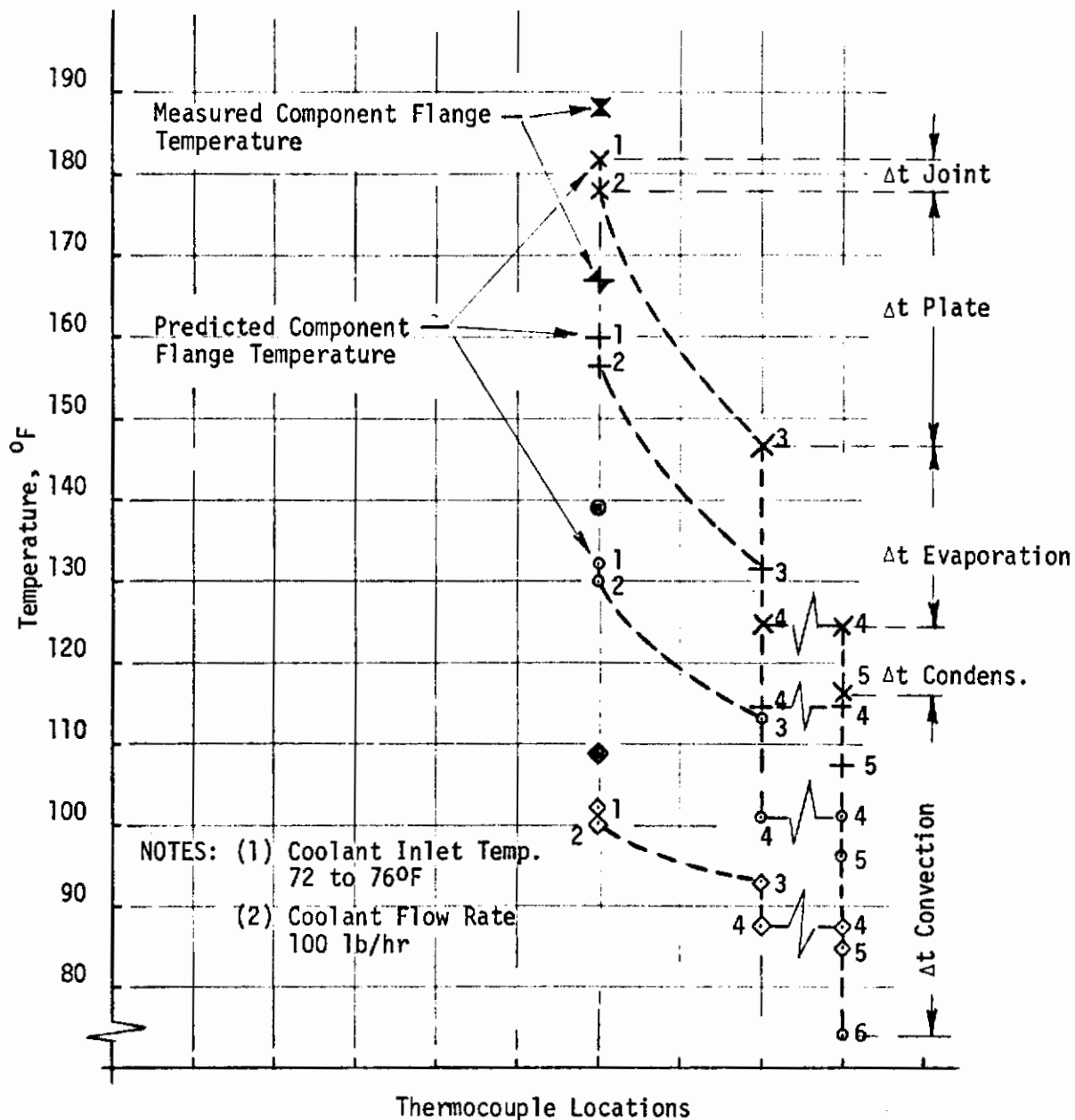


FIGURE 31. TEMPERATURE DISTRIBUTION FROM COMPONENT 3 MOUNTING FLANGE TO COOLANT

shows conditions where both "dummy" components "3" were energized, and Figure 32 when all of the "dummy" components were energized. Because of limitations imposed by availability of temperature recorders, it was not possible to obtain complete actual temperature readings throughout the cold plate. Only the components' mounting base or flange actual temperatures, therefore, are shown and the overall distributions represent analytically determined values. A certain inconsistency between the analytical and experimental results can also be observed here. Under a total power input rate of 270 watts (all four components energized), the actual component "2" mounting base temperature was 14⁰F lower than predicted, while component "3" actual mounting flange temperature was 12⁰F higher than predicted.

The inconsistency could be caused by differences in the mounting joint thermal resistances and variations in the welded joints connecting the mounting plates to the heat pipe passages. Particularly large differences in the mounting joint thermal resistance could occur at the flange mounted components because the surface of the plate was not machined.

b. Sample Calculation

A sample calculation for determining heat transfer and temperature distributions from "dummy" component 1, attached to Cold Plate No. 3 as shown on Figure 21, will be performed. Thermal resistances, starting from the component's mounting base to the circulating coolant, will be determined analytically, and temperature differentials found from the resistances and heat flow rates. Comparison between the analytical and experimental results, based on the same power dissipation rates and coolant inlet temperature, is shown on Figure 29.

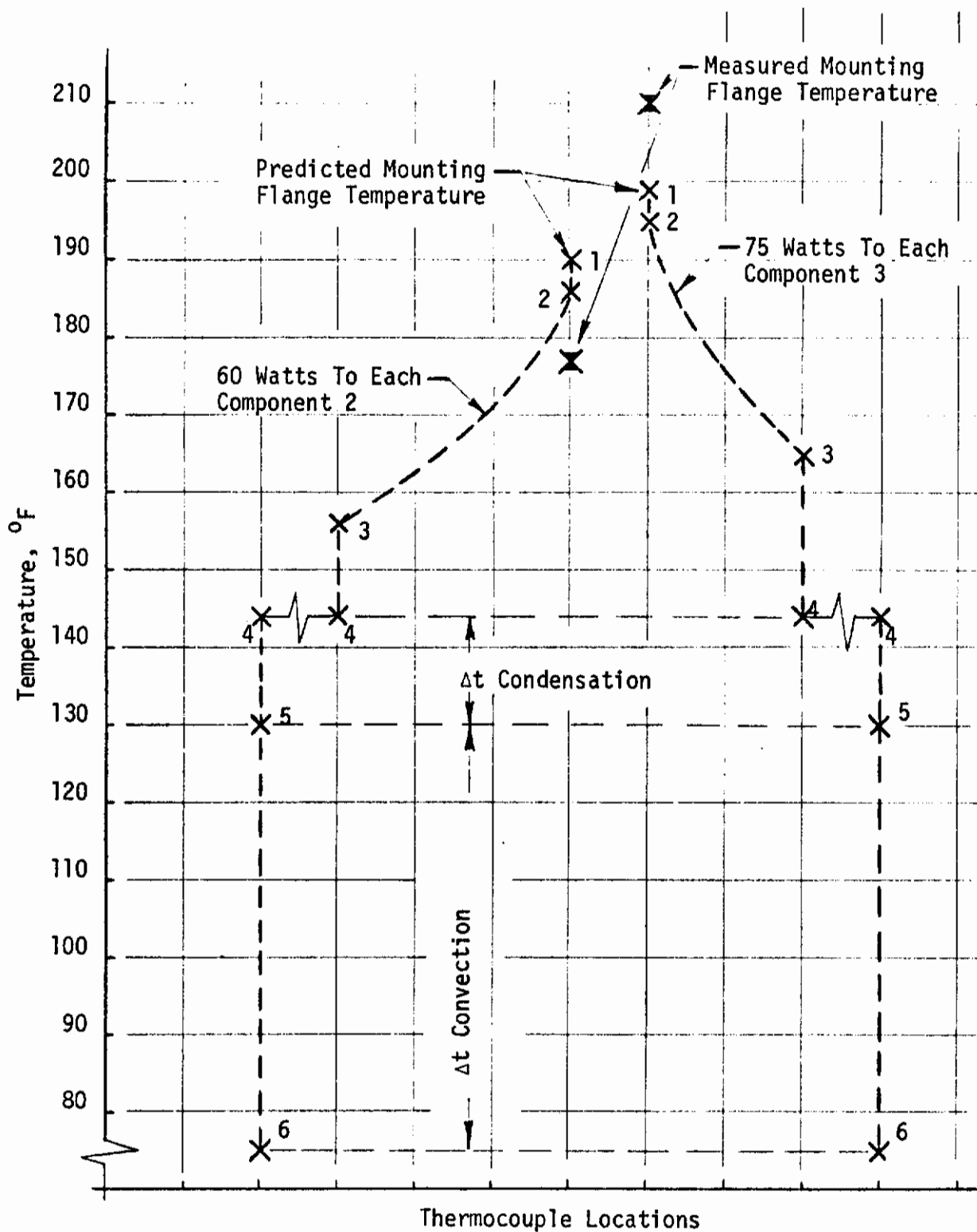


FIGURE 32. TEMPERATURE DISTRIBUTION OF COLD PLATE NO. 3 (SHORT SIDE) - ALL COMPONENTS ENERGIZED

(1) Thermal Resistance of Mounting Joint

Based on a stud torque of $T = 35$ in-lb, aluminum plate thermal conductance $k = 100$ Btu/hr ft $^{\circ}$ F and component copper mounting base thermal conductance $k = 180$ Btu/hr ft $^{\circ}$ F, the joint thermal conductance of the direct contact area was determined to be

$$k_j = 12,800 \text{ Btu/hr ft}^2 \text{ } ^{\circ}\text{F}$$

or, for the direct contact area of $A_c = 0.0023$ ft 2 .

$$K_j = 12,800 (.0023) = 29.4 \text{ Btu/hr } ^{\circ}\text{F}$$

and the mounting joint thermal resistance

$$R_j = \frac{1}{K_j} = \frac{1}{29.4} = 0.034 \text{ hr } ^{\circ}\text{F/Btu}$$

(2) Thermal Resistance of Plate

From Equations 51a and 51b the thermal conductance is expressed as

$$K = b S k$$

and the thermal resistance, therefore, is

$$R_1 = \frac{1}{b S_1 k}, \quad R_2 = \frac{1}{b S_2 k}$$

where

$$S_1 = \frac{N_1}{M_1} \quad \text{and} \quad S_2 = \frac{N_2}{M_2}$$

$$b = 0.125/12 = 0.0104 \text{ ft}$$

$$k = 100 \text{ Btu/hr ft } ^{\circ}\text{F}$$

From Figure 22, $S_1 = 0.80$, $S_2 = 1.0$

$$R_1 = \frac{1}{(.0104) (.8)(100)} = 1.2 \text{ hr } ^{\circ}\text{F/Btu}$$

$$R_2 = \frac{1}{(.0104) (1)(100)} = 0.96 \text{ hr } ^{\circ}\text{F/Btu}$$

Thermal resistance of the plate can be expressed as

$$\frac{1}{R_{pl}} = \frac{1}{R_1} + \frac{1}{R_2}$$

$$\frac{1}{R_{pl}} = \frac{1}{1.2} + \frac{1}{0.96} = 0.83 + 1.04 = 1.87$$

$$R_{pl} = \frac{1}{1.87} = 0.535 \text{ hr } ^\circ\text{F}/\text{Btu}$$

(3) Thermal Resistance of Evaporator Section

Because there are practically no analytical techniques for determining evaporative heat transfer coefficients from wick covered surfaces, an approximate value of 375 Btu/hr ft² °F was estimated for this particular evaporator arrangement. The heat pipe passage side wall effectiveness was estimated to be 50 percent, and the evaporative heat transfer area was estimated to be approximately 0.0232 ft². The thermal resistance was determined to be

$$R_w = \frac{1}{hA} = \frac{1}{375(.0232)} = 0.115 \text{ hr } ^\circ\text{F}/\text{Btu}$$

(4) Thermal Resistance of Condenser Section

Because only a small portion of the condenser section is covered with wick, the following simplified equation was used for determining the thermal resistance:

$$R_c = \frac{1}{h_c A_c}$$

Applying Equation 26 the condensation heat transfer coefficient was determined to be $h_c = 440 \text{ Btu/hr ft}^2 \text{ } ^\circ\text{F}$. The condensing surface area was determined by adding the external surface area of the tube and upper and lower portions of the condenser channel. This area was determined to be 0.125 ft².

$$R_C = \frac{1}{440(.125)} = 0.0182 \text{ hr } ^\circ\text{F}/\text{Btu}$$

(5) Thermal Resistance of Forced Convection

Neglecting resistance of tube wall, the convection thermal resistance can be expressed by the following simplified equation:

$$R_{CV} = \frac{1}{h_{CV}A}$$

The convection coefficient h_{CV} has been determined by the equation recommended by McAdams

$$\begin{aligned} h_{CV} &= 6.2 \frac{k}{D} \left(\frac{\dot{w}_C}{kL} \right)^{0.2} = 6.2 \frac{0.223}{0.0254} \left(\frac{60(.75)}{.223(1.1)} \right)^{0.2} \\ &= 150 \text{ Btu/hr ft}^2 \text{ } ^\circ\text{F} \end{aligned}$$

Convection coefficients determined by the above equation correlate quite well for ethylene-glycol-water coolants at the lower temperature ranges and streamline flow. At higher temperature ranges (somewhat over 100°F) temperature correction factors must be introduced.

While the whole surface area of one section of the tube (located within the condenser channel) can be considered as transferring heat, only a portion of the other section is effective. The convection heat transfer area was determined to be approximately $10.5 \text{ in}^2 = 0.073 \text{ ft}^2$.

$$R_{CV} = \frac{1}{150(.073)} = 0.091 \text{ hr } ^\circ\text{F}/\text{Btu}$$

At a condenser surface temperature of approximately 120°F , a temperature correction factor of 1.25 was introduced, and the convection thermal resistance, therefore, becomes

$$R_{CV} = \frac{1}{150(1.25)(.073)} = 0.073 \text{ hr } ^\circ\text{F}/\text{Btu}$$

Contrails

After the thermal resistances have been determined, temperature differentials across each of the resistances can be determined from the following equation:

$$Q = \frac{\Delta t}{R}$$

or $\Delta t = QR$

To calculate the Δt values, the heat flow rates in each of the resistance network branches must also be known. Two different levels of electric power input were applied to each of the dummy components.

$$Q_1 = 20 \text{ watts} = 20(3.4) = 68 \text{ Btu/hr}$$

$$Q_2 = 40 \text{ watts} = 40(3.4) = 136 \text{ Btu/hr}$$

Figure 33 shows resistance network of the evaporator section where "dummy" components are attached.

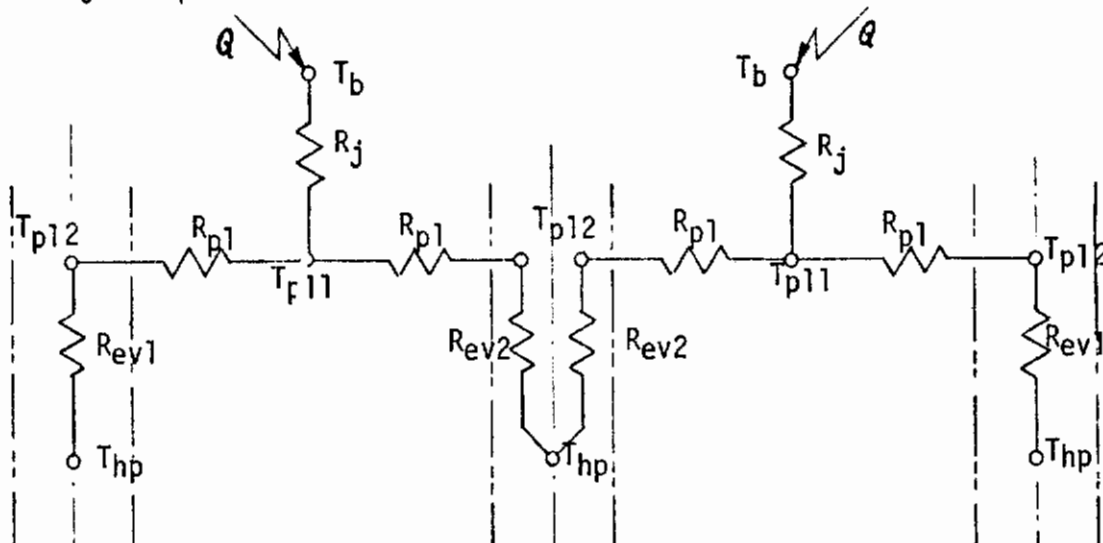


FIGURE 33. RESISTANCE NETWORK OF THE EVAPORATOR SECTION

It has been estimated that approximately 15 percent of the total heat input was dissipated to the ambient air. The 15 percent heat loss was further divided in 5 percent from the component itself, and 10 percent from the plate. Thus, 95 percent of the total component heat load was transferred across the joint, and 85 percent by the heat pipe.

A certain amount of heat from the evaporator to the condenser section is also transferred by the plate. This amount, however, because of the large distance is small, and no attempt, therefore, was made to estimate its value.

(6) Determination of Temperature Distribution

Temperature Drop Across Joint

$$\Delta t_j = Q R_j$$

$$\Delta t_{j1} = Q_1 R_j = 64(.034) = 2.2^\circ\text{F}$$

$$\Delta t_{j2} = Q_2 R_j = 130(.034) = 4.4^\circ\text{F}$$

Temperature Drop Within Mounting Plates

$$\Delta t_{p1} = Q R_{p1}$$

Under symmetrical heat load conditions (equal electric power inputs to both components) the heat flow will be equal in each of the two sections which can be simplified as shown in Figure 34.

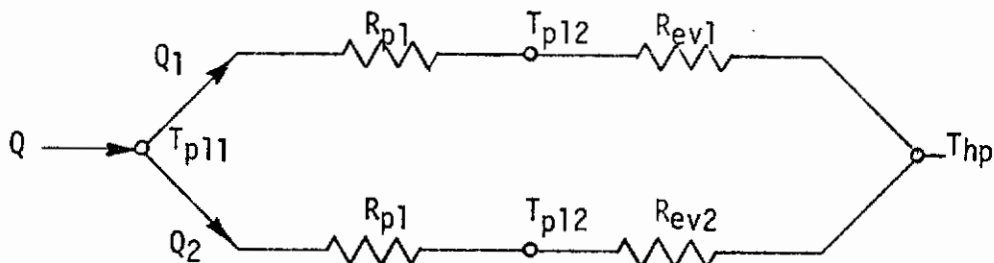


FIGURE 34. RESISTANCE NETWORK OF SYMMETRICAL SECTION

Similarly as division of current flow in parallel branches, the total heat flow in a parallel circuit divides between the branches. Heat flow in each branch is proportional to the conductance in that branch, or inversely proportional to the resistance of that branch. Referring

to Figure 34 containing two parallel resistances R_1 and R_2 , the heat flow in R_1 may be expressed as

$$Q_1 = Q_{in} \times \frac{R_2}{R_1 + R_2}$$

and the heat flow in R_2

$$Q_2 = Q_{in} \times \frac{R_1}{R_1 + R_2}$$

where

$$R_1 = R_{p1} + R_{ev1}$$

$$R_2 = R_{p1} + R_{ev2}$$

The evaporator thermal resistances of each branch will be different, because the central heat pipe has to absorb a portion of the heat generated by each of the components. It is assumed that (because of symmetrical and equal heat load conditions) only half of the total heat transfer area for each of the central heat transfer branches can be utilized.

From previous calculations

$$R_{ev1} = \frac{1}{hA_1} = \frac{1}{375(.0232)} = 0.115 \text{ hr } ^\circ\text{F/Btu}$$

$$R_{ev2} = \frac{1}{hA_2} = \frac{1}{375(.0116)} = 0.23 \text{ hr } ^\circ\text{F/Btu}$$

Substituting values

$$R_1 = 0.535 + 0.115 = 0.650 \text{ hr } ^\circ\text{F/Btu}$$

$$R_2 = 0.535 + 0.230 = 0.765 \text{ hr } ^\circ\text{F/Btu}$$

For the lower heat dissipation rates

$$Q_1 = 58 \frac{.765}{.65 + .765} = 58(.54) = 31.3 \text{ Btu/hr}$$

$$Q_2 = 58 \frac{.65}{.65 + .765} = 58(.46) = 26.7 \text{ Btu/hr}$$

For the higher heat dissipation rate

$$Q_1 = 116 \frac{.765}{.65 + .765} = 116(.54) = 62.6 \text{ Btu/hr}$$

$$Q_2 = 116 \frac{.65}{.65 + .765} = 116(.46) = 53.4 \text{ Btu/hr}$$

As can be expected, the heat load is not evenly distributed among the three heat pipe channels, the central heat pipe receives the highest heat load, although heat flow through the plate is smaller in the central direction. This means that the temperature drop within the plate will not be the same in both directions. A smaller temperature drop will occur in the central direction; however, because of the larger total heat load to the central heat pipe channel, a larger temperature drop will occur in the evaporator section.

$$\Delta t_{p1} = Q R_{p1}$$

$$\Delta t_{p1_1} = 31.3(.535) = 16.7^{\circ}\text{F}$$

$$\Delta t_{p1_2} = 62.6(.535) = 33.5^{\circ}\text{F}$$

$$\Delta t_{p2_1} = 26.7(.535) = 14.3^{\circ}\text{F}$$

$$\Delta t_{p2_2} = 53.4(.535) = 28.6^{\circ}\text{F}$$

Temperature Drop Across Evaporator Section

Assuming same evaporator surface areas, the temperature drop across the heat pipe evaporator section can be determined for both the central and outer heat pipes.

$$\Delta t_{ev1} = 31.3(.115) = 3.6^{\circ}\text{F}$$

$$\Delta t_{ev1} = 62.6(.115) = 7.2^{\circ}\text{F}$$

$$\Delta t_{ev2} = 26.7(2)(.115) = 6.1^{\circ}\text{F}$$

$$\Delta t_{ev2} = 53.4(2)(.115) = 12.3^{\circ}\text{F}$$

Temperature Drop Across Condenser Section

$$\Delta t_c = Q R_c$$

where Q represents all the heat generated by the components

$$Q_1 = 2(58) = 116 \text{ Btu/hr}$$

$$Q_2 = 2(116) = 232 \text{ Btu/hr}$$

and with blanket heater also on

$$Q_3 = 232 + 434 = 666 \text{ Btu/hr}$$

$$\Delta t_{c1} = 116(.0182) = 2.1^{\circ}\text{F}$$

$$\Delta t_{c2} = 232(.0182) = 4.2^{\circ}\text{F}$$

$$\Delta t_{c3} = 666(.0182) = 12.1^{\circ}\text{F}$$

Convection Temperature Drop

$$\Delta t_{cv} = Q R_{cv}$$

$$\Delta t_{cv1} = 116(.091) = 10.6^{\circ}\text{F}$$

$$\Delta t_{cv2} = 232(.091) = 21.2^{\circ}\text{F}$$

$$\Delta t_{cv3} = 666(.073) = 48.6^{\circ}\text{F}$$

Based on the coolant inlet temperatures of 71, 73 and 75^oF for the total heat input rates of 136 Btu/hr, 272 Btu/hr and 780 Btu/hr respectively, the following "dummy" component mounting flange temperatures were predicted:

$$t_{f1} = t_{in} + \Delta t_{cv} + \Delta t_c + \Delta t_{ev} + \Delta t_{p1} + \Delta t_j$$

Substituting values

$$t_{f1_1} = 71 + 10.6 + 2.1 + 6.1 + 14.3 + 2.2 = 106.3^{\circ}\text{F}$$

$$t_{f1_2} = 73 + 21.2 + 4.2 + 12.3 + 28.6 + 4.4 = 143.7^{\circ}\text{F}$$

$$t_{f1_3} = 75 + 48.6 + 12.1 + 12.3 + 28.6 + 4.4 = 181^{\circ}\text{F}$$

Data provided by the manufacturer for an actual silicon rectifier diode indicates maximum junction temperature $t_j (\text{max}) = 150^{\circ}\text{C} = 302^{\circ}\text{F}$,

and thermal resistance from junction to base $R_{j-b} = 1.1^{\circ}\text{C/watt}$ or $1.98^{\circ}\text{F/watt}$. The expected junction temperature for an actual device at the different power dissipation rates would be:

$$t_{j1} = t_{b1} + 1.98 (\text{watts}) = 106.1 + 1.98(20) = 145.7^{\circ}\text{F}$$

$$t_{j2} = 143.7 + 1.98(40) = 222.8^{\circ}\text{F}$$

$$t_{j3} = 181 + 1.98(40) = 260^{\circ}\text{F}$$

As can be seen, under all heat load conditions the diode junction temperature is within safe operating limits. Furthermore, the manufacturers data indicate that when the diode is attached to an ordinary air cooled heat sink providing a base temperature of 125°C (257°F) a maximum power of 22 watts can be dissipated. This component when mounted on a cold plate of the design shown, could dissipate more than double of the rated power without exceeding the maximum junction temperature.

There is, however, one more item to be considered in determining thermal resistance of mounting joints. Under many conditions the electronic components must be electrically isolated from the cold plate by application of insulating washers. Such washers, depending on the insulation requirements, can induce quite a significant additional thermal resistance and corresponding temperature drop.

c. Cold Plate No. 4 Results

Figure 35 shows cold plate no. 4 fabricated by McDonnell Douglas Astronautics Company. The cold plate is made of aluminum and contains one continuous 0.5 inch heat pipe bent in U-shape, thus forming two evaporator and one condenser sections. Copper tubing, 1/4 inch outside diameter, is attached to the condenser section of the heat pipe through

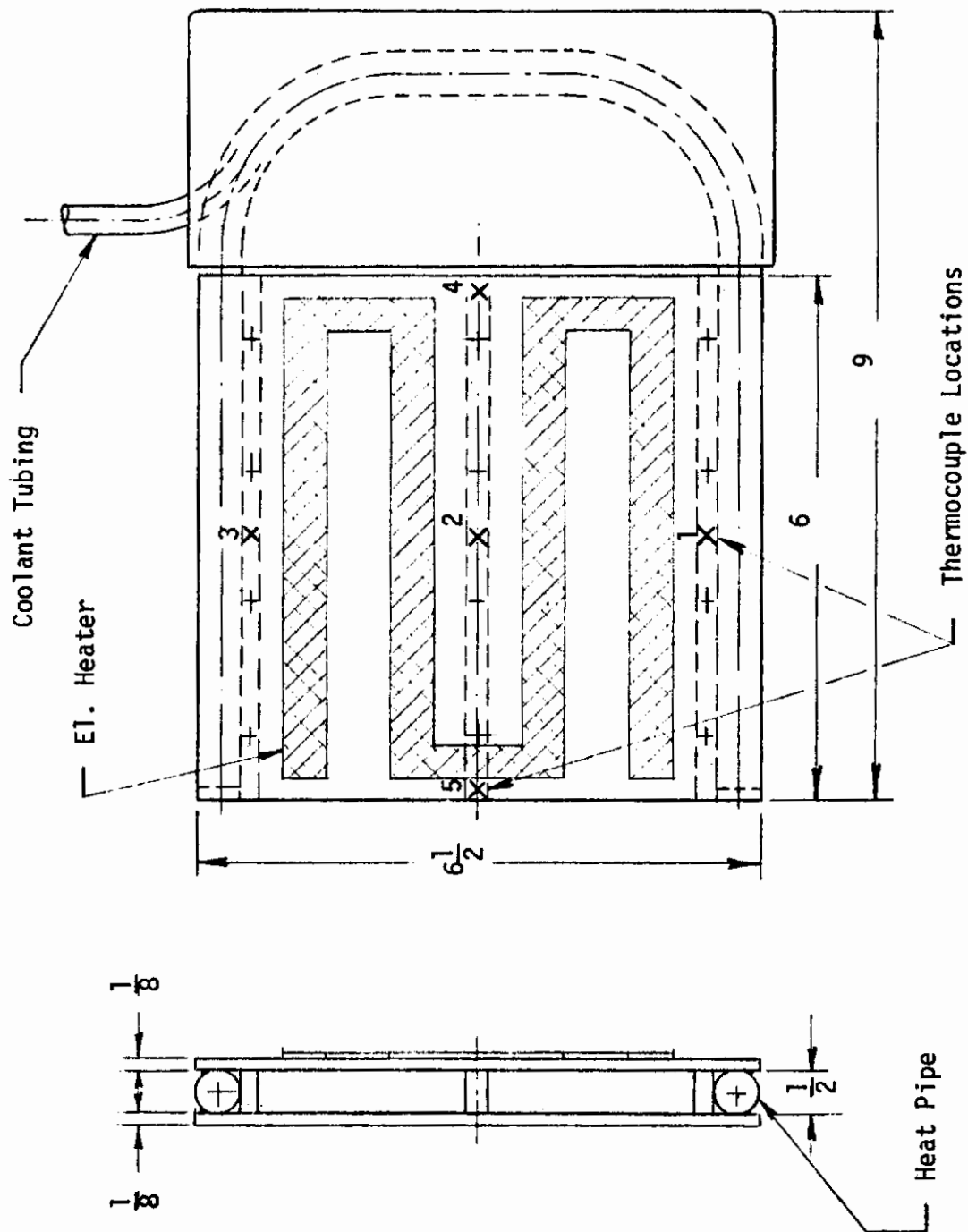


FIGURE 35. EXPERIMENTAL ELECTRONIC EQUIPMENT COLD PLATE NO. 4

Contrails

which coolant is circulated. A tape type electric heater, attached to the plate as shown, was used to simulate the equipment dissipated heat load. The heat pipe was designed for a heat load of approximately 100 watts (340 Btu/hr) and ammonia is used as the working fluid.

Figure 36 shows temperature distribution at the central section of Cold Plate No. 4 at the four different electric power input rates to the tape heater. As can be seen the temperature distribution is completely uniform. This condition, however, is exceptional and can be explained by two main reasons: First, uniform heat input from the tape heater throughout the length of the plate, and second, the evaporator section of the plate is completely separated from the condenser section and no axial conduction heat transfer takes place.

Figure 37 shows temperature changes of Cold Plate No. 4 (thermocouple #2 readings) resulting from electrical power input changes. The temperature change is linear up to an electric power input rate of 75 watts, with some deviation thereafter. This phenomena could be caused by some noncondensable gas left in the heat pipe, or more heat dissipation to the ambient air at the higher plate temperature.

Figure 38 shows also Cold Plate No. 4 (McDonnell Douglas) with two Westinghouse 2N1016 silicon power transistors, and a "dummy" component used in previous experiments attached to it. The tape electric heater was removed and the plate modified by drilling mounting holes for the components. The transistors were attached to the plate with the manufacturer's recommended torque of 50 in-lbs. Also the "dummy" component's mounting screws were tightened with 50 in-lbs torque. Thermal tests of the power transistors were performed with and without

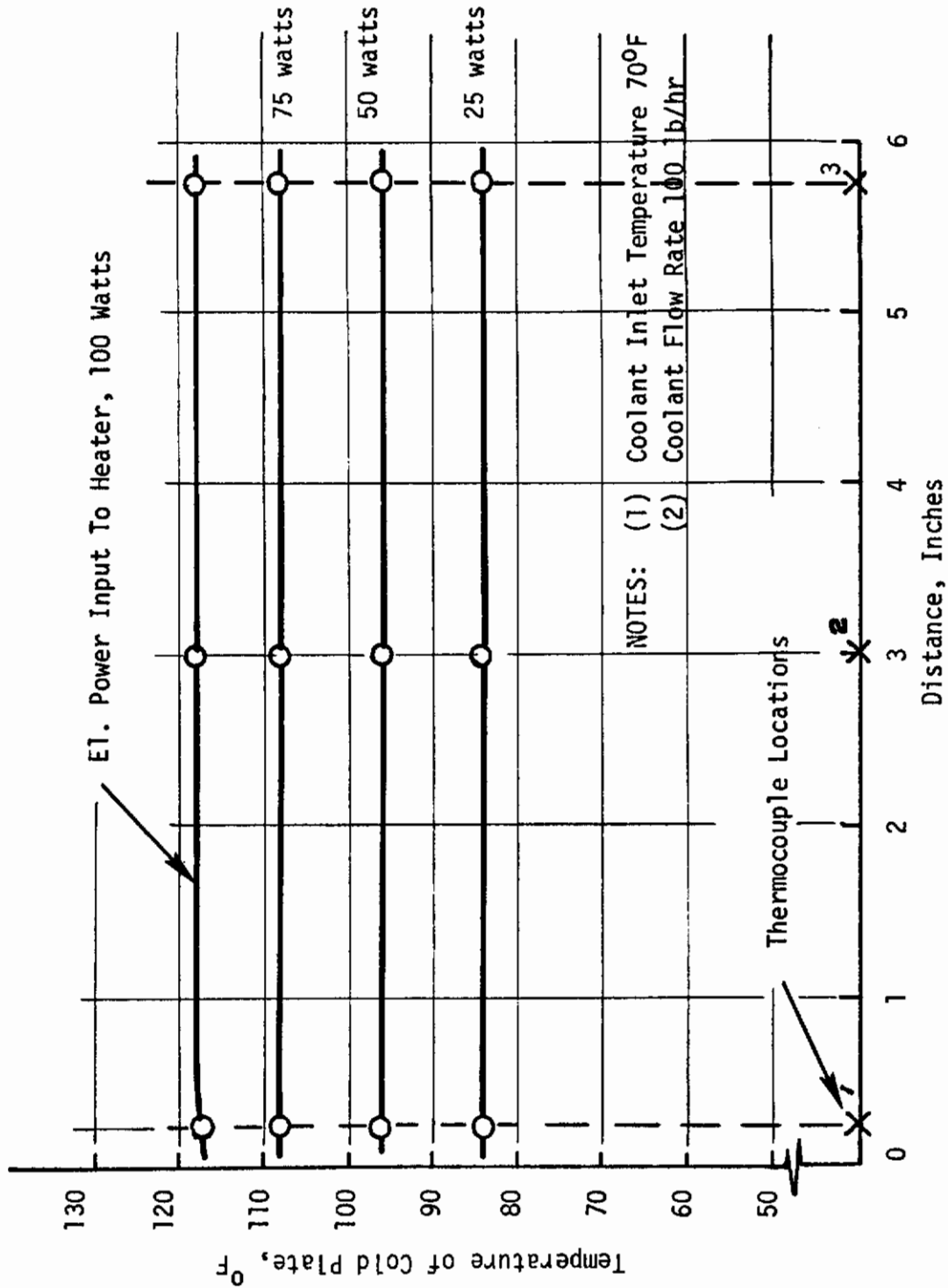


FIGURE 36. TEMPERATURE DISTRIBUTION OF COLD PLATE NO. 4

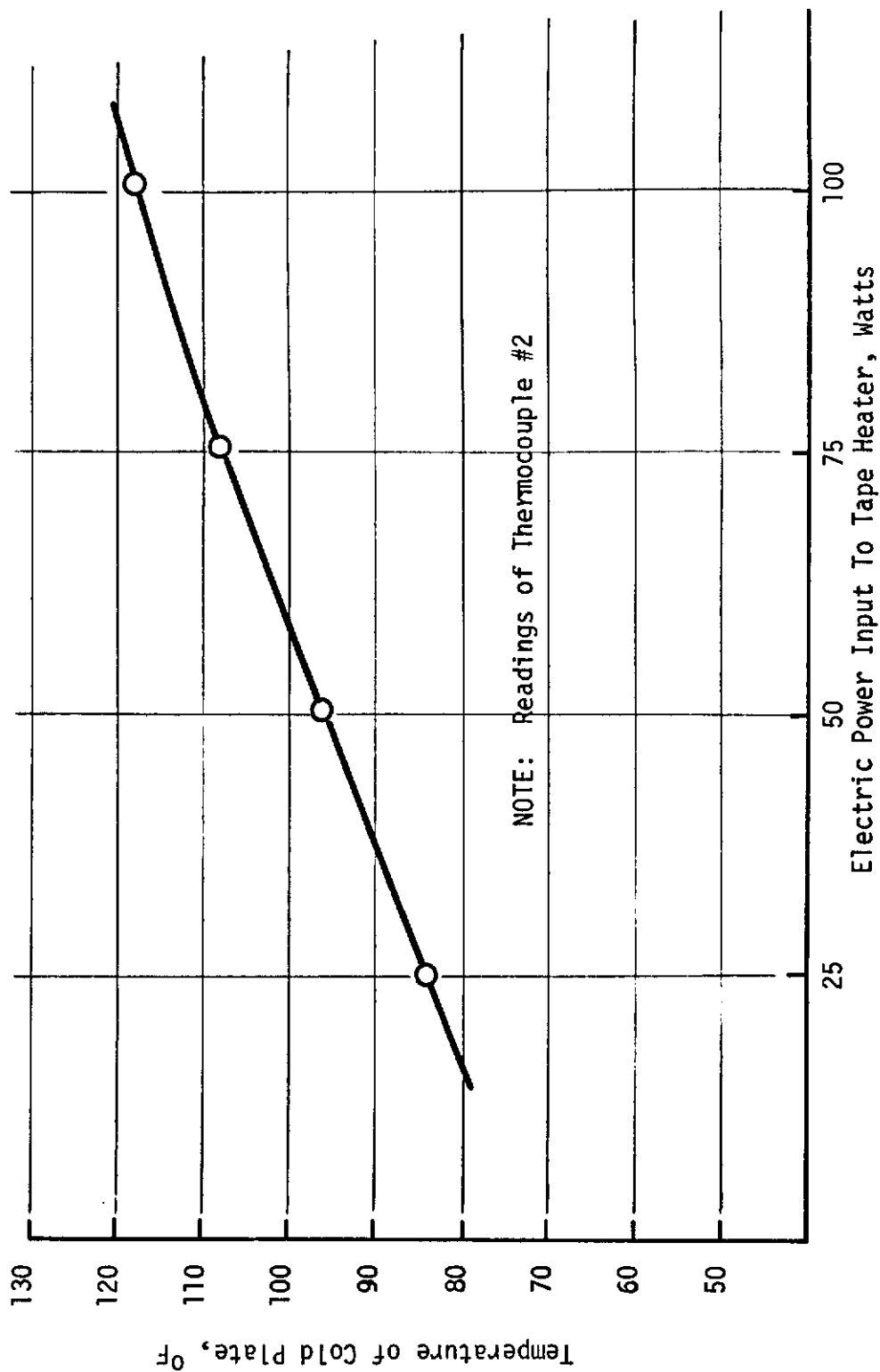


FIGURE 37. TEMPERATURE CHANGES OF COLD PLATE NO. 4 VS EL. POWER INPUT RATES

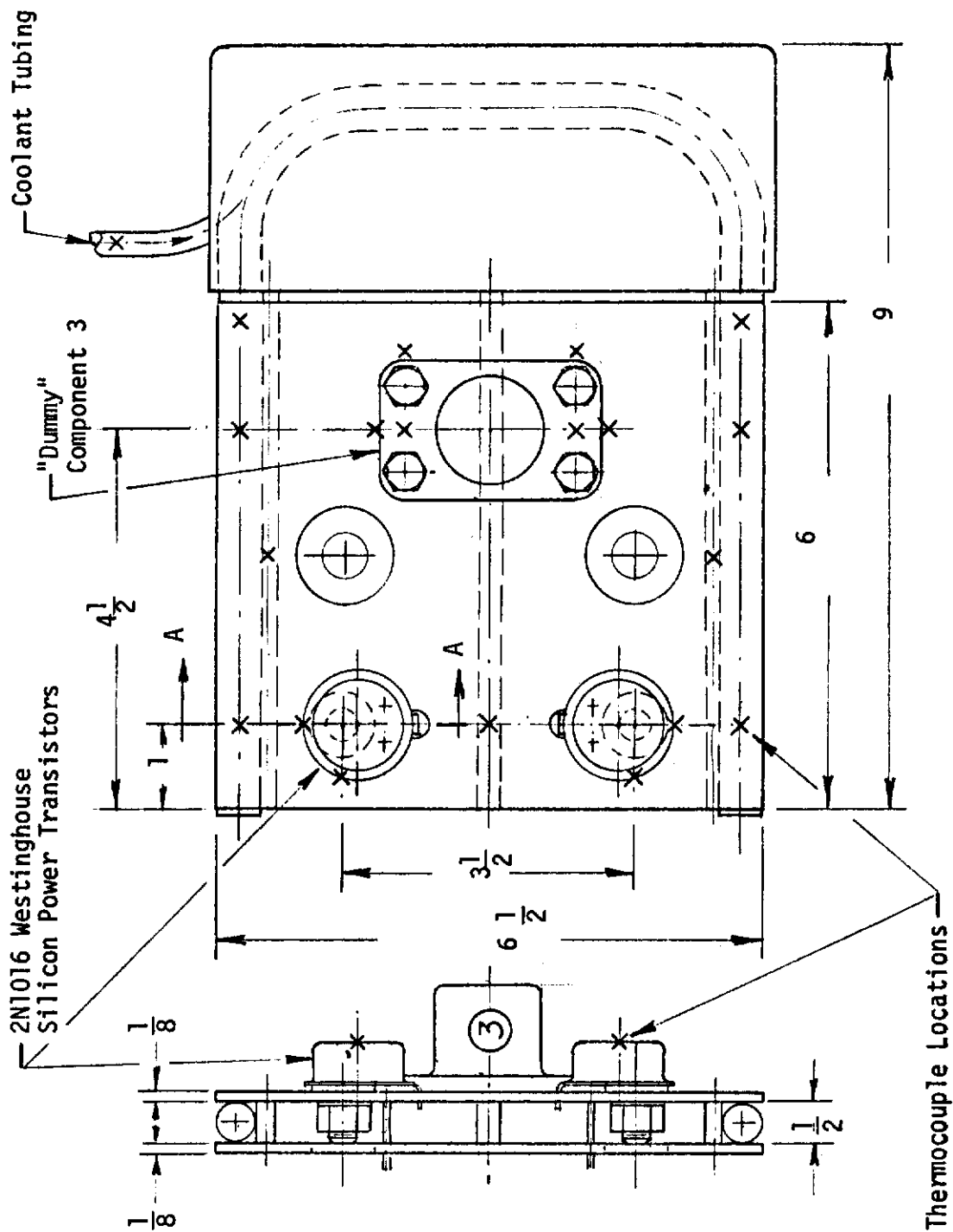


FIGURE 38. EXPERIMENTAL ELECTRONIC EQUIPMENT COLD PLATE NO. 4 WITH TWO POWER TRANSISTORS AND A "DUMMY" COMPONENT

the use of mounting kits consisting of 0.003 inch thick mica washers and insulating spacers as shown on Figure 39. No electrical insulating washers were used with the dummy component; it was mounted directly to the plate. Before attaching the components to the plate, the mating surfaces were cleaned with a fine emery paper and glass wool. Effects of application of silicon grease on the transistor mounting surfaces were also investigated.

Temperature measurements were made with copper-constantan thermocouples inserted into small holes drilled in the plate and component mounting flanges and/or studs. The thermocouples were secured in place by adhesive tape or steel wires.

Figure 39 shows Section A-A of Figure 38 - Cold Plate No. 4. As already indicated, the transistors were attached to the plate by a 50 in-lbs torque, and thermal tests performed with and without the mica washers. The transistor temperatures were measured on the mounting stud and external surface of the case as shown. No attempt was made to measure the junction temperature. This temperature can be determined from the known power dissipation and the manufacturer's given junction to base thermal resistance ($R_{j-b} = 0.7^{\circ}\text{C}/\text{watt}$ for the 2N1016) from Equation (33).

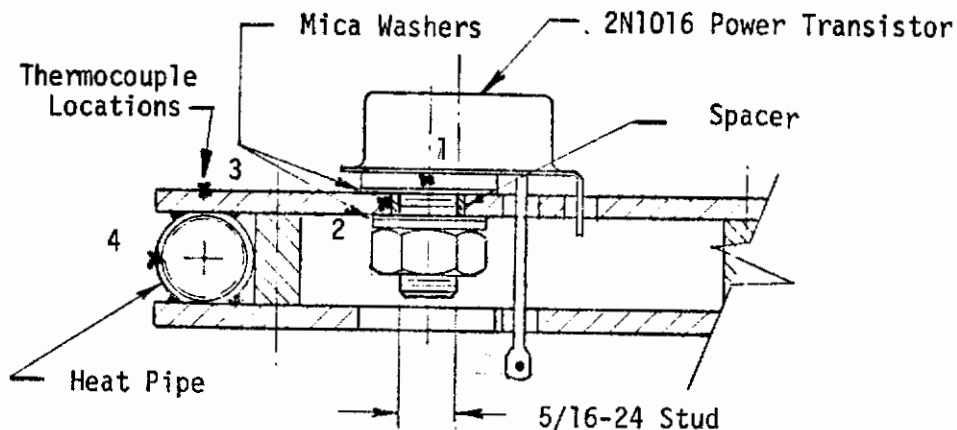


FIGURE 39. SECTION A-A OF COLD PLATE NO. 4

The transistors were energized by applying a constant collector voltage of 20 volts DC from a power supply. Change of the power dissipation was achieved by changing the base current with a variable resistance.

An analytical prediction of the temperature distribution throughout the plate and component mounting base was not performed, because design details of the heat pipe, bonding material thermal properties and joining techniques were not known.

Figure 40 shows comparison of temperature distribution of Cold Plate No. 4 under conditions when the plate was cooled by circulating liquid coolant and natural convection to the ambient air. Electric power input rates to both transistors were the same under both conditions. As expected, there is a significant temperature difference of the transistor mounting base, thus showing the effectiveness of liquid cooling.

It must be noted that temperature of the heat pipe increased by 69°F without the coolant flow, and was uniform throughout the plate, except around the energized transistor mounting base. Temperature increase of the components would be much larger for an ordinary liquid cooled cold plate without coolant flow. The heat pipe cold plate can provide a significant advantage as a heat sink under emergency conditions by increasing the fin effectiveness and thus the heat dissipation rate.

Figure 41 shows temperature distributions for Cold Plate No. 4 from power transistor mounting base to circulating coolant at two different power input rates to the transistors (35 watts and 50 watts to each transistor). The transistors were attached directly to the plate without using any electrical isolation or silicon grease. It

- ◇ Coolant Flow 100 lb/hr
- No Coolant Flow

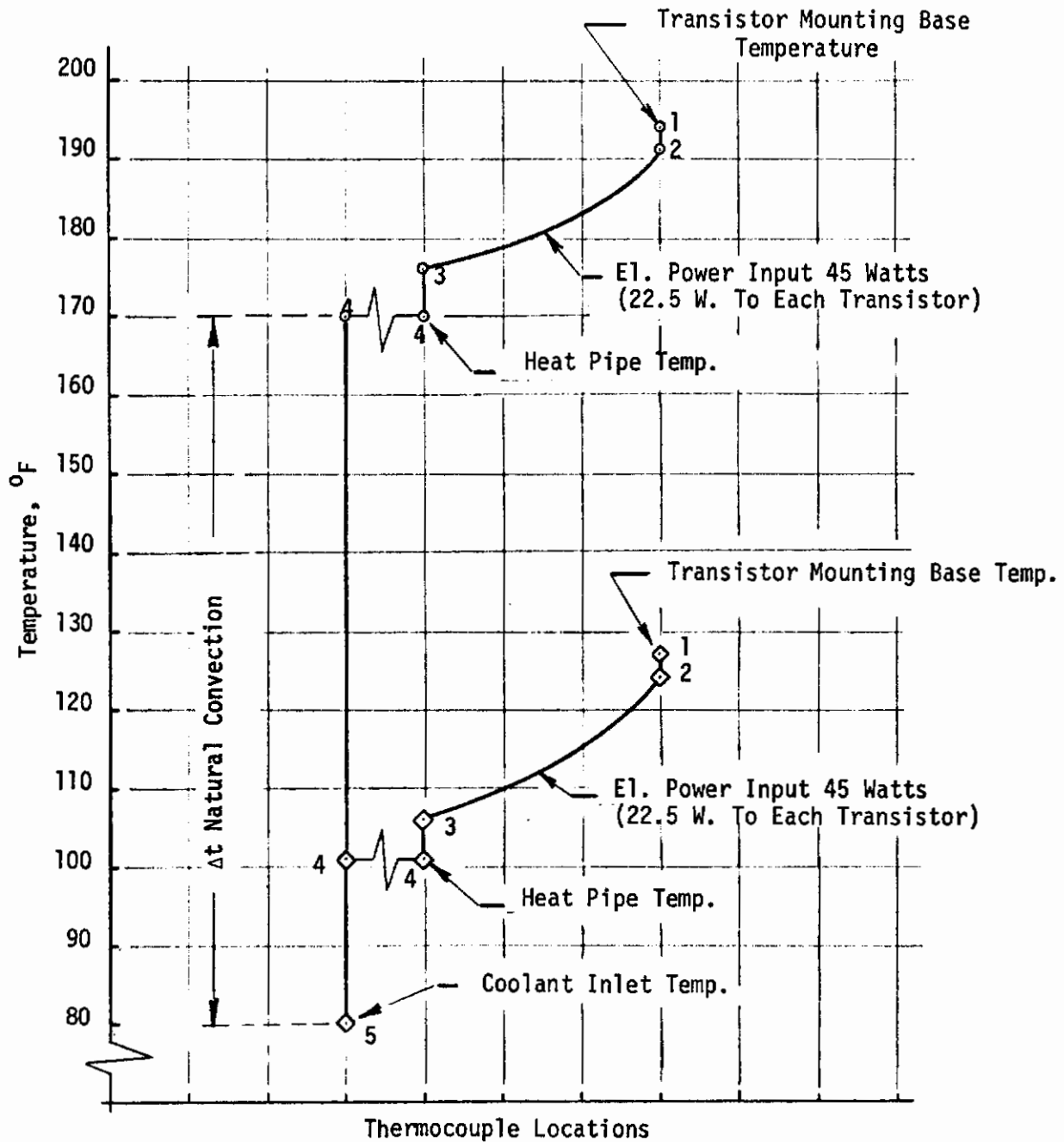


FIGURE 40. TEMPERATURE DISTRIBUTION OF COLD PLATE NO. 4 UNDER COOLANT FLOW AND NO FLOW CONDITIONS

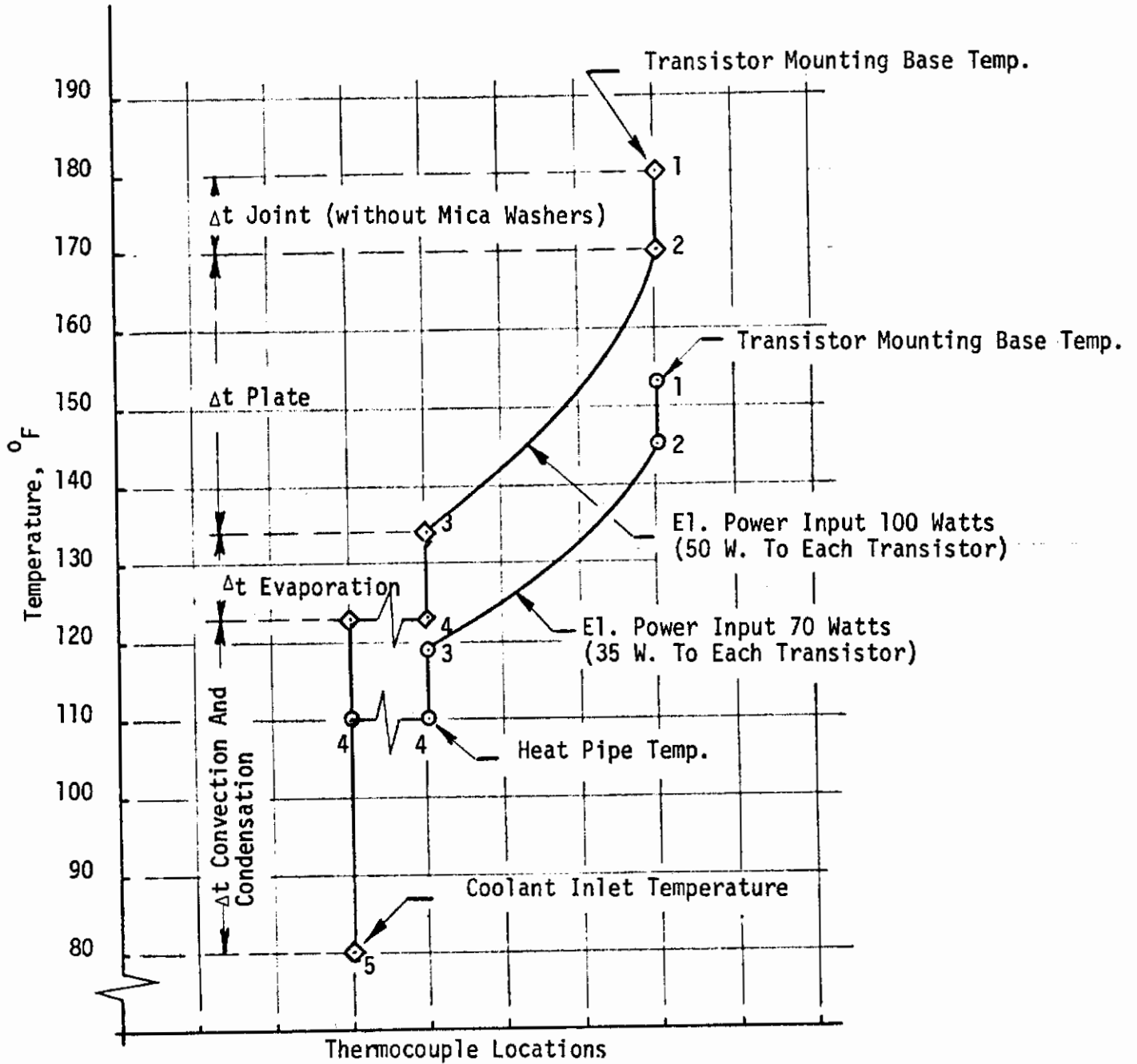


FIGURE 41. TEMPERATURE DISTRIBUTION OF COLD PLATE NO. 4 AT TWO DIFFERENT EL. POWER INPUT RATES TO TRANSISTORS

is apparent from the figure that the largest temperature drops occur at the condenser section and within the mounting plates. These temperature drops could be reduced by increasing the convection heat transfer area, using thicker mounting plates or reducing the spacing of heat pipe passages.

Figure 42 shows temperature distributions for Cold Plate No. 4 at the two indicated electrical power input rates to the transistors. Two mica washers and a spacer were used to electrically isolate the transistors from the plate (see Figure 39). As can be seen, with this mounting technique, the largest temperature drop occurs across the mounting joint.

Figure 43 shows a comparison of temperature distributions for the following three transistor mounting techniques. (1) mica washers used for electrical isolation; (2) same as (1) except silicone grease applied to all mating surfaces; and (3) transistors mounted directly to the cold plate. The comparison was made at approximately the same electrical power input rates to the transistors. Based on the test results, the following joint thermal resistances were determined: (1) transistors mounted directly to plate, $R = 0.11^{\circ}\text{C/Watt}$; (2) mica washers used for electrical isolation, $R = 0.72^{\circ}\text{C/watt}$; (3) same as above, except silicone grease applied to all mating surfaces, $R = 0.51^{\circ}\text{C/Watt}$.

Figure 44 shows temperature distributions for Cold Plate No. 4 at four different electrical power input rates to the "dummy" component. No insulating washers were used for mounting the component to the cold plate. Similarly as in the previous experiments, significant temperature drops occurred within the mounting surfaces.

d. Cold Plate No. 5 Results

Figure 45 shows Cold Plate No. 5 fabricated by McDonnell Douglas

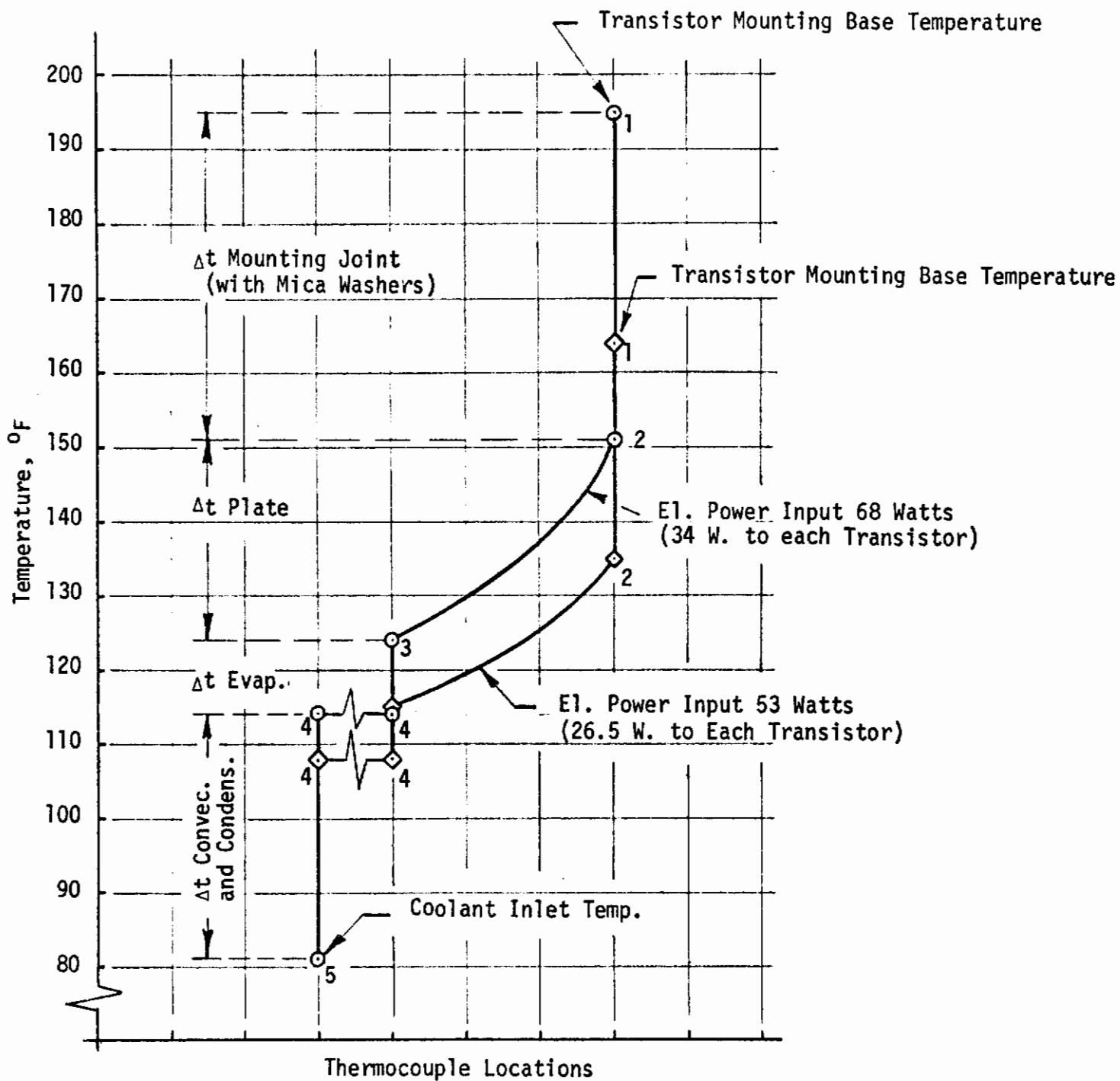


FIGURE 42. TEMPERATURE DISTRIBUTION OF COLD PLATE NO. 4 - MICA WASHERS USED AT TRANSISTOR MOUNTING JOINTS

- Mica Washers Used For Mounting Transistors To Cold Plate (El. Power Input 34 W to Each Transistor)
- ◇ Mica Washers and Silicon Grease Used For Mounting Transistors To Cold Plate (El. Power Input 35 W to Each Transistor)
- Transistors Mounted Directly To Cold Plate (El. Power Input 35 W. to Each Transistor)

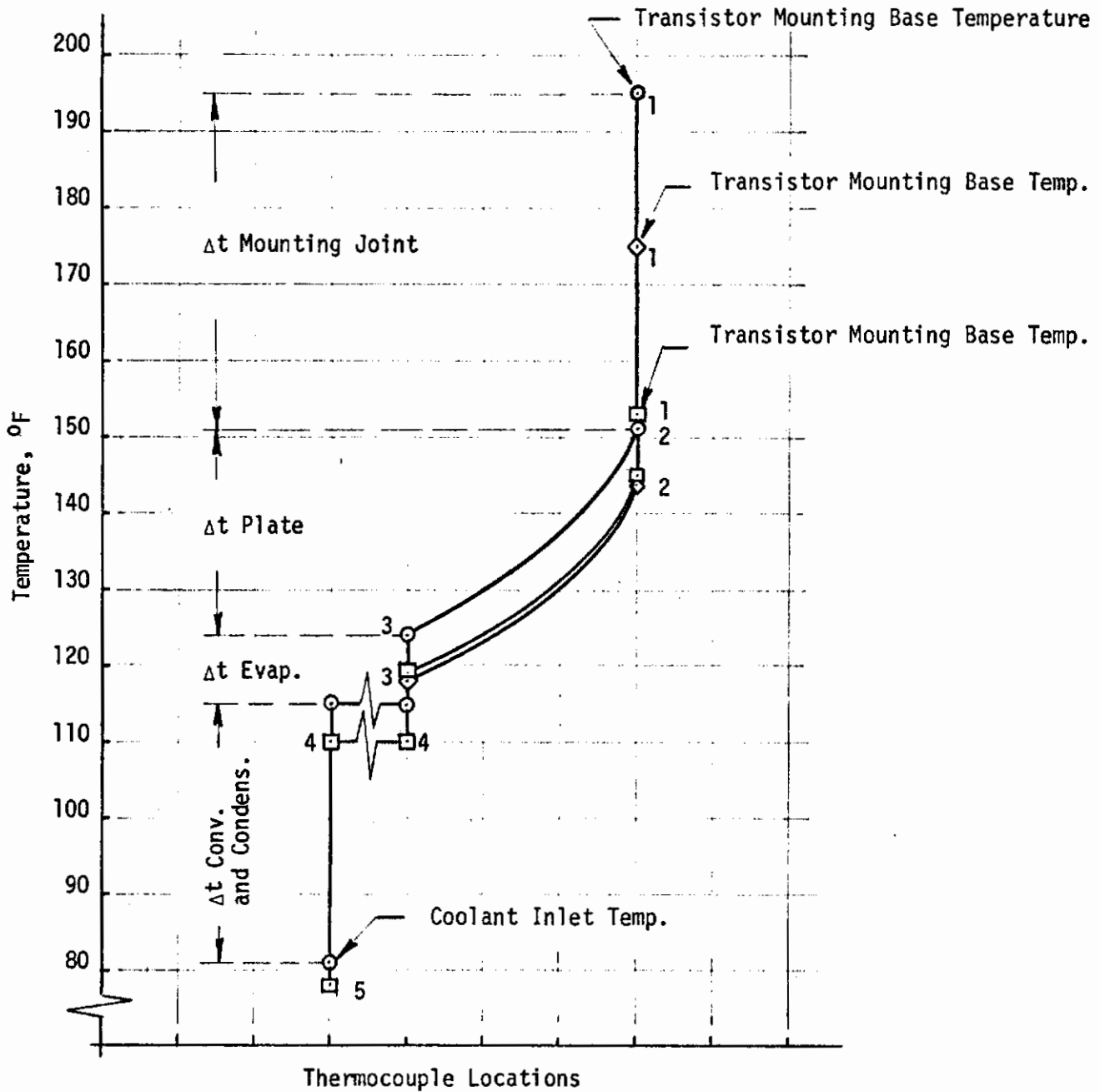


FIGURE 43. TEMPERATURE DISTRIBUTION OF COLD PLATE NO. 4
COMPARISON OF DIFFERENT TRANSISTOR MOUNTING
TECHNIQUES

- × El. Power Input To "Dummy" Component 125 Watts
- El. Power Input to "Dummy" Component 100 Watts
- ◇ El. Power Input to "Dummy" Component 75 Watts
- El. Power Input to "Dummy" Component 50 Watts

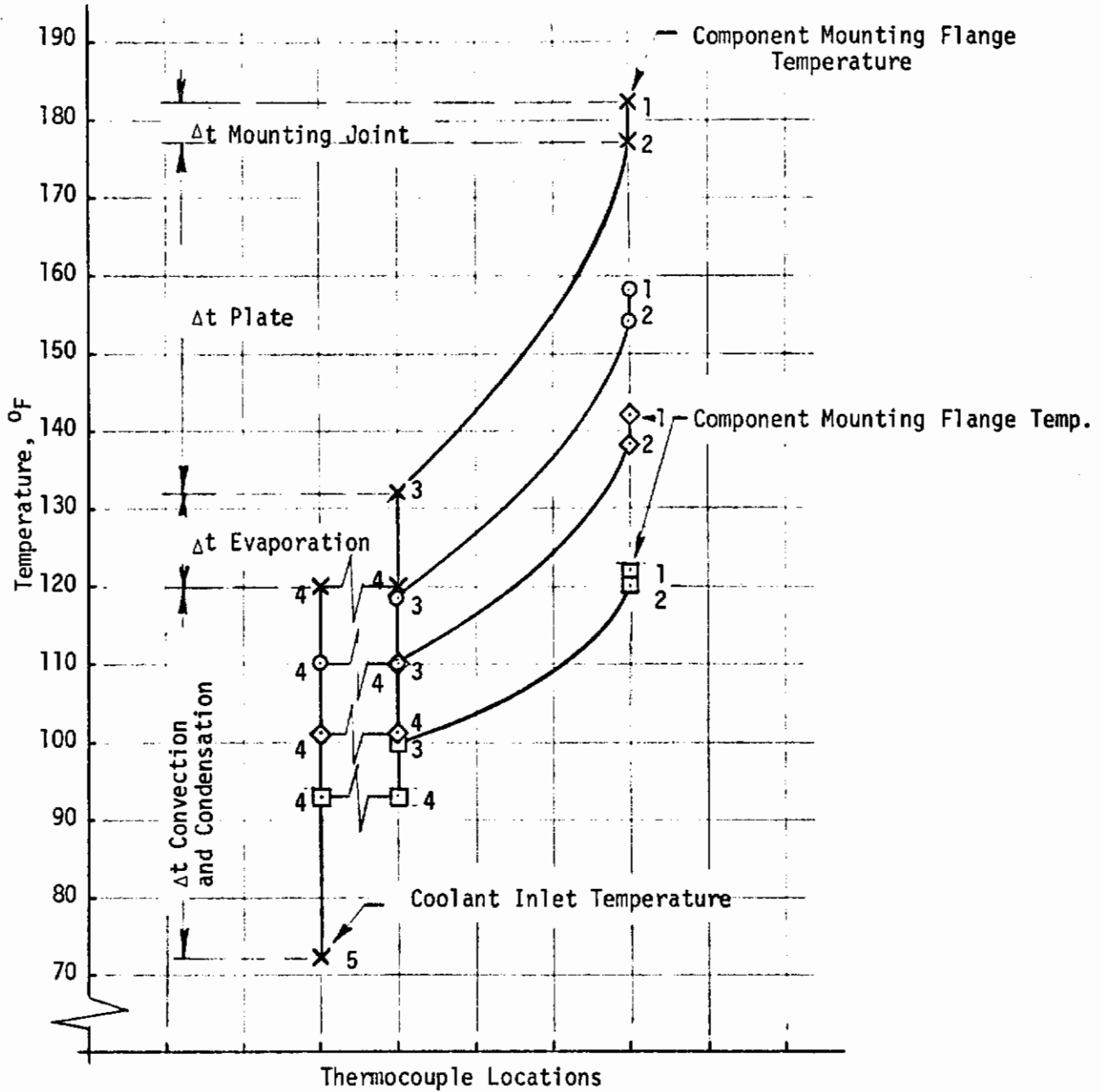


FIGURE 44. TEMPERATURE DISTRIBUTION OF COLD PLATE NO. 4 AT DIFFERENT EL. POWER INPUT RATES TO "DUMMY" COMPONENT 3

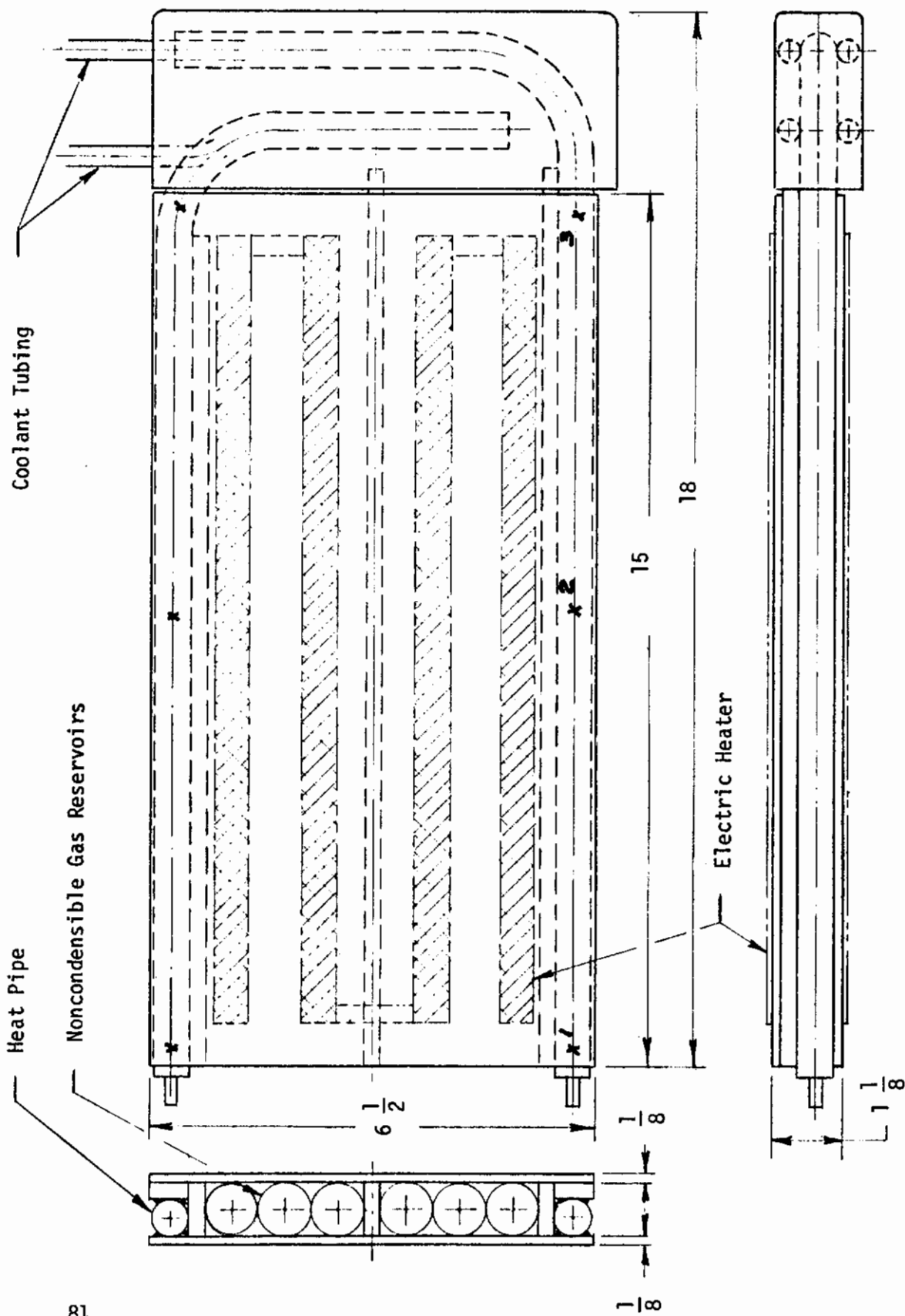


FIGURE 45. EXPERIMENTAL ELECTRONIC EQUIPMENT COLD PLATE NO. 5
(VARIABLE CONDUCTANCE COLD PLATE)

Astronautics Company. The cold plate is made of aluminum and consists of two 1/8 inch thick plates and two 1/2 inch diameter heat pipes each of which is provided with three 3/4 inch diameter by 14 inch long tubes as noncondensable gas reservoirs. A device, located between the heat pipe and the reservoir, prevents liquid ammonia from flowing into the reservoirs. Heat is removed by circulating coolant through the 1/4 inch diameter copper tubing attached to the condenser section of the heat pipes. The plates and heat pipes are bonded together with aluminum epoxy. The cold plate is designed for a total heat load of 250 watts.

The helium gas filled reservoirs provide temperature control of the plate under conditions when the heat load is changing. At low heat load the noncondensable gas extends quite far into the condenser section, and resistance to heat flow is, therefore, increased. When the heat load of the plate is increased, the vapor generation and flow rates, and thus also the pressure are increased pushing the noncondensable gas back into the reservoir. The displaced gas will expose a larger condenser surface area for condensation, thus promoting heat transfer of the heat pipe. Temperature of the plate can be maintained constant and stable because of the variable conductance of the condenser.

The cold plate was instrumented with 30-gage copper-constantan thermocouples attached to internal and external surfaces of the plate. The equipment heat load was simulated by tape heaters attached to both sides of the plate. DC power supplies were used to provide controllable electric power input to the heaters.

Figures 46 and 47 show temperature distributions for Cold Plate No. 5 at different electric power input rates to the heaters, and two different

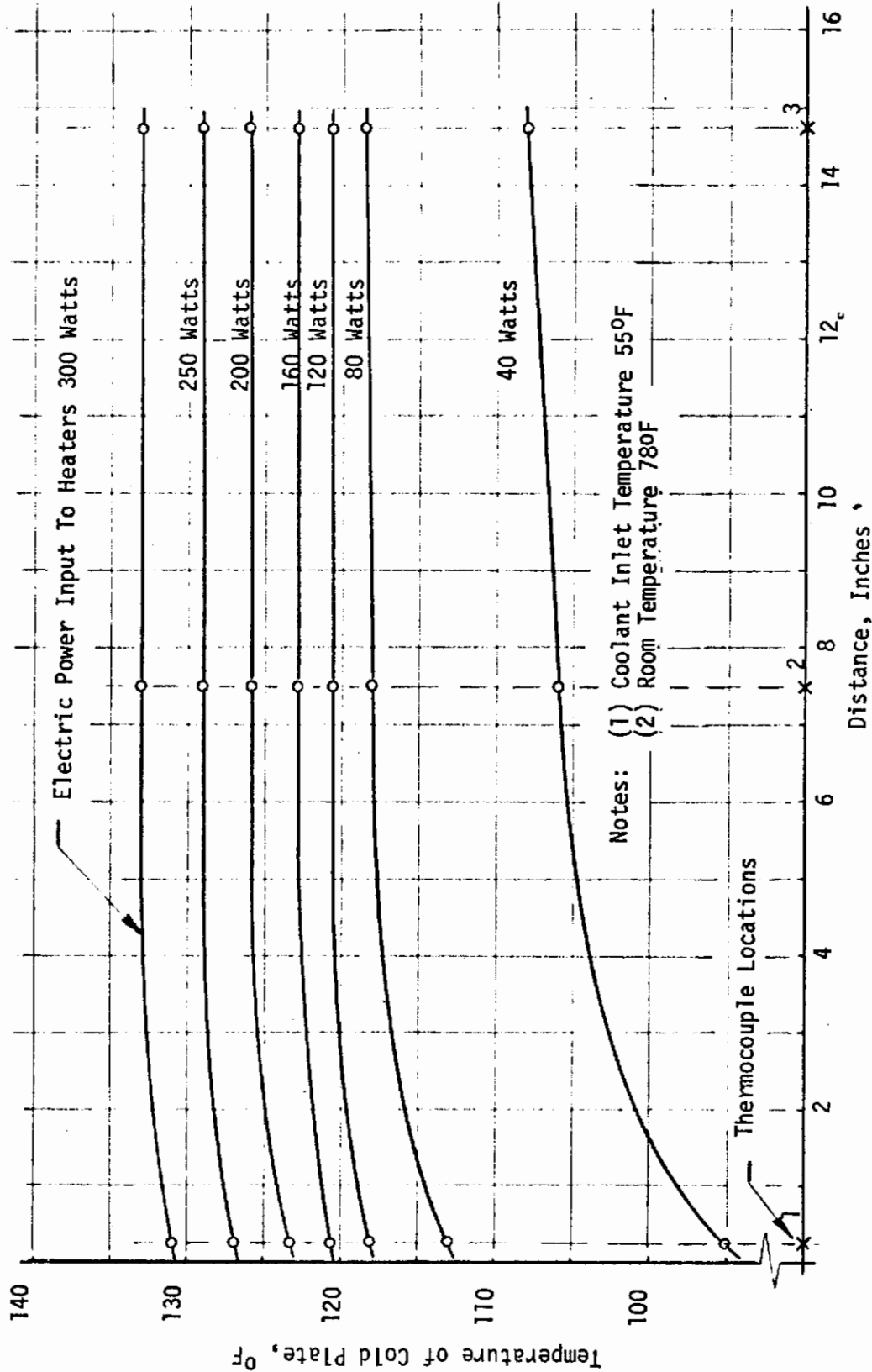


FIGURE 46. TEMPERATURE DISTRIBUTION OF COLD PLATE NO. 5

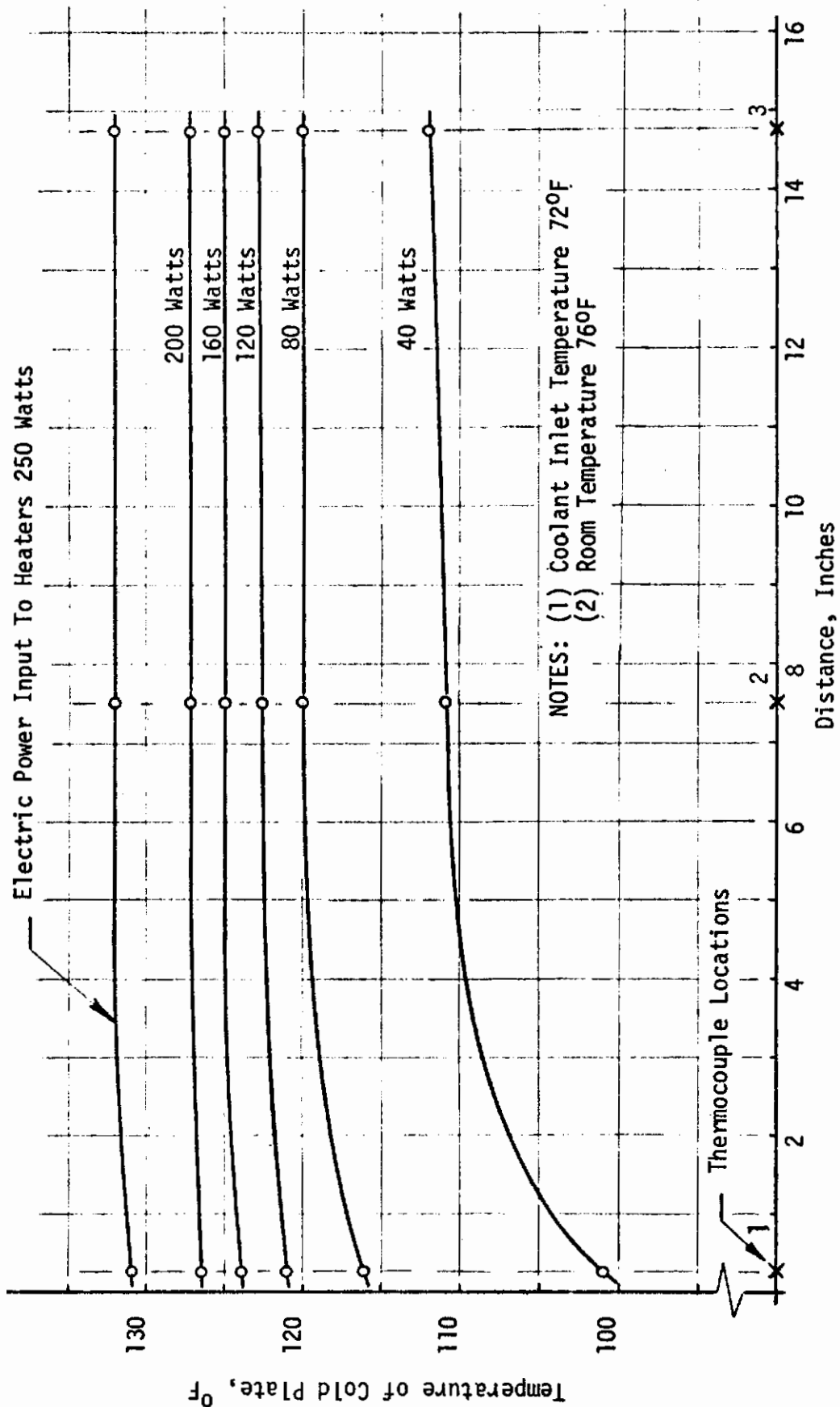


FIGURE 47. TEMPERATURE DISTRIBUTION OF COLD PLATE NO. 5

coolant inlet temperatures (55°F and 72°F). The charts show temperature measurements taken near an edge of the plate (along the heat pipe).

As can be expected, temperature distribution along the plate is nonuniform at the lower heat input rates because the noncondensable gas occupies a large portion of the condenser. However, when the heat load is increased, the vapor flow rate and pressure are also increased exposing a larger surface area for condensation and this forces the noncondensable gas into the reservoir. As a result, only a small temperature increase of the plate occurs. Somewhat larger temperature changes and also higher temperatures could be observed at the plate's central section (between the heat pipes). This condition was caused by the thermal resistance of the plates.

Figure 48 shows temperature changes (readings taken near the edge located at the middle section of the plate) of Cold Plate No. 5 resulting from heat load changes. Comparison is also made here between conditions when the coolant inlet temperatures were 55°F and 72°F . As can be seen, above a heat load of 80 watts, the temperature change is quite small and linear. A heat load change from 80 watts to 240 watts caused a plate temperature change of only 10°F . It is also interesting to note that a coolant inlet temperature change of 17°F caused a plate temperature change of only 2°F . This indicates that not much can be gained by reducing coolant inlet temperature below a certain limit.

Figure 49 shows effects of orientation upon temperature distribution of Cold Plate No. 5. Orientation effects were determined under both conditions - condenser end at the higher location, and evaporator end at the higher location. When the plate was tilted approximately 15

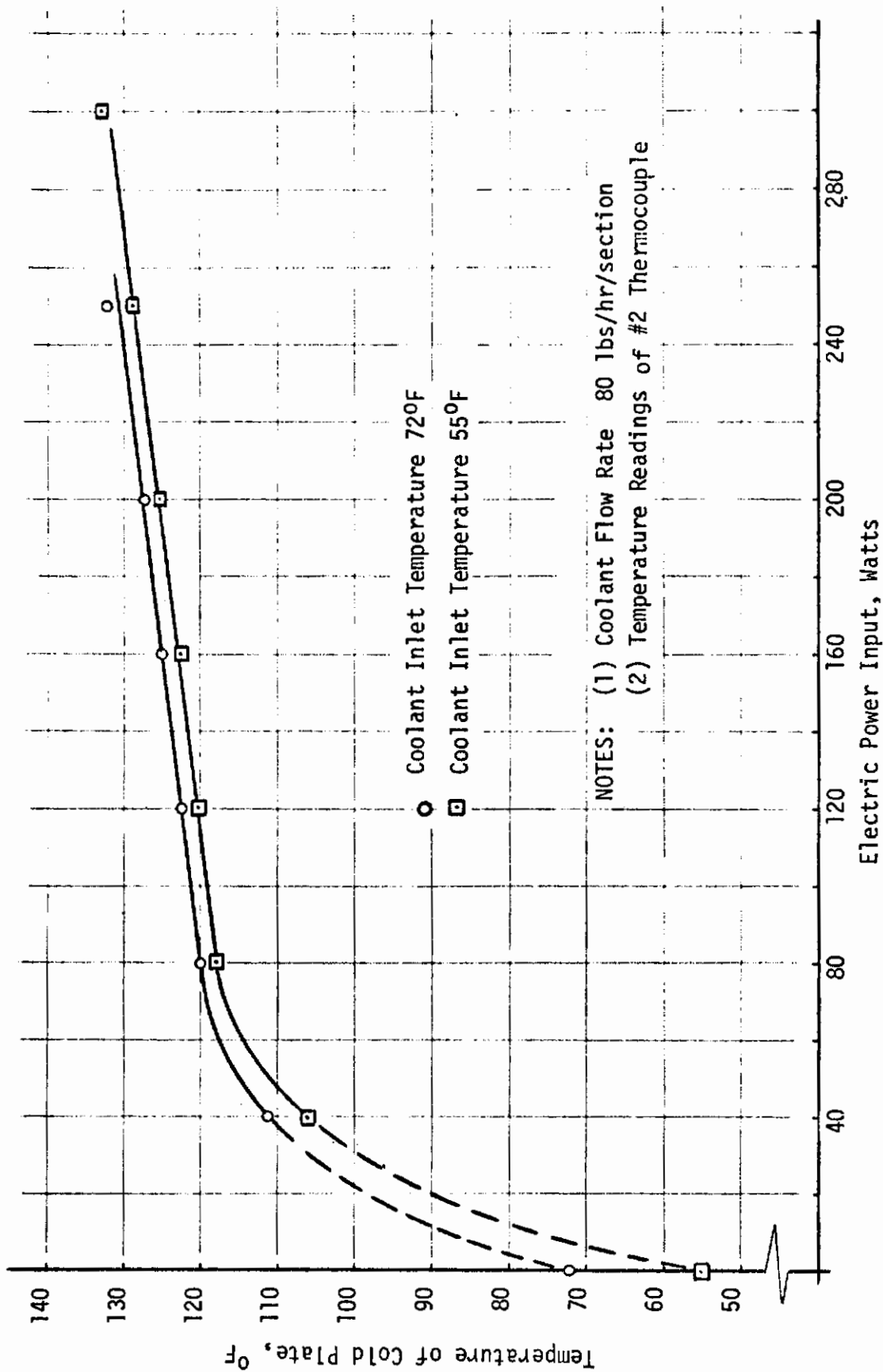


FIGURE 48. TEMPERATURE CHANGES OF COLD PLATE NO. 5 VS. ELECTRIC POWER INPUT RATES TO HEATERS

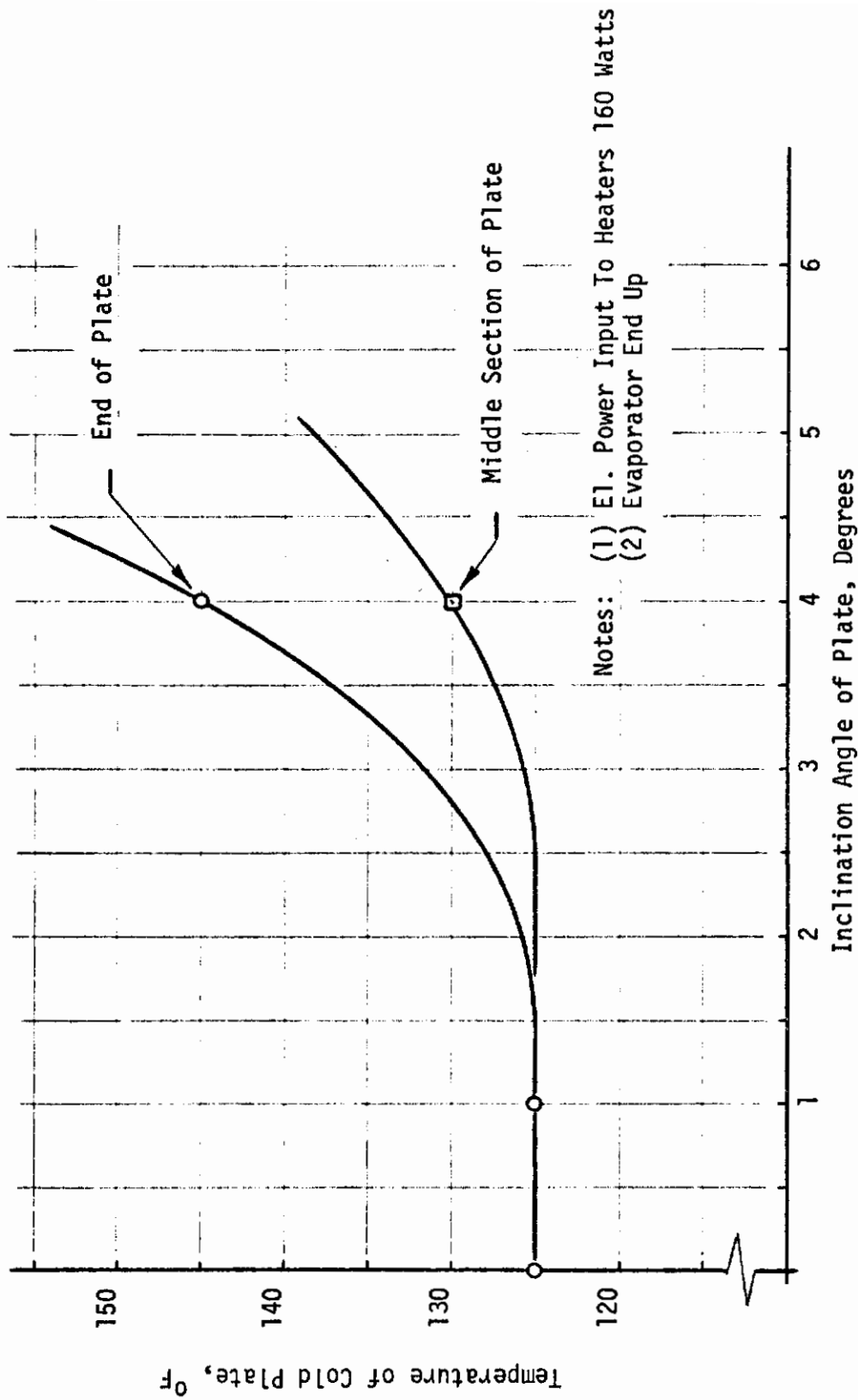


FIGURE 49. EFFECTS OF ORIENTATION UPON COLD PLATE'S NO. 5 THERMAL PERFORMANCE

degrees with the condenser end up, a hardly noticeable temperature change took place. However, when the plate was tilted with the evaporator end up, temperature distribution started to show effects above an inclination angle of approximately 2 degrees. At approximately 4 degrees inclination a temperature rise of 20⁰F took place at the evaporator end of the plate, while only 5⁰F rise occurred at the middle section. No temperature change could be observed at the condenser end. Further inclination caused quite a significant temperature increase at the evaporator end indicating dry out of the wick.

In order to investigate the thermal performance of different mounting techniques, Cold Plate No. 5 was altered as shown on Figure 50. The electronic components were mounted on brackets made of 3/16 inch thick aluminum angles. The brackets were attached to the cold plate by 1/4-20 hexagon head machine screws as shown in Section A-A, Figure 51. Silicone grease was used on all joints and the components fastened to the brackets with the recommended torque. The components selected were N-P-N stud mounted power transistors widely used in many electronic systems.

Figures 51, 52 and 53 show temperature distributions from the power transistor 2N1724, 2N2109 and 2N1016 mounting bases to Cold Plate No. 5. Transistors 2N1724 and 2N1016 were electrically isolated from the mounting bracket by mica washers and teflon spacers, while transistor 2N2109 was mounted directly to the bracket without any electrical isolation. To show effects of heat dissipation rates upon temperature distribution, two electric power input levels were used and are shown on each of the charts.

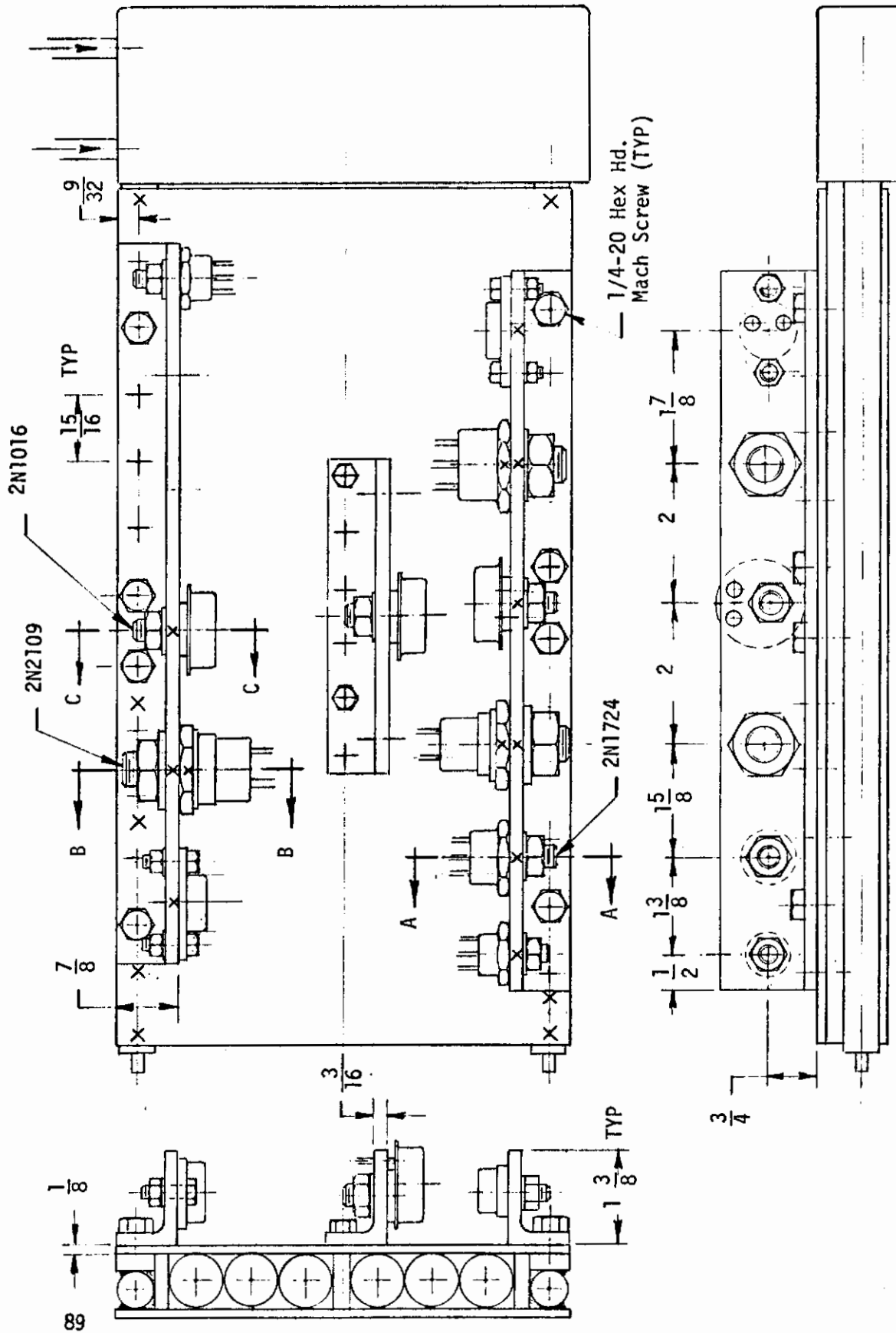
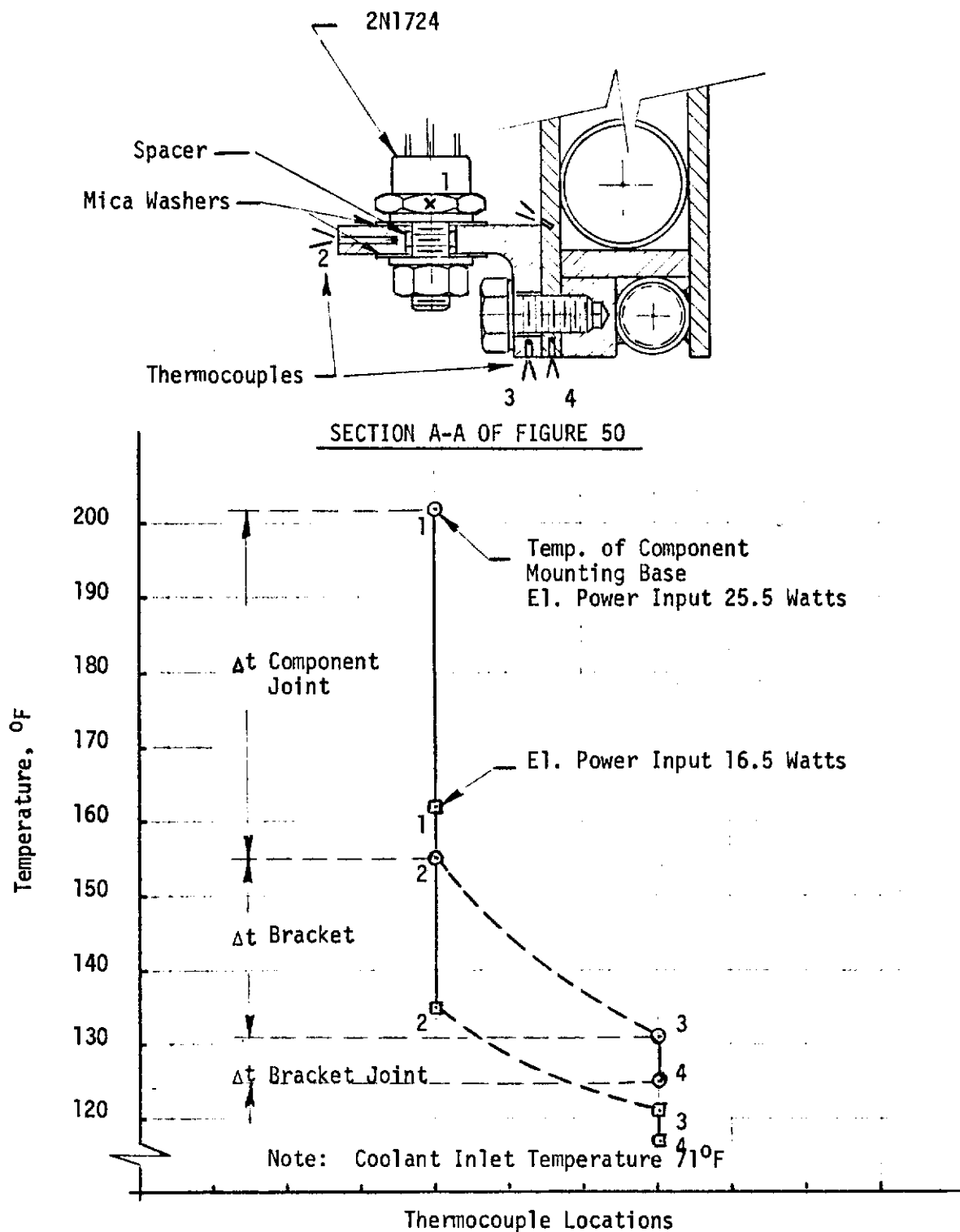
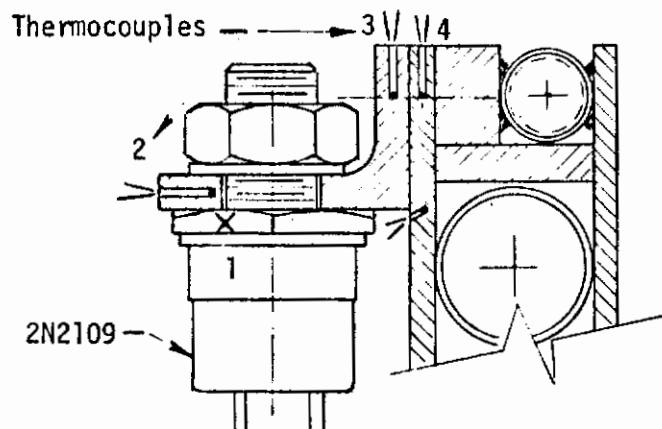


FIGURE 50. EXPERIMENTAL ELECTRONIC EQUIPMENT COLD PLATE NO. 5 WITH ATTACHED ELECTRONIC COMPONENTS





SECTION B-B OF FIGURE 50

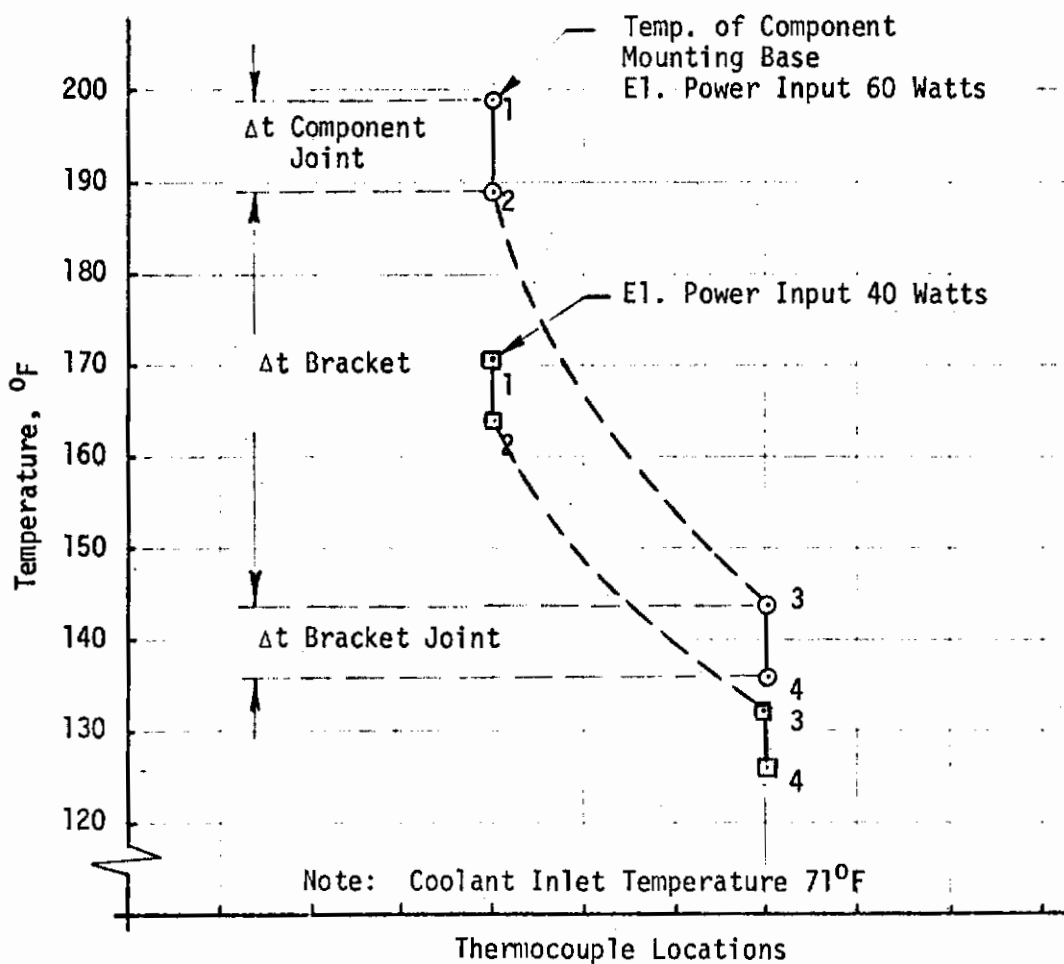
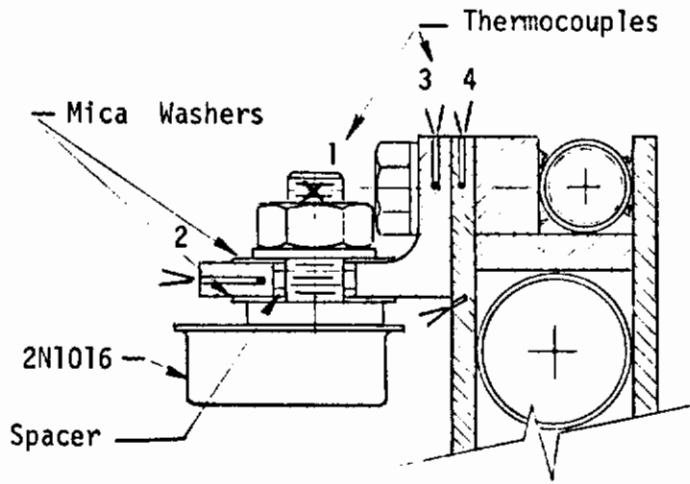


FIGURE 52. TEMPERATURE DISTRIBUTION FROM COMPONENT MOUNTING BASE TO COLD PLATE



SECTION C-C OF FIGURE 50

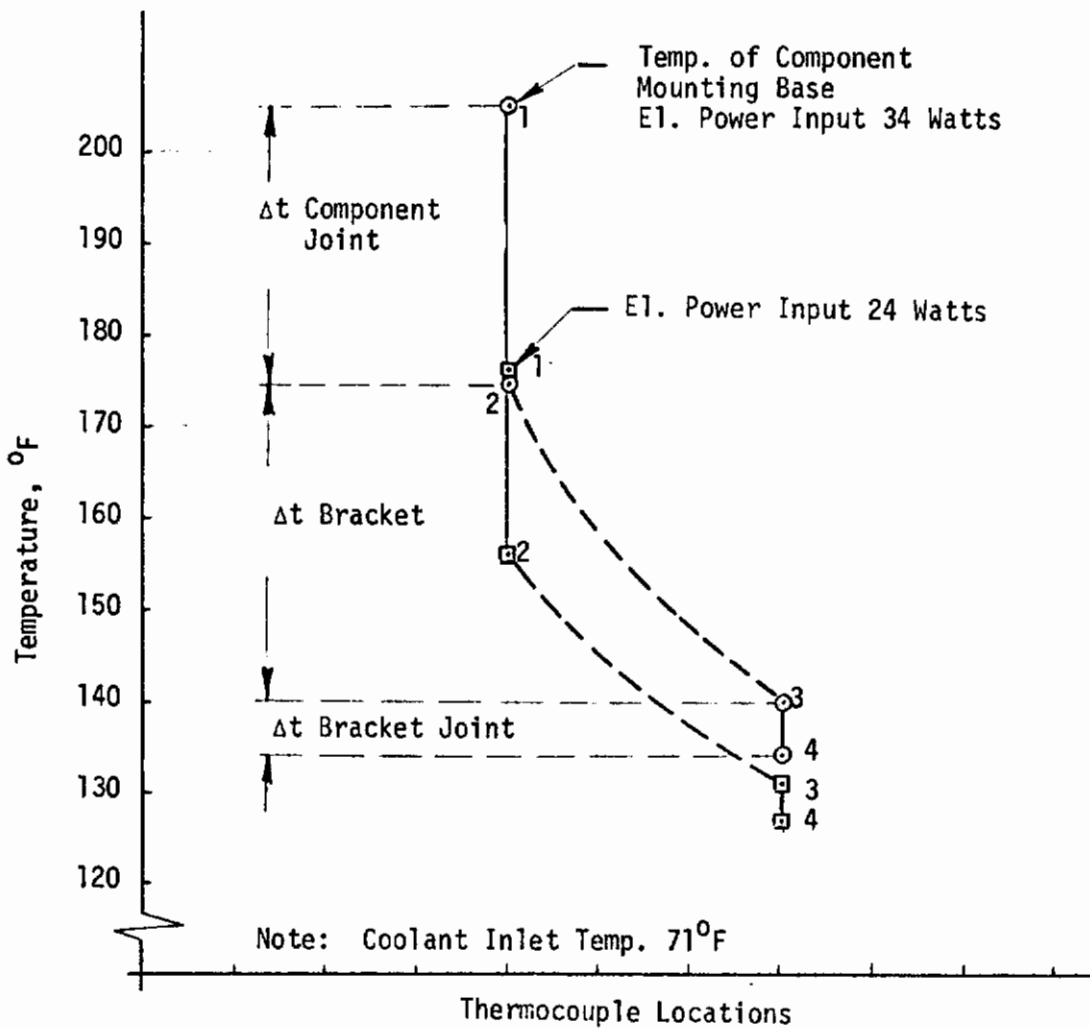


FIGURE 53. TEMPERATURE DISTRIBUTION FROM COMPONENT MOUNTING BASE TO COLD PLATE

The temperature measurements were performed by copper-constantan thermocouples inserted into small holes drilled into the component's base or stud and bracket as shown. The thermocouples were secured in place by steel wires pressed into the holes after the thermocouples were inserted. Temperature distribution throughout the cold plate is not shown on these charts, because it has been done previously. It must be noted, however, that the concentrated heat loads caused certain distortions of the temperature uniformity. It is apparent from the charts that the largest temperature differentials occurred in the brackets and component mounting joints when mica washers were used. Based on the heat input rate and temperature measurements, the joint thermal resistances, expressed in $^{\circ}\text{F}/\text{watt}$, were determined from the following equation:

$$W = \frac{\Delta t}{R}, \text{ watts}$$

$$R = \frac{\Delta t}{W}, \text{ }^{\circ}\text{F}/\text{Watt}$$

TABLE 1. JOINT THERMAL RESISTANCES

Component	Component Mtg. Joint Thermal Resistance $^{\circ}\text{F}/\text{Watt}$	Bracket - Plate Thermal Resistance $^{\circ}\text{F}/\text{Watt}$
2N1724	1.85	0.23
2N2109	0.167	0.135
2N1016	0.88	0.175

The results indicate quite a significant difference in the component mounting joint thermal resistances, particularly between joints with and without mica washers. Comparing component 2N1724 and 2N1016 mounting joint thermal resistances (mica washers used on both components), a

difference of approximately 100% is apparent. This large difference could be caused by the different joint surface area, stud size and torque, and particularly the thickness of the mica washers. While some of the washers were less than 0.003 inches thick, others were over 0.005 inches thick. Furthermore, the larger and black surface area of the 2N1016 case causes larger heat dissipation rates to the surroundings by both radiation and natural convection. The bracket-cold plate thermal resistance is quite small.

e. Cold Plate No. 6 Results

Thermal tests performed on all of the conventionally designed (fin-tube arrangement) cold plates indicated that a significant temperature drop occurred within the mounting surfaces. This condition introduces restrictions for the application of cold plates to components of high power dissipation rates, unless very thick plates are used. To eliminate this restriction and improve performance characteristics of equipment cooling plates, a new design was devised. Figure 54 shows this design identified as Cold Plate No. 6. The plate is made of two rather thin sheets forming a 3/16 inch wide continuous cavity which is provided with a screen as wick and is charged with a working fluid. Because of fabrication reasons the plate was made of copper instead of aluminum, which would be a more realistic material for airborne applications. The components, generally silicone power transistors, are mounted to inserts or fixtures shown in Sections A-A and B-B of Cold Plate No. 6. Heat, generated by the electronic components, is transferred through the inserts to the

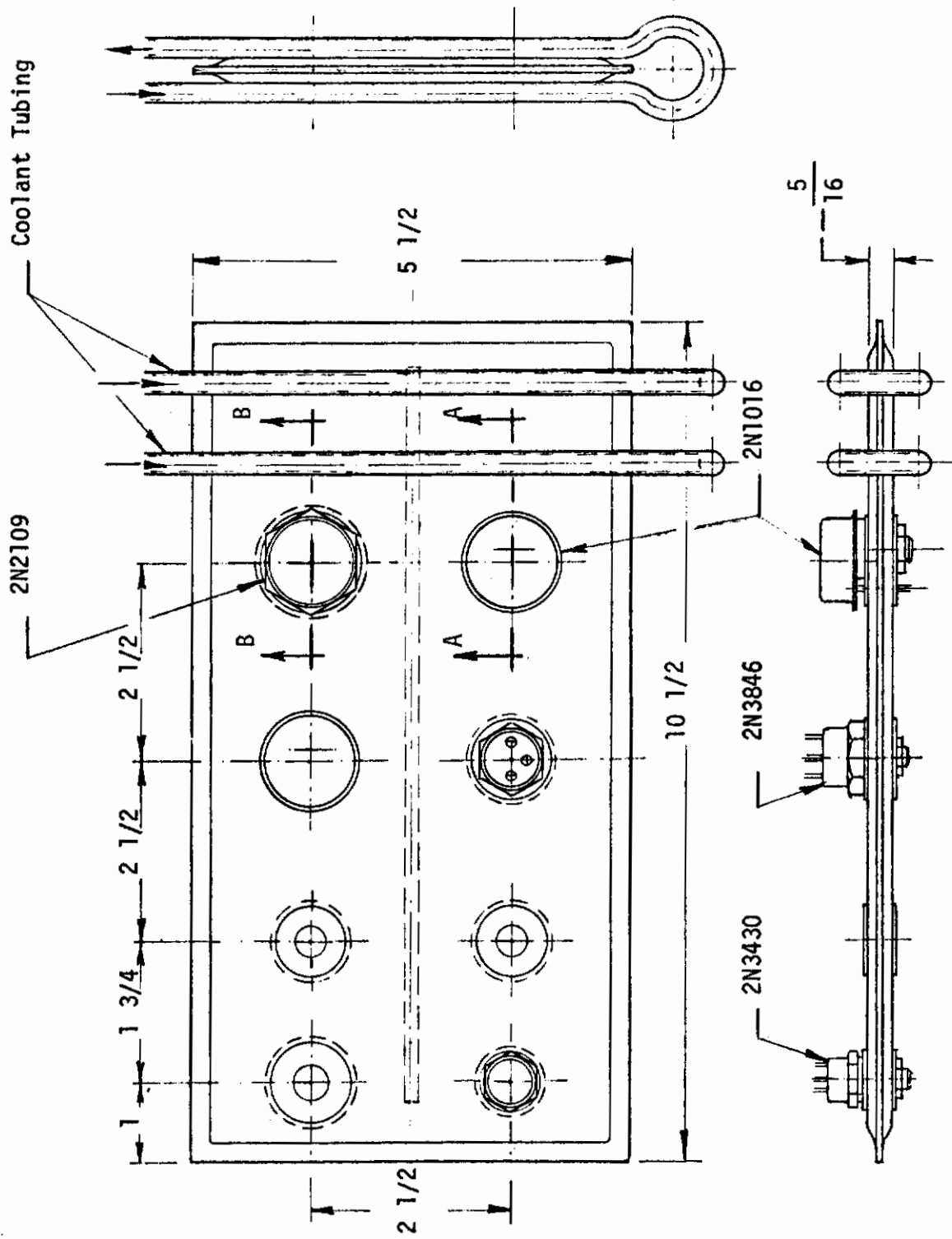


FIGURE 54. EXPERIMENTAL ELECTRONIC EQUIPMENT COLD PLATE NO. 6

working fluid, and from there to the coolant circulated through 1/4 inch diameter tubing attached to the condenser section of the plate.

Arrangement of the heat pipe cavity and component mounting surface shortens the conduction path significantly and thus reduces the temperature differential from the insert to the working fluid. Evaporative heat transfer will take place from the insert and also both sheets or plates. The plates act as radial fins and dissipate heat by evaporation from the internal surfaces, and by natural convection and radiation from the external surfaces. The largest portion of the waste heat, however, because of the much higher evaporative heat transfer coefficients, will be transferred to the working fluid.

In order to allow performance prediction of such cold plates, the basic analytical techniques for establishing the R-C network will be outlined.

The evaporative heat transfer rate from the insert can be determined from the following equation:

$$Q = h\pi Db(\Delta t) \quad (63)$$

D - diameter of insert, ft

b - width of insert, ft

Heat dissipated from a radial fin can be determined from equation given in Reference 18.

$$Q_o = 2\pi R_o \delta k m \theta_o \left[\frac{I_1(mR_L) K_1(mR_o) - K_1(mR_L) I_1(mR_o)}{I_o(mR_o) K_1(mR_L) + I_1(mR_L) K_o(mR_o)} \right] \quad (64)$$

Or, when calculations are based on fin efficiency:

$$\eta = \frac{Q_o}{Q_i} \quad (65)$$

Contrails

$$Q_i = 2\pi (R_L^2 - R_0^2) h \theta_0 \quad (66)$$

and $Q_o = \eta Q_i \quad (67)$

Q_i is the ideal heat dissipated when the fin temperature would be uniform.

$$\eta = \frac{2R_0}{m(R_L^2 - R_0^2)} \left[\frac{I_1(mR_L)K_1(mR_0) - K_1(mR_L)I_1(mR_0)}{I_0(mR_0)K_1(mR_L) + I_1(mR_L)K_0(mR_0)} \right] \quad (68)$$

Determination of m can be based on two conditions

- a. both sides of fin are effective

$$m = \sqrt{\frac{2h}{k\delta}} \quad (69)$$

- b. only one side of fin is effective

$$m = \sqrt{\frac{h}{k\delta}} \quad (70)$$

R_0 = radius of fin base or root, ft

R_L = radius of fin, ft

I = modified Bessel function, first kind

K = modified Bessel function, second kind

$$\theta_0 = t_0 - t_s$$

t_0 = fin base temperature

t_s = surrounding temperature

Figure 55 shows the resistance network from the component base to the working fluid of a heat pipe. This resistance can be expressed as follows:

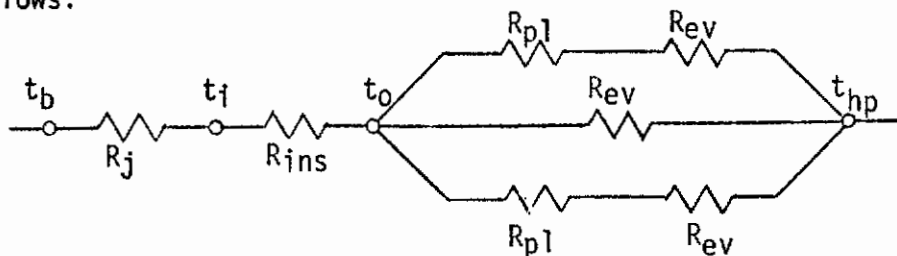


FIGURE 55. RESISTANCE NETWORK OF EVAPORATOR SECTION

$$R = R_j + R_{ins} + \frac{1}{\frac{1}{R_{p1} + R_{ev}} + \frac{1}{R_{ev}} + \frac{1}{R_{p1} + R_{ev}}} \quad (71)$$

Where

R_j - thermal resistance of joint

R_{ins} - thermal resistance of insert

R_{p1} - thermal resistance of plate

R_{ev} - thermal resistance of evaporation

Thermal resistances of mounting joints and evaporation have been discussed previously; heat flow and a simplified, one dimensional thermal resistance determination of cylinders and disks will be discussed here. Radial heat conduction in a cylinder or disk of thickness δ can be expressed with the following equation:

$$Q = k \delta 2 \pi r \frac{dt}{dr} \quad (72)$$

Integrating within the limits r_1 and r_2

$$Q = k \delta 2 \pi \frac{\Delta t}{\ln r_1 - \ln r_2} \quad (73)$$

When R-C networks are used for thermal analysis, it is more convenient to have a simple expression for the heat flow through a disk of the same form as through a plane wall. This requires the determination of the mean area, A_m

$$A_m = \frac{A_2 - A_1}{\ln A_2 - \ln A_1} \quad (74)$$

and

$$Q = k \frac{A_m}{r_2 - r_1} \Delta t \quad (75)$$

also

$$Q = \frac{\Delta t}{R} \quad (76)$$

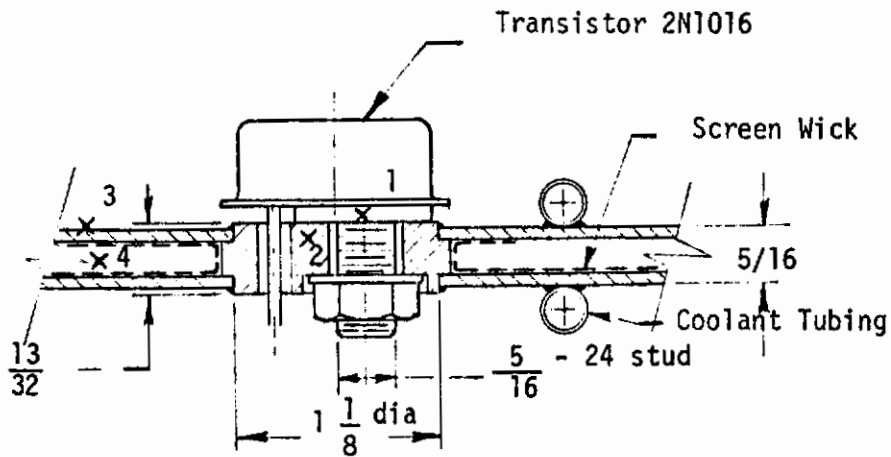
where

$$R = \frac{r_2 - r_1}{kA_m}, \text{ hr } ^\circ\text{F/Btu} \quad (77)$$

r_1 and r_2 are the internal and external radii of the disk or radial fin.

Figures 56 and 57 show the temperature distribution from power transistors 2N1016 and 2N2109 mounting bases to the plate's heat sink-circulating coolant, at three different power dissipation rates. The transistors were mounted directly to the plate without using any electrical isolation. As can be seen, temperature differentials caused by conduction heat transfer within the mounting surfaces are almost completely eliminated. Such a design can provide a significant advantage for cooling electronic components of high heat dissipation rates. The largest temperature drop occurs at the condenser section of the plate and is mainly caused by the convection heat transfer to the circulating coolant. This temperature differential, however, can be reduced by providing larger convection heat transfer surface area.

Figure 58 shows the temperature distribution under conditions when the power transistor 2N1016 was electrically isolated from the plate by application of mica washers. The significant increase in mounting joint thermal resistance is apparent. This thermal resistance can be reduced by selecting washers with higher thermal conductivity or reducing thickness of the washers. It has been already pointed out that the thickness of the mica washers varied quite significantly. This variation also caused quite a significant change of the joint thermal resistance.



SECTION A-A OF COLD PLATE NO. 6

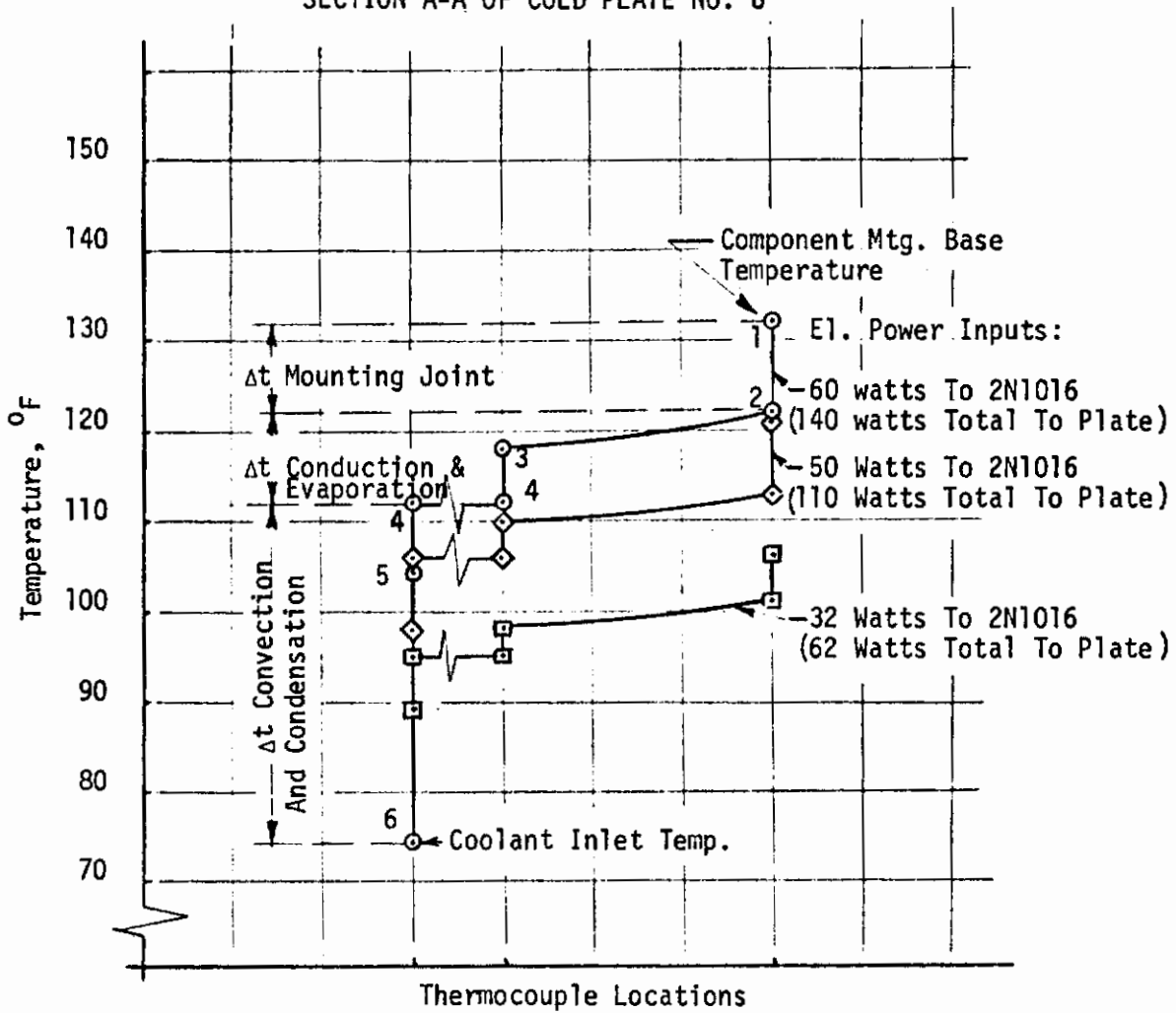
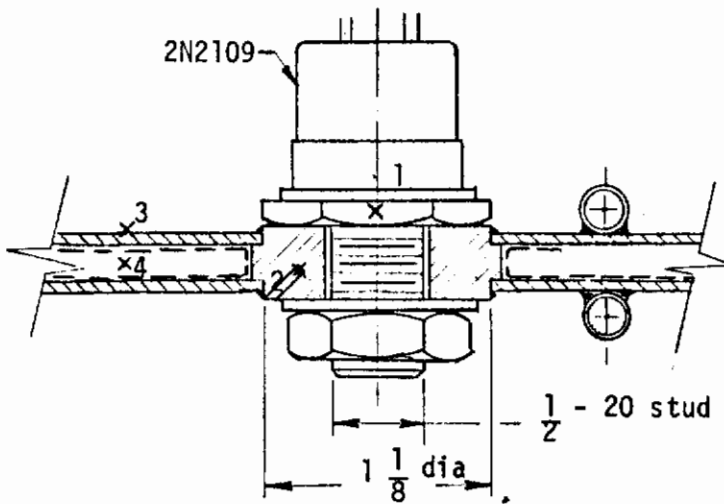


FIGURE 56. TEMPERATURE DISTRIBUTION OF COLD PLATE NO. 6 AT DIFFERENT POWER INPUT RATES TO TRANSISTOR



SECTION B-B OF COLD PLATE NO. 6

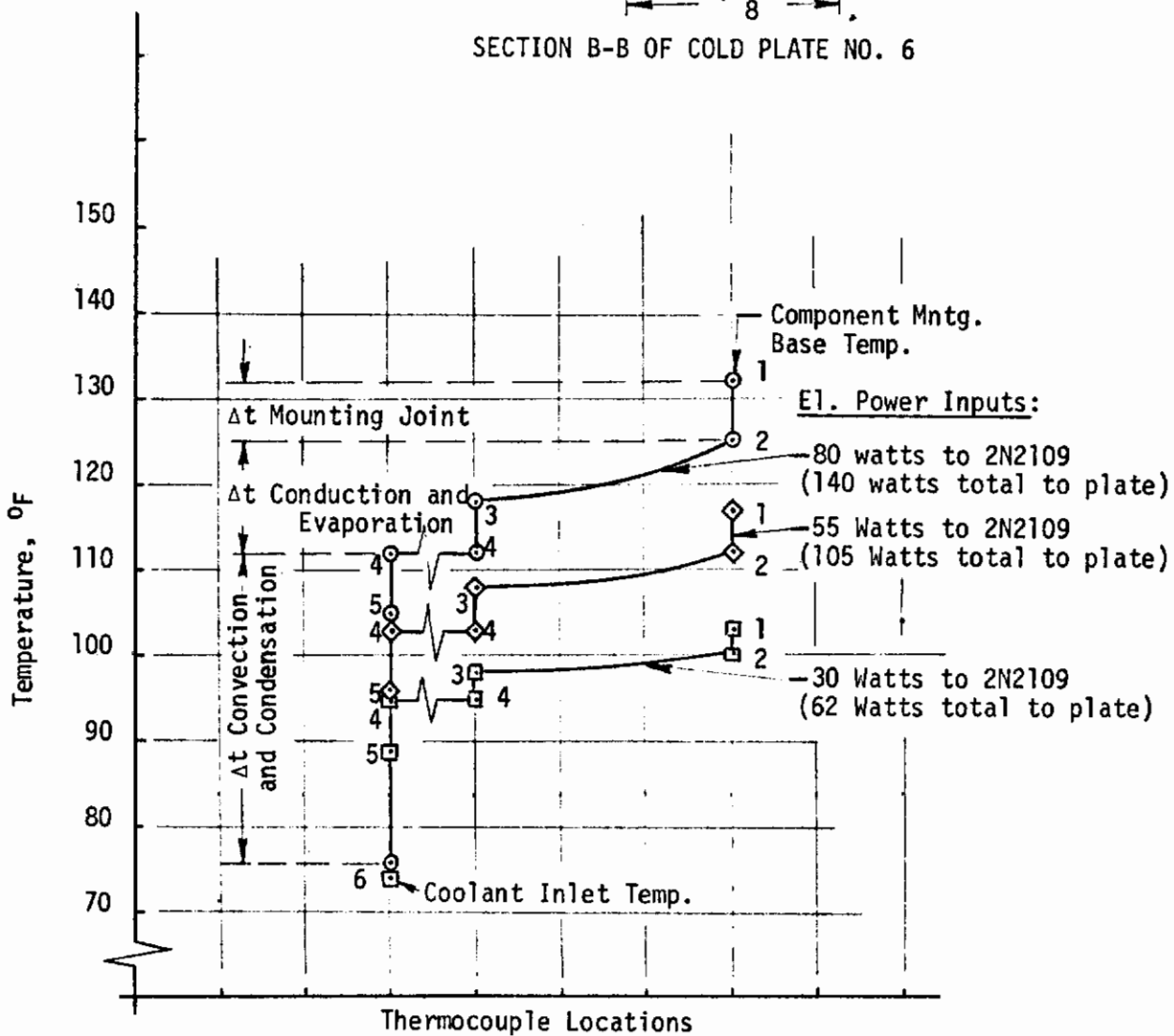


FIGURE 57. TEMPERATURE DISTRIBUTION OF COLD PLATE NO. 6 AT DIFFERENT POWER INPUT RATES TO TRANSISTORS

Contrails

- Total El. Power Input To Plate 182 Watts
- ◇ Total El. Power Input To Plate 120 Watts

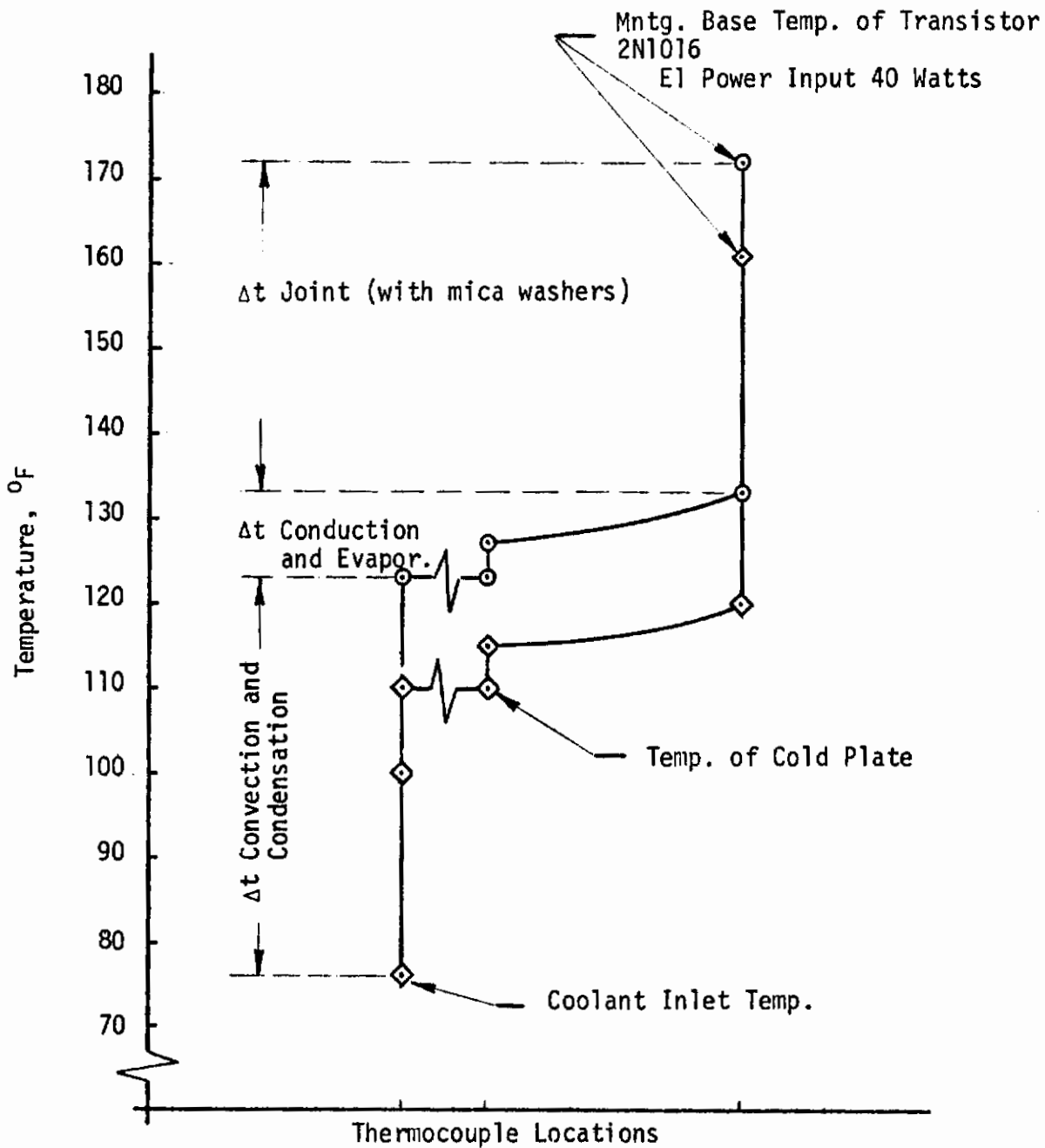


FIGURE 58. TEMPERATURE DISTRIBUTION OF COLD PLATE NO. 6 AT TWO DIFFERENT EL. POWER INPUT RATES

Contrails

The mounting joint thermal resistance, as obtained from temperature and heat flow rate measurements, was determined to be

$$R = \frac{\Delta t}{Q} = 0.294 \text{ hr } ^\circ\text{F/Btu} = 1.0^\circ\text{F/watt}$$

Two types of working fluids were used in the cold plate, Freon 11 and methanol. However, more uniform temperature throughout the cold plate was achieved with Freon 11, particularly at the lower heat input rates. An attempt was also made to determine the maximum possible concentrated heat load removal rate with this cooling technique. An electric power input of 165 watts was applied to the 2N2109 power transistor without any indication of dry-out of the wick. Because of the cold plate's internal pressure and transistor temperature considerations, no further increase was made in the electric power input. At an electrical power input of 165 watts, the transistor case temperature reached a value of 180°F . Based on a junction to case thermal resistance of $R_{jC} = 0.63^\circ\text{F/watt}$, the transistor junction temperature was determined to be

$$T_j = T_c + R_{jC} P = 180 + (.63)(165) = 284^\circ\text{F} = 140^\circ\text{C}$$

This temperature is below the maximum allowable junction temperature of 175°C .

V. SUMMARY OF RESULTS

A total of six different experimental electronic equipment cold plates provided with integral heat pipes have been thermally tested. Copper and aluminum materials were used for fabrication of the cold plates, and 100 mesh copper screen was used as a wick material. Freon 11, Freon 113 and methanol were used as working fluids. The plates were tested in an ethylene glycol-water cooling loop provided with a refrigeration unit and tap water as heat sinks.

All of the cold plates tested can be divided into four general categories: (1) conventional fin-tube design provided with heat of fusion materials or evaporative coolant, (2) conventional fin-tube design with heat pipes, (3) conventional fin-tube design provided with temperature control capabilities, and (4) flat, continuous cavity (vapor fin) configuration. Electric heaters, "dummy" and actual electronic components were used as heat loads.

The test results indicate that all the cold plates performed satisfactorily as long as the orientation was horizontal or inclined with the condenser section up. Inclination with the evaporator end up caused thermal degradation with temperature rise at the evaporator section, and at the electronic components.

Cold plates charged with heat of fusion materials can provide a limited heat sink under emergency conditions, or reduce thermal cycling under conditions when the heat load or heat sink temperature changes. Evaporative cooling, depending on temperature and time requirements, can provide much more effective emergency heat sinks. For example, 262 cubic centimeters of water in Cold Plate No. 2 extended the operating

Contrails

time of the cold plate for a 50 watt heat load to over four hours.

Cold plates of the conventional fin-tube design induced significant temperature differentials within the mounting surfaces when highly concentrated heat loads were applied. Application of such designs will be limited to components of low or medium power dissipation rates. It is possible, however, to reduce this deficiency by increasing the thickness of the mounting surfaces, and/or reducing the spacing of the heat pipe passages.

Cold plates provided with temperature control capabilities by introducing noncondensable gas into the condenser section of the plate can provide quite a close temperature control under variable heat load conditions, or when the heat sink temperature changes. A heat load change of from 80 watts to 240 watts caused a plate temperature change of only 10°F. A coolant inlet temperature change from 55°F to 73°F caused the plate temperature change of approximately 2°F.

The flat, continuous cavity (vapor fin) cold plate showed quite a significant improvement in temperature distribution and heat removal. A concentrated heat load of 165 watts was removed from a power transistor without reaching its maximum operating temperature or wick dry out condition. This design can be further improved and still larger concentrated heat loads removed.

Comparing performance of the different working fluids, Freon 11 showed the best results as far as temperature uniformity of the cold plates was concerned. Limits of the maximum heat fluxes were not investigated.

For comparison purposes a direct liquid cooled cold plate with a design similar to that of Cold Plate No. 6 was also tested. Instead of

Contrails

evaporative heat transfer, ethylene glycol-water coolant was circulated through the cavity, and component heat was removed by forced convection. The test results indicated that the temperature of individual components could be maintained at lower levels with the conventional liquid cooled cold plate. However, large temperature differentials occurred between components which had different heat dissipation rates. Significant thermal cycling was caused by heat load changes. More severe component temperature changes could also be observed when coolant temperature and flow rate changed.

VI. CONCLUSIONS

The application of heat pipes to electronic equipment cooling can provide significant improvements in equipment reliability and performance by improving temperature uniformity and reducing the amplitude of thermal cycling. Regardless of the design configuration, temperature distributions throughout the plates were always excellent. As long as heat was applied somewhere at the plate's surface by energizing one or more of the components, the heat was distributed throughout the plate, and all of the unenergized or low dissipation rate components attached to the plate's surface assumed its temperature. This condition, regardless of the different heat dissipation rates, reduced thermal gradients among components and also thermal cycling caused by changes in heat dissipation rates.

A simple, accurate and reliable temperature control can be provided by introducing noncondensable gas into the condenser section of the heat pipe. Application of this technique can significantly improve the thermal environment of electronic components by reducing temperature cycling caused by equipment duty cycles or heat sink temperature changes.

Furthermore, application of heat pipes to equipment cooling plate design will simplify the whole thermal control system by reducing the length of tubing, number of fittings and weight of coolant. Such cooling systems will be lighter, require less pumping power, and have improved reliability because of reduced vulnerability to general leaks and battle damage.

Heat of fusion materials and evaporative coolants can provide thermal protection for electronic systems under emergency conditions

and will reduce the amplitude of thermal cycling. A short time emergency protection method can also be provided by installing safety valves in the cold plates and using excessive working fluid. Even without the above precautions, such cold plates will be much more effective heat dissipators when the coolant loop fails.

Two general problem areas which resulted from the experimental work must be pointed out:

1. All of the cold plates tested were quite sensitive to orientation. Tilting the plate by only a few degrees with the evaporator end up caused thermal performance degradation. It must be noted, however, that all the cold plates were designed for horizontal or near horizontal operation.

2. At the higher heat loads a significant temperature drop occurred at the condenser section of the cold plates. This problem will always be present in designing cold plates with integral heat pipes. When temperature differentials must be reduced, particular attention should be paid to designing the condenser section of the cold plates with sufficiently large convection and condensation heat transfer surface areas.

REFERENCES

1. C. D. Parker, "Integrated Silicon Device Technology", ASD-TDR-63-316, Volume XV, Air Force Avionics Laboratory, Wright-Patterson AFB, Ohio, May 1967.
2. W. F. Hilbert and F. H. Kube, "Effects on Electronic Equipment Reliability of Temperature Cycling in Equipment", Grumman Aircraft Engineering Corp. Report EC-69-400, Feb 1969.
3. D. M. Cawthon and J. I. Gonzalez, "Effects of Aircraft Environmental Thermal Transients on Component Part Thermal and Electrical Parameters," Martin Marietta Corporation, Report OR 10,164, Dec 1969.
4. C. M. Ryerson et al, RADC Reliability Notebook, Volume II, RADC-TR-67-108, Sept 1967.
5. James P. Welsh et al, "Methods of Cooling Semiconductor Devices", RADC-TR-60-22, May 1960.
6. Alfred T. Batch, "Heat Sinking Solid State Devices with Diamonds", Electronic Packaging and Production, Volume 10, Number 8, Aug 1970.
7. T. P. Cotter, "Theory of Heat Pipes", Los Alamos Scientific Laboratory Report LA-3246-MS, March 1965.
8. E. C. Phillips, "Low Temperature Heat Pipe Research Program", NASA CR-66792 (N69-29839).
9. M. W. Leidy, "The Effect of Nucleate Boiling on Heat Pipe Operation", Naval Postgraduate School, Monterey, Calif, April 1969.
10. W. D. Allingham and J. A. McEntire, "Determination of Boiling Film Coefficient for a Heated Horizontal Tube in Water-Saturated Wick Material", ASME Paper No. 60-HT-11, Sept 1960.
11. R. S. Gill, "Pool Boiling in the Presence of Capillary Wicking Materials", M. S. Thesis, Massachusetts Institute of Technology, Aug 1967.
12. H. R. Kunz et al, "Vapor-Chamber Fin Studies", NASA CR-812, June 1967.
13. A. E. Bergles et al, "Cooling of High-Power Density Computer Components," Massachusetts Institute of Technology, Report DSR-70712-60, November 1968.
14. J. D. Lenk, Practical Semiconductor Data Book for Electronic Engineers and Technicians, Prentice-Hall, Inc. Englewood Cliffs, N. J. 1970.
15. C. J. Feldmanis, "Investigation of Passive Electronic Equipment Temperature Control Devices", Air Force Flight Dynamics Laboratory, Wright Patterson Air Force Base, Ohio, Technical Memorandum, TM-69-13-FDFE, Aug 1969.

Contrails

16. J. E. Fontenot, "Thermal Conductance of Contacts and Joints", Boeing Document No. D5-12206.
17. K. G. Lindh et al, "Studies on Heat Transfer in Aircraft Structural Joints", University of Calif. Report No. 57-50, May 1957.
18. Allan D. Kraus, Extended Surfaces, Spartan Books, Inc., 1964.

Unclassified

Security Classification

DOCUMENT CONTROL DATA - R & D

(Security classification of title, body of abstract and indexing annotation must be entered when the overall report is classified)

1. ORIGINATING ACTIVITY (Corporate author) AF Flight Dynamics Laboratory Wright-Patterson AFB, Ohio		2a. REPORT SECURITY CLASSIFICATION Unclassified	
		2b. GROUP	
3. REPORT TITLE Application of Cold Plates to Electronic Equipment Cooling			
4. DESCRIPTIVE NOTES (Type of report and inclusive dates) June 1971 to November 1972			
5. AUTHOR(S) (First name, middle initial, last name) Carl J. Feldmanis			
6. REPORT DATE November 1972		7a. TOTAL NO. OF PAGES 110	7b. NO. OF REFS 18
8a. CONTRACT OR GRANT NO.		9a. ORIGINATOR'S REPORT NUMBER(S) AFFDL-TR-72-128	
b. PROJECT NO. 6146			
c. Task No. 614617		9b. OTHER REPORT NO(S) (Any other numbers that may be assigned this report)	
d. Work Unit No. 61461713			
10. DISTRIBUTION STATEMENT Distribution limited to U. S. Government agencies only; test and evaluation; statement applied May 1972. Other requests for this document must be referred to Air Force Flight Dynamics Laboratory (FEE), Wright-Patterson Air Force Base, Ohio 45433.			
11. SUPPLEMENTARY NOTES		12. SPONSORING MILITARY ACTIVITY Air Force Flight Dynamics Laboratory AF Systems Command Wright-Patterson AFB, Ohio	
13. ABSTRACT <p>Analytical and experimental work have been performed to investigate the feasibility for heat pipe technology for electronic equipment thermal control. Temperature level and uniformity, amplitude and the frequency of thermal cycling have significant adverse effect upon the reliability and operational characteristics of electronic equipment. In order to promote heat transfer and improve the temperature distribution, the electronic equipment cooling plates (cold plates) were provided with integral heat pipes. The experimental cold plates which were tested can be divided into three general categories. (1) conventional fin-tube configurations, (2) fin-tube configuration provided with temperature control capabilities (constant temperature or variable conductance cold plate), and (3) flat, continuous cavity configuration. Actual and simulated electronic components were attached to the plates and used as heat loads.</p> <p>Test results have shown that the high thermal conductance of the heat pipes provided excellent temperature distribution throughout the plates, thus maintaining all of the equipment attached to them at a uniform temperature. Close temperature control of the plate could be achieved by utilizing variable conductance heat pipes with noncondensable gas reservoirs. Thermal cycling caused by equipment duty cycles or heat sink temperature changes was significantly reduced. Application of heat of fusion materials or evaporative coolants within the cold plates can also reduce thermal cycling or extend operational time for the safety of flight equipment under emergency conditions.</p>			

DD FORM 1 NOV 65 1473

Unclassified

Security Classification

Unclassified

Security Classification

14. KEY WORDS	LINK A		LINK B		LINK C	
	ROLE	WT	ROLE	WT	ROLE	WT
Electronic Equipment Cooling Cold Plates Heat Pipes						

Unclassified

Security Classification